THE UNIVERSITY OF CHICAGO

CIRCUITRY MECHANISMS UNDERLYING NOISE RESILIENCE OF RETINAL MOTION COMPUTATION

A DISSERTATION SUBMITTED TO
THE FACULTY OF THE DIVISION OF THE BIOLOGICAL SCIENCES
AND THE PRITZKER SCHOOL OF MEDICINE
IN CANDIDACY FOR THE DEGREE OF
DOCTOR OF PHILOSOPHY

COMMITTEE ON COMPUTATIONAL NEUROSCIENCE

BY
QIANG CHEN

CHICAGO, ILLINOIS
DECEMBER 2018

Abstract

We rely on visual information to navigate through natural environment. The extraction of visual features by the nervous system first arises in the retina. Retina sends processed visual information to cortical and sub-cortical brain regions through 20∼40 types of retinal ganglion cells (RGCs), each encodes specific aspect of visual scene. One of the most prominent visual processing in the retina is computation of motion direction, implemented by retinal direction selective circuit. While our notions about retinal direction circuit has come from usage of simple parametric stimuli, natural scenes are rarely homogeneous, but full of competing signals. This thesis focuses on understanding the underlying mechanisms of noise resilience of retinal direction computation. In chapter 1, we review the recent understanding of dynamic engagement of circuitry and synaptic mechanisms for robust retinal directional selectivity under various visual conditions. Chapter 2 described the protocol we developed for recording and functional imaging of retinal neurons under two-photon microscopy in the laboratory. In chapter 3, we used synapse-specific genetic manipulation to dissect the role of distinct sets of inhibitory motifs for motion processing. We found that the functional circuitries that process bright versus dark moving objects are not mirrored symmetric. Furthermore, Lateral inhibitory motifs in retinal direction selective circuit are only recruited in noisy visual condition in On pathway. Based upon findings in chapter 3, chapter 4 further investigated mechanistic implementation of noise resilience by lateral inhibition motif. We found that one particular form of lateral inhibition, the mutual inhibition of lateral inhibition, prevents use-

dependent synaptic suppression triggered by competing signals, thus maintains the strength and fidelity of synaptic transmission in the circuitry. Since feature selectivity, including direction selectivity, relies on the veto of spiking activities to "null" stimuli. This silencing of neuronal spiking requires timely cancellation of excitation by inhibition. In chapter 5, we investigated how retinal direction selective circuit maintains the $\sim ms$ time-scale covariation of inhibition and excitation for robust direction selectivity.

For my family, without whom I couldn't have made this journey

Contents

List of Figures

Acknowledgements

As long as our brain is a mystery, the universe, the reflection of the structure of the brain will also be a mystery. —Cajal

Over the years, I had the fortune to work with many incredible people both in and out of labs. My initial encounter with neuroscience started with Dr. Guoqiang Bi's lab back in my *alma mater* at University of Science and Technology of China as a physics major undergraduate. Bi showed me the characters being a good scientist: focus, dedication, and hard-working. It is in the Bi lab that I came to know some enthusiastic future scientists, with whom I still keep a close friendship after we came to the States together. Among them are Pengcheng Zhou now at Columbia, and Xun Wang now at Caltech, Xiaokang Zhang now a faculty at Zhejiang University. My development as a neuroscientist, however, really started in the Wei lab at Chicago. The Wei lab has been relatively small over the years, but the atmosphere was fabulous. While each individual naturally went through some up-and-downs in graduate school, Wei has been extremely supportive and patient throughout our training. Being one of the first graduate students, I am really fortunate to be able to work alongside with Wei on rigs as well as help build out portion of the lab. This early hands-on training turns out to be extremely helpful in my transitioning from a theorist into an experimentalist. While the title of "professor" might create some distance between the PI and students, I can't express more gratitude towards Wei for being a sister-like figure in the lab when we need her.

The members of the Wei lab are the key for making the past a few years both productive and full of fun. We learned from each other from different aspects, because of our diverse backgrounds both in terms academic training and life endeavors. David Koren, Hector Ledesma, and me are the early trio in the lab. We joined the lab around similar time and traveled together to conferences, had nights of discussion of science and life. Jenny Pei, a former postdoc, collaborated with me on my first two published work. Lindsay Huang, has been enthusiastic towards science since day one in the lab. Other current and former lab members I would like to thank includes Chen Zhang, James Grove, Benno Giammarinaro, Jennifer Ding, etc.

The members of my thesis committee: Stephanie Palmer, Nicolas Brunel, Ruth Anne Eatock, all provided incredible feedbacks throughout my graduate career. They insightful advices helped me to approach research projects from different perspectives.

My parents have been on my back since early on. I got the complete freedom to choose my own way. They always trust me in making the right decisions. I didn't fully realize how luxurious this has been for those growing up in China. I am grateful towards them for letting me explore my life freely.

Last but no least, I would like to thank my wife Flora for her love, companion, and support. While working on the thesis, we welcomed little Alvin to the family. This journey has really been an endeavor of the whole family!

1

Stimulus-dependent engagement of neural mechanisms for reliable motion detection in the mouse retina

This Chapter is a full reprint of Chen et al., Journal of Neurophysiology, in which I was the primary author.The work is included with permission from all authors.

Relevant Publication

Qiang Chen, Wei Wei. "Stimulus-dependent engagement of neural mechanisms for reliable motion detection in the mouse retina". J. Neurophysiol. 2018 Jun 13. doi: 10.1152/jn.00716.2017.

1.1 Abstract

Direction selectivity is a fundamental computation in the visual system and is first computed by the direction-selective circuit in the mammalian retina. While landmark discoveries on the neural basis of direction selectivity have been made in the rabbit, many technological advances designed for the mouse have emerged, making

this organism a favored model for investigating the direction-selective circuit at the molecular, synaptic, and network levels. Studies using diverse motion stimuli in the mouse retina demonstrate that retinal direction selectivity is implemented by multilayered mechanisms. This review begins with a set of central mechanisms that are engaged under a wide range of visual conditions, and then focuses on additional layers of mechanisms that are dynamically recruited under different visual stimulus conditions. Together, recent findings allude to an emerging theme: robust motion detection in the natural environment requires flexible neural mechanisms.

1.2 introduction

Direction selectivity, a classic model of neural computation, has inspired scientists in both experimental and computational disciplines for decades (Hassenstein and Reichardt 1956; Hubel and Weisel 1959; Barlow et al. 1964; Poggio and Reichardt 1973; Ferster 1998; Borst 2000). In mammals, direction-selective ganglion cells (DSGCs) were first discovered in the rabbit retina (Barlow and Hill 1963; Barlow et al. 1964). These cells fire maximally to images moving in their preferred direction and are silenced by movement in the opposite (null) direction. Based on the activity of DSGCs during sequential presentation of a pair of stationary light flashes in the preferred and null directions, Barlow and Levick proposed the null-direction inhibition model that attributes direction selectivity of DSGCs to a stronger inhibitory mechanism during motion in the null direction (Barlow and Levick 1965). Since then, uncovering neural mechanisms underlying null-direction inhibition has been a major goal in visual neuroscience.

During the quest to identify the neural mechanisms of retinal direction selectivity, the rabbit has been the prevalent model organism for a series of remarkable discoveries at the cellular and synaptic levels. In the past ten years, an increasing repertoire of cell

type-specific genetic markers and molecular tools available for the mouse retina has prompted the field to gradually transition to the mouse as a model for probing the developmental and mature mechanisms of retinal direction selectivity. The ability to target specific DSGC subtypes and their key presynaptic partner, the starburst amacrine cell (SAC), has accelerated the analysis of this circuit (Watanabe et al. 1998; Kim et al. 2008; Yonehara et al. 2008; Huberman et al. 2009; Kay et al. 2011; Rivlin-Etzion et al. 2011; Trenholm et al. 2011; Dhande et al. 2013). Based on the results from both rabbit and mouse studies, the neural substrate of the null-direction inhibition model originally proposed by Barlow and Levick (1965) has been pinpointed at the GABAergic connections between SACs and DSGCs (Figure 1.1a).

The triumph of understanding the null-direction inhibition at the level of SAC-DSGC interactions marks the beginning, rather than the end of our search for the neural basis of direction selectivity. SACs and DSGCs, the cell types that have been in the spotlight, are embedded in the extensive retinal network consisting of around 100 types of neurons (Masland 2012; Sanes and Masland 2015; Baden et al. 2016). Immediately connected to the SAC-DSGC microcircuit are the diverse sets of synapses from multiple types of bipolar cells and amacrine cells (Figure 1.1b). These connections profoundly shape the light responses of both SACs and DSGCs, making them sensitive or resilient to various features of visual input. A comprehensive understanding of motion detection therefore requires an integrated circuit model that encompasses all relevant neurons and their radiating connections, with the ultimate goal of a complete functional wiring diagram for motion detection in the natural environment.

The two major DSGC types, On and On-Off DSGCs, are both dependent on SACs for their direction selectivity but exhibit interesting differences in other receptive field properties and visual functions (reviewed by Vaney et al. 2012). Most of the literature focuses on On-Off DSGCs, due to their higher density compared to that

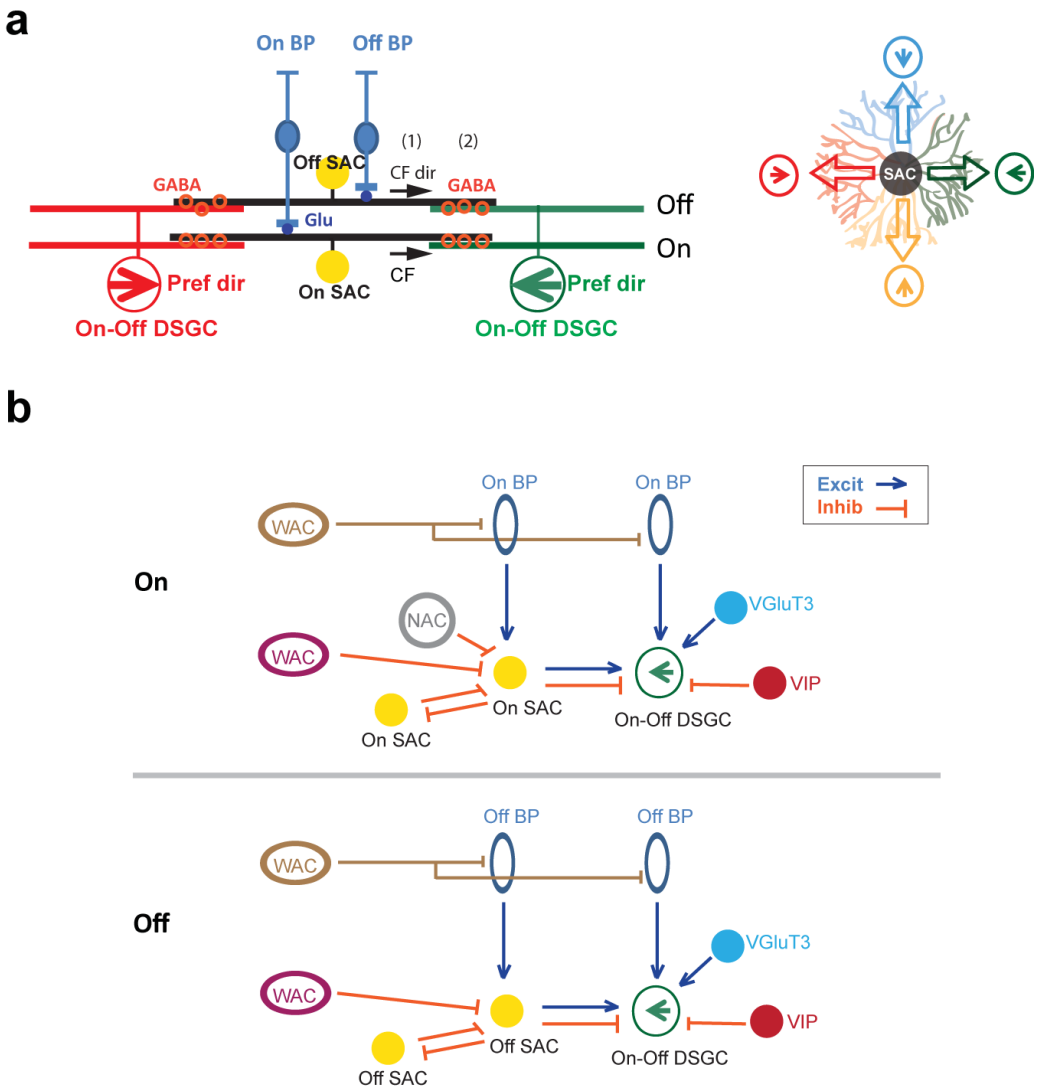

FIGURE 1.1: Wiring diagrams of retinal direction selectivity.
a. Model of null-direction inhibition. Left: Schematic shows side view of glutamatergic bipolar cell (BP) inputs to the proximal dendrites of On and Off SACs, and GABA release (orange circles) from SAC distal dendrites to two On-Off DSGCs of opposite preferred directions. The preferred directions of On-Off DSGCs are represented by the green and red arrows. Directional inhibition from SACs to the DSGC depends on two properties. (1) Centrifugal (CF) direction selectivity of SAC dendrites. CF direction of SAC dendrites is represented by black arrows. (2) Asymmetric wiring between SACs and DSGCs. SAC dendrites oriented to the right form GABAergic synapses with the DSGC whose preferred direction is to the left. Right: Top view shows the asymmetric inhibition from a SAC (center) to four DSGCs that prefer four different cardinal directions. Each SAC dendritic quadrant preferentially forms GABAergic synapses with the DSGC with the same color.
b. Schematic shows anatomically and/or functionally identified connections in the inner plexiform layer that participate in the direction-selective circuit. Upper: On pathway; lower: Off pathway.

of On DSGCs in the retina and the availability of multiple subtype-specific markers. The preferred directions of On-Off DSGCs are grouped into four clusters (Oyster et al. 1967) that correspond to the forward/backward and upward/downward directions of translational motion (Sabbah et al. 2017). On-Off DSGCs project to two major visual nuclei, the dorsal lateral geniculate nucleus (dLGN) and superior colliculus (Huberman et al. 2009; Kay et al. 2011; Rivlin-Etzion et al. 2011; Cruz-Martn et al. 2014). In the superior colliculus, direction-selective retinal inputs give rise to direction selectivity in collicular neurons (Shi et al. 2017). In the dLGN, thalamic neurons in the region innervated by axons of On-Off DSGCs exhibit direction and orientation selectivity (Marshel et al. 2012; Piscopo et al. 2013; Cruz-Martn et al. 2014), suggesting an instructive role of direction-selective retinal inputs in feature selectivity in the dLGN. Furthermore, perturbing retinal direction selectivity has been shown to alter the receptive field properties of direction-selective neurons in the mouse primary visual cortex (Hillier et al. 2017).

In this review, we first summarize the recent literature on the core mechanisms underlying direction selectivity in On-Off DSGCs that are invariant in a wide range of visual stimulus conditions. For a more comprehensive summary of the rich literature on this topic and the developmental aspects of retinal direction selectivity, readers are encouraged to consult other excellent reviews (Vaney et al. 2012; Morrie and Feller 2016; Mauss et al. 2017). The rest of this review focuses on the recently discovered neural mechanisms in the mouse retina that are selectively recruited or modulated by specific features of motion stimuli. These findings indicate that direction selectivity in the retina is not implemented by a rigid set of mechanisms. Rather, dynamic and flexible sets of mechanisms are engaged and tailored to the specific visual conditions to ensure reliable and robust motion detection as the animal navigates in the versatile natural environment.

1.3 Core mechanisms

1.3.1 Null-direction inhibition of DSGCs

As a key mechanism of direction selectivity, the inhibitory inputs onto DSGCs are strongly tuned to motion in the null direction. This directional inhibition is provided by On and Off SACs, which are axonless, monostratified amacrine cells releasing GABA and acetylcholine onto the On and Off dendritic layers of the bistratified On-Off DSGCs (Figure 1.1a). When GABAergic synapses between SACs and DSGCs is genetically disrupted by knocking out vesicular GABA transporter (Vgat) in SACs, the direction selectivity of DSGCs is severely reduced (Pei et al. 2015).

Two properties of SAC-DSGC GABAergic synapses are required to generate directional inhibition of DSGCs.

- SAC dendrites are direction-selective and prefer motion in the centrifugal direction (away from the soma, Figure 1.1a) (Euler et al. 2002). The centrifugal direction selectivity of SAC dendrites has been attributed to multiple mechanisms. In the mouse retina, spatially segregated synaptic inputs and outputs along the dendrites have been implicated in generating this centrifugal preference. Glutamatergic inputs from bipolar cells and inhibitory inputs from neighboring amacrine cells are enriched in the proximal dendrites of mouse SACs (Ding et al. 2016; Vlasits et al. 2016). This proximal distribution of synaptic inputs in the mouse is in contrast to the more uniform distribution of inputs along the SAC dendrites in the rabbit (Famiglietti 1991). On the other hand, neurotransmitters GABA and acetylcholine (Ach) are released from varicosities in the outer third of SAC dendritic arbors in both rabbits and rodents (Brecha et al.1988; Kosaka et al. 1988; Vaney and Young 1988; OMalley and Masland 1989; Famiglietti 1991). Computational modeling indicates that the

proximal distribution of synaptic inputs and distal distribution of synaptic outputs in the mouse SAC contributes to the centrifugal direction selectivity of SACs (Ding et al. 2016; Vlasits et al. 2016).

Although the SAC dendritic branches are tuned to different linear motion directions, motion-evoked dendritic activation of individual sectors is not completely isolated from other sectors. Computational modeling suggests that global signal integration across the dendritic field contributes to the centrifugal response of SAC distal dendrites (Tukker et al. 2004). A role of global dendritic signal integration is experimentally demonstrated by a mulitphoton calcium imaging experiment, in which the centrifugal activation of SAC distal dendrites during full-field linear motion stimuli is stronger and starts earlier compared to the centrifugal response locally generated within a dendritic sector (Koren et al. 2017).

The balance between signal integration and compartmentalization in SAC dendrites is maintained by intricate interactions between passive and active membrane properties (Ozaita et al. 2004; Tukker et al. 2004; Koren et al. 2017) and regulated by metabotropic glutamate receptor 2 (mGluR2) signaling (Koren et al. 2017). mGluR2 blockade increases voltage-gated calcium channel activity and thereby reduces the electrotonic isolation between SAC sectors. This leads to enhanced propagation of centrifugal response from one dendritic sector to the opposite, centrifugally activated sector. As a result, centrifugal direction selectivity of SAC dendrites is impaired during mGluR2 blockade (Figure 1.2) (Koren et al. 2017). The molecular targets of mGluR2 activation include N- and P/Q-types of voltage-gated calcium channels in SACs, which are inhibited shortly after bath application of an mGluR2 agonist. However, mGluR2 blockade specifically promotes cross-sector signal propagation, but does not affect signal processing within a sector. Therefore, the site of endogenous mGluR2

action is likely the perisomatic/proximal dendritic compartment, without directly inhibiting the presynaptic calcium channels at the distal dendritic tips. Although the subcellular distribution of mGluR2 along SAC dendrites is not yet known, glutamate release onto the SAC from bipolar cells are skewed to SAC proximal dendrites in the mouse retina (Ding et al. 2016; Vlasits et al. 2016). Concomitant activation of ionotropic and metabotropic glutamate receptors in the proximal dendrites may serve as a homeostatic mechanism to prevent aberrant backpropagation of local depolarization of SAC dendrites when the glutamatergic drive to the SAC is strong. Future studies that investigate mGluR2 signaling under different visual stimulus conditions will elucidate the intriguing link between visually evoked activity and the flexible dendritic computation algorithm modulated by mGluR2 signaling. Interestingly, voltage-gated KV_3 potassium channels (Ozaita et al. 2004) and GABAergic inputs (Ding et al. 2016) are also concentrated in the proximal dendrites of SACs and contribute to local dendritic processing (Ozaita et al. 2004; Poleg-Polsky et al. 2018), making the proximal dendritic region well-equipped for regulation of compartmentalized signaling of SAC dendrites.

- The GABAergic connections between SACs and DSGCs are highly asymmetric along the preferred-null axis. Each DSGC is selectively inhibited by SAC dendrites that are oriented in the DSGC's null direction (Fried et al. 2002; Lee et al. 2010; Briggman et al. 2011; Wei et al. 2011; Yonehara et al. 2011) (Figure 1.1a). In the mouse, this asymmetry emerges during the second postnatal week before eye opening (Wei et al. 2011; Yonehara et al. 2011) due to increased number of synapses between null-direction-oriented SAC dendrites and DSGCs (Morrie and Feller 2015). The establishment of direction selectivity is not af-

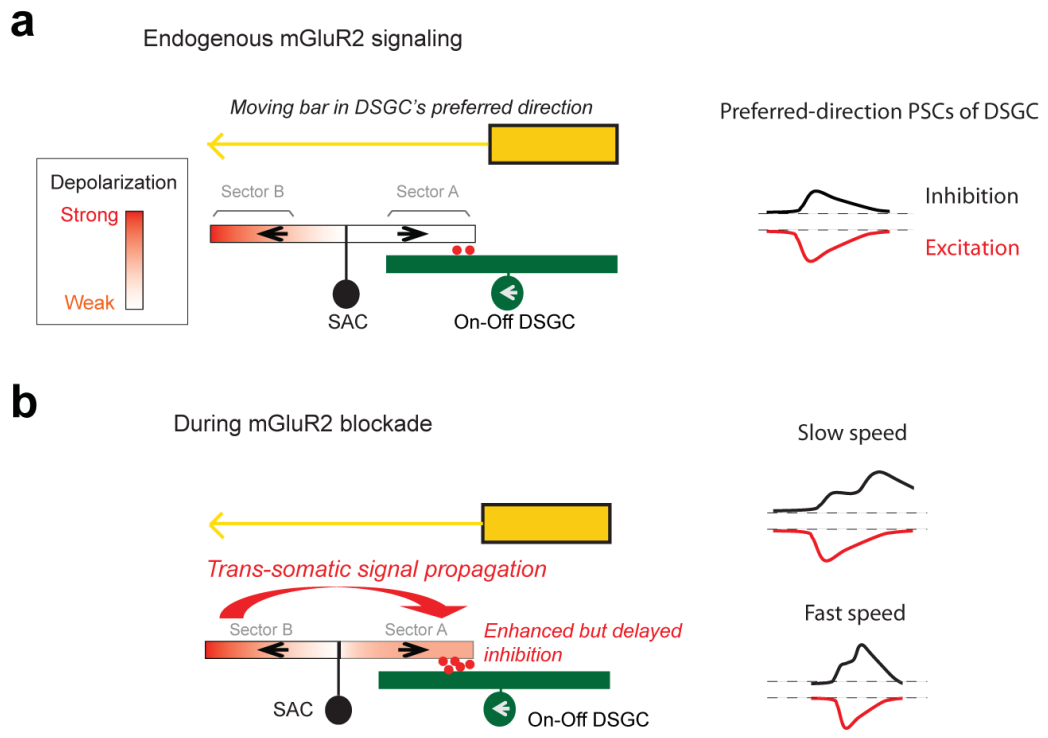

FIGURE 1.2: mGluR2-mediated electrotonic isolation of SAC dendritic sectors is required for broad speed tuning of On-Off DSGCs. (Adapted from Koren et al Neuron, 2017)
a. A model of mGluR2-dependent dendritic compartmentalization in SACs. Left:Endogenous mGluR2 signaling promotes the electrotonic isolation between SAC dendritic branches. A bar moving in the preferred direction of the DSGC (leftward) triggers minimal GABA release (red dots) from the centripetally activated sector A of the SAC. Subsequent activation of sector B in the centrifugal direction does not propagate efficiently to sector A to trigger GABA release. Right: Weak centripetal activation of SAC dendrites leads to weak IPSC of the DSGC in the preferred direction.
b. Left: During mGluR2 blockade, electrotonic isolation between SAC branches is reduced. Therefore, the strong centrifugal response of sector B propagates more efficiently to sector A. This leads to enhanced dendritic activation of sector A and more GABA release onto the DSGC during motion in the DSGC's preferred direction. Right: Since the relative timing of sector B and A activation depends on the speed of the moving bar, the enhanced component of IPSC during mGluR2 blockade is more delayed and shows less overlap with EPSC at slower speed. Therefore, preferred-direction spiking of DSGC is less affected. At higher speed, enhanced IPSC shows more overlap with EPSC, leading to reduced firing of DSGC.

fected by pharmacological blockade of neural activity (Sun et al. 2011; Wei et al. 2011), while the clustering of the four preferred directions is refined by visual activity after eye opening (Bos et al. 2016).

Together, the centrifugal direction selectivity of SAC dendrites and the asymmetric wiring of SAC-DSGC GABAergic synapses result in directionally tuned

inhibition of DSGCs. Motion in the null direction of the DSGC activates its presynaptic SAC dendrites in the centrifugal direction, causing strong GABAergic inputs from SACs to DSGCs (Figure 1.1a).

1.3.2 Directional excitation onto DSGCs

Stronger preferred-direction excitation of DSGCs has been consistently observed in multiple studies using whole-cell voltage clamp recordings, although the tuning of EPSCs appears weaker compared to that of inhibitory postsynaptic currents (IPSCs) (Taylor and Vaney 2002; Fried et al. 2005; Lee et al. 2010; Park et al. 2014; Pei et al. 2015). EPSCs of DSGCs consist of the glutamatergic component and the SAC-mediated cholinergic component. When the glutamatergic component is examined with alternative methods such as calcium imaging in bipolar cell terminals and glutamate imaging in DSGCs with a fluorescent glutamate sensor,iGluSnFR, it does not appear to be directional (Yonehara et al. 2013; Chen et al. 2014; Park et al. 2014). One complication of voltage-clamp recording is that EPSCs in the null direction may be distorted by the concomitant strong inhibitory inputs due to imperfect space clamp, leading to an underestimation of EPSCs in the null direction (Poleg-Polsky and Diamond 2011). However, recent studies indicate that directional excitation is not simply a voltage-clamp artifact. First, the tuning strength of excitation is not well correlated with the tuning strength or absolute amplitude of inhibition in wild type rabbits (Percival et al. 2017) or in mutant mice that lack SAC-DSGC inhibition (Pei et al. 2015), suggesting that directional excitation is not solely due to voltage clamp errors. Second, abolishing directional inhibition by genetically removing GABA release from SACs does not fully eliminate directional excitation or directional spiking activity of DSGCs (Pei et al. 2015). Although direction selectivity of DSGCs in mutant mice is significantly reduced, a subset of the On-Off DSGCs

still receive directional cholinergic excitation and exhibit residual, albeit weakened, directional tuning of their spiking activity (Pei et al. 2015). These results indicate that directional excitation is a physiological mechanism that contributes to the direction selectivity of DSGC spiking activity, together with the more universal and prominent null-direction inhibition. The contribution of cholinergic excitation to direction selectivity may depend on visual stimuli, since earlier studies report different effects of nicotinic receptor antagonists on direction selectivity of DSGCs during moving bar and drifting grating stimuli (Grzywacz et al.1998a, 1998b).

The synaptic circuitry underlying directional excitation remains poorly understood. The cholinergic excitation from SACs to DSGCs is isotropic when the SACs are stimulated by depolarizing voltage steps in dual voltage clamp recordings. However, these cholinergic synapses are activated in a directional manner during the presentation of moving stimuli (Fried et al. 2005; Lee et al. 2010; Pei et al. 2015). Bath application of GABA-A receptor antagonists abolishes directional excitation (Fried et al. 2005; Lee et al. 2010; Pei et al. 2015), suggesting that an upstream inhibitory circuit mediates the directional acetylcholine release from SACs. The neural substrate of this inhibitory mechanism is not yet identified.

1.3.3 Postsynaptic mechanisms at DSGC dendrites

After the arrival of the patterned excitatory and inhibitory inputs at DSGC dendrites, synaptic inputs are further integrated and processed by postsynaptic mechanisms to amplify the direction selectivity of DSGC spiking response through NMDA receptor signaling (Poleg-Polsky and Diamond 2016a) and local dendritic spike generation (Oesch et al. 2005; Schachter et al. 2010; Sivyer and Williams 2013; Brombas et al. 2017). Furthermore, the fluctuations of excitatory and inhibitory inputs (also termed "synaptic noise") during motion stimuli show direction-dependent covaria-

tion. Synaptic noise covariation during null-direction motion is stronger compared with that during the preferred direction motion, leading to more efficient cancellation of excitatory and inhibitory inputs onto DSGC dendrites during motion in the null direction (Cafaro and Rieke 2010).

1.4 Stimullus-dependent mechanisms

1.4.1 Contrast

Direction selectivity of DSGCs is robust over a wide range of stimulus contrast (Grzywacz et al. 1998b; Poleg-Polsky and Diamond 2016b). In the mouse retina, multiple mechanisms have been reported to maintain robust direction selectivity at different contrasts. Inhibitory circuits have been shown to play a role at high contrast conditions since bath application of GABA-A receptor antagonist SR95531 leads to a more severe reduction of the centrifugal direction selectivity of On SAC dendrites at higher contrast compared to low contrast (Ding et al. 2016). However, selective removal of GABA-A receptors from On SACs does not affect the centrifugal direction selectivity of SAC dendrites over a range of contrast levels (Chen et al. 2016), suggesting that the locus of inhibition is at the bipolar terminals presynaptic to SACs (refer to Figure 1.1b for the sources of inhibition of SACs).

Excitatory inputs to DSGCs are also modulated by contrast. The bipolar cells that drive SACs exhibit higher contrast sensitivity compared to those that drive DSGCs (Poleg-Polsky and Diamond 2016b). However, the glutamatergic inputs undergo nonlinear transformation by SAC dendrites, likely caused by the nonlinear activation of synaptic calcium channels, which results in a reduced contrast sensitivity of ACh and GABA release from SAC presynaptic terminals (Poleg-Polsky and Diamond 2016b). As a result, the contrast sensitivity of GABAergic and cholinergic inputs matches that of bipolar cell-mediated glutamatergic inputs onto DSGCs. This balanced exci-

tation/inhibition ratio in DSGCs ensures reliable direction selectivity independent of contrast (Poleg-Polsky and Diamond 2016b). In an alternative model, the contrast sensitivity of SAC-mediated inputs to DSGCs does not match that of bipolar cell-mediated glutamatergic inputs. Different contrast sensitivities of SACs and DSGCs arise from different compositions of their glutamate receptors (Sethuramanujam et al. 2016, 2017). Cholinergic inputs dominate DSGC excitation at low contrast due to the and work in conjunction with GABAergic inputs to implement direction selectivity (Sethuramanujam et al. 2016). By comparison, a different strategy has been reported in guinea pigs and rabbits. In these animals, excitatory inputs onto DSGCs vary more linearly with contrast to encode contrast information in preferred-direction spiking activity, while strong null-direction inhibitory inputs exhibit highly nonlinear contrast sensitivity and saturate at low contrast (Lipin et al. 2015). Saturated inhibition ensures sufficient suppression of null-direction spiking across different contrast levels and therefore safeguards direction selectivity. It is noteworthy that the background light intensity and the contrast range differ across studies. Therefore, differences in results reported from different studies may be explained by differences in experimental, or stimulus conditions.

1.4.2 On/Off contrast polarity

Segregation of the On and Off pathways is a general feature of the synaptic organization in the inner retina. For On-Off DSGCs, direction selectivity for bright and dark contours is processed in the On and Off layers of DSGC dendrites that receive synaptic inputs from the On and Off SACs respectively. While the asymmetric wiring between SACs and DSGCs is mirrored in the On and Off pathways (Briggman et al. 2011), recent studies demonstrate notable differences in the neural mechanisms underlying the direction selectivity of On and Off SAC dendrites.

First, inhibitory inputs to On and Off SACs show functional and anatomical divergence. In the On pathway, inhibitory inputs onto On SACs are not required for direction selectivity of On SACs and the On response of DSGCs during a simple moving bar stimulus against a uniform background (Chen et al. 2016). However, feed-forward inhibition from non-SAC amacrine cells to Off SACs contributes to direction selectivity in the Off pathway under the same stimulus condition (Chen et al. 2016). Interestingly, connectomic analysis shows that Off SACs receive a higher fraction of wide-field amacrine cell inputs than On SACs (Ding et al. 2016), consistent with a more prominent role of inhibition from non-SAC amacrine cells to Off SACs. On the other hand, On SACs, but not Off SACs, receive inputs from a class of narrow-field amacrine cells (Ding et al. 2016). These results highlight that the inhibitory circuitry impinging on the On and Off SACs are not identical. Additionally, NMDA receptor function has been reported to differ between the two SAC populations, since NMDA receptor antagonist affects the temporal response of Off but not On SACs (Fransen and Borghuis 2017).

In addition to the distinct mechanisms underlying direction selectivity of On and Off SACs,interactions between On and Off pathways have been implicated under specific visual stimulation conditions. Crossover excitation of Off SACs from the On pathway originated from rod and M-cone signaling has been reported in the mouse retina (Rosa et al. 2016, but see Kittila and Massey 1995 in rabbit). In another study, the polarity of excitatory inputs to On and Off SACs can be reversed by a short period of repetitive drifting grating stimulation (Vlasits et al. 2014), which may underlie the reversal of the preferred direction of DSGCs under the same condition (Rivlin-Etzion et al. 2012).

Together, these recent studies indicate that motion of bright and dark contours is not processed by completely mirror symmetric mechanisms in the On and Off pathways in the mouse retina. Instead, divergent circuit motifs and synaptic properties as well

as the interactions between the two pathways collectively shape the directionally tuned On and Off responses of DSGCs.

1.4.3 Noise

A moving bar stimulus over a uniform background has been pivotal to uncovering many key mechanisms of direction selectivity. However, visual motion in the natural environment is usually accompanied by other non-motion features that put extra strains on the direction-selective circuit. To maintain robust direction selectivity in the presence of these competing features or "noise", the retina recruits additional layers of neural mechanisms that are selectively engaged when visual noise is present in motion stimuli. One example is the NMDA receptor signaling in DSGCs that amplifies correlated excitation and improves the fidelity of direction selectivity in noisy conditions (Poleg-Polsky and Diamond 2016a). When the background and bar intensities vary independently and randomly, direction selectivity of DSGCs deteriorates upon NMDA receptor blockade (Poleg-Polsky and Diamond 2016a). By contrast, NMDA receptor blockade has no effect on direction selectivity during noise-free moving bar stimuli (Kittila and Massey 1997; Poleg-Polsky and Diamond 2016a). Visual noise also recruits specific microcircuit motifs to the direction-selective circuit. This is exemplified by selective activation of lateral inhibition onto On SACs (Chen et al. 2016). In the absence of background noise, the direction selectivity of the On SACs and On component of DSGCs does not require lateral inhibition onto On SACs. However, when a randomly flickering checkerboard is introduced in the background, the lack of GABAergic inputs onto On SACs significantly impairs direction selectivity in the On pathway, highlighting the importance of lateral inhibition in preserving feature selectivity under complex visual conditions.

1.4.4 Speed

Direction-selective firing of On-Off DSGCs exhibits broad speed tuning. In the null direction, to ensure reliable suppression of DSGC spiking, strong inhibitory inputs need to be generated in time to sufficiently coincide with excitation at all speeds. Steep saturation of inhibitory inputs onto DSGCs has been shown in rabbits and guinea pigs to render the strong null-direction inhibition speed-invariant (Lipin et al. 2015). In the temporal domain, cholinergic and GABAergic inputs onto DSGCs are well correlated in the null direction across a range of speeds due to the co-release of ACh and GABA from the centrifugally activated SAC dendrites. The fast onset of GABAergic inhibition onto DSGCs in the null direction also ensures a timely cancellation of glutamatergic excitation from bipolar cells. This fast onset of strong null-direction inhibition depends on global signal integration across the entire SAC dendritic field along the motion trajectory (Koren et al. 2017).

In the preferred direction, mGluR2-dependent electronic isolation of SAC dendrites is involved in maintaining the broad speed tuning of DSGC spiking (Koren et al. 2017). When mGluR2 is blocked, the strong centrifugal activation of one sector propagates more readily into the opposite, centripetally activated sector and thereby enhances the preferred-direction inhibition of DSGCs (Figure 1.2). This timing of the enhanced centripetal response during mGluR2 blockade depends on the speed of linear motion across SAC dendrites. At faster motion speed, back-propagating signals arrive faster and enhance preferred-direction GABAergic inputs onto DSGCs during concomitant excitation. Therefore, blockade of endogenous mGluR2 signaling significantly reduces the preferred-direction firing of DSGCs at faster speeds. The impact of mGluR2 blockade on DSGC preferred-direction spiking is less prominent at lower speed due to the reduced overlap between excitation and aberrant but more delayed inhibition of DSGCs (Figure 1.2).

1.5 Anatomical substrates for an extended neural network of direction selectivity

The stimulus-dependent neural mechanisms discussed above indicate that the receptive field properties of SACs and DSGCs are intricately influenced by the extended neural circuitry under different stimulus conditions. Recently, physiological studies reveal two new types of amacrine cells that provide synaptic inputs onto DSGCs. The VGluT3 amacrine cells provide glutamatergic excitation to On-Off and On DSGCs (Lee et al. 2014, 2016; Kim et al. 2015), while the VIP positive amacrine cells send GABAergic inhibition to On-Off DSGCs (Park et al. 2015).

Connectomic analysis reveals a separate set of narrow and wide amacrine cell types that are connected to SACs and bipolar cells (Hoggarth et al. 2015; Ding et al. 2016). Reconstruction of the direction-selective circuit at the electron microscopic level also delineates partially overlapping sets of bipolar cell types that innervate the On-Off DSGCs, On and Off SACs (Helmstaedter et al. 2013; Kim et al. 2014; Ding et al. 2016). In the On layer, both DSGC and On SAC receive inputs from cone bipolar cell CBC5 subtypes, but only On SAC receives additional CBC7 inputs at proximal dendrites. In the Off layer, both DSGC and Off SAC receive inputs from CBC3 and CBC4, but Off SAC receives additional inputs from CBC1 and CBC2 at proximal dendrites. These findings will inspire future studies that unite anatomy with function for these new cellular players in order to generate a more comprehensive model of direction selectivity under diverse visual conditions.

1.6 Summary

An intuitive assumption of visual processing in the retina is that computations need to be robust so that visual features can be faithfully reported to the higher visual centers in the brain. This is in contrast to many cortical circuits that feature flexible

input-output relationships such as circuits involved in learning and memory (Holtmaat and Caroni 2016). However, robust computation does not necessarily imply a rigid circuit. Instead, the direction-selective circuit uses a highly dynamic set of mechanisms both at the circuit and dendritic levels. This flexibility is necessary because visual motion in the natural environment is complex, dynamic and often obscured by other visual features. A rigid set of mechanisms may quickly fail in the large parameter space of natural stimuli. By acute modulation and selective engagement of multi-layered mechanisms, retinal circuits are well-equipped to meet the challenges of feature extraction in the ever-changing natural environment, and reliably convey visual information to downstream visual areas.

Acknowledgements

We thank lab members Hector Acaron Ledesma, Xiaolin Huang and Jennifer Ding for helpful comments on the manuscript. This work was supported by NIH R01 EY024016 (WW). The authors declare no competing financial interests.

1.7 References

Baden T, Berens P, Franke K, Romn Rosn M, Bethge M, Euler T. The functional diversity of retinal ganglion cells in the mouse. Nature 529: 345350, 2016.

Barlow HB, Hill RM. Selective sensitivity to direction of movement in ganglion cells of the rabbit retina. Science 139: 4124, 1963.

Barlow HB, Hill RM, Levick WR. Retinal ganglion cells responding selectively to direction and speed of image motion in the rabbit. J Physiol 173: 377407, 1964.

Barlow HB, Levick WR. The mechanism of directionally selective units in rabbits retina. J Physiol 178: 477504, 1965.

Borst A. Models of motion detection. Nat Neurosci: 11681168, 2000.

Bos R, Gainer C, Feller MB. Role for Visual Experience in the Development of Direction-Selective Circuits. Curr Biol 26: 136775, 2016.

Brecha N, Johnson D, Peichl L, Wssle H. Cholinergic amacrine cells of the rabbit retina contain glutamate decarboxylase and gamma-aminobutyrate immunoreactivity. Proc Natl Acad Sci USA 85: 618791, 1988.

Briggman KL, Helmstaedter M, Denk W. Wiring specificity in the direction-selectivity circuit of the retina. Nature 471: 1838, 2011.

Brombas A, Kalita-de Croft S, Cooper-Williams EJ, Williams SR. Dendro-dendritic cholinergic excitation controls dendritic spike initiation in retinal ganglion cells. Nat Commun: 15683, 2017.

Cafaro J, Rieke F. Noise correlations improve response fidelity and stimulus encoding. Nature 468: 9647, 2010.

Chen M, Lee S, Park SJH, Looger LL, Zhou ZJ. Receptive field properties of bipolar cell axon terminals in direction-selective sublaminas of the mouse retina. J Neurophysiol 112: 195062,2014.

Chen Q, Pei Z, Koren D, Wei W. Stimulus-dependent recruitment of lateral inhibition underlies retinal direction selectivity. Elife, 2016.

Cruz-Martn A, El-Danaf RN, Osakada F, Sriram B, Dhande OS, Nguyen PL, Callaway EM, Ghosh A, Huberman AD. A dedicated circuit links direction-selective retinal ganglion cells to the primary visual cortex. Nature 507: 358361, 2014.

Dhande OS, Estevez ME, Quattrochi LE, El-Danaf RN, Nguyen PL, Berson DM, Huberman AD. Genetic dissection of retinal inputs to brainstem nuclei controlling image stabilization. J Neurosci 33: 17797813, 2013.

Ding H, Smith RG, Poleg-Polsky A, Diamond JS, Briggman KL. Species-specific wiring for 392 direction selectivity in the mammalian retina. Nature 535: 10510, 2016.

Euler T, Detwiler PB, Denk W. Directionally selective calcium signals in dendrites

of starburst amacrine cells. Nature 418: 84552, 2002.

Famiglietti E V. Synaptic organization of starburst amacrine cells in rabbit retina: analysis of serial thin sections by electron microscopy and graphic reconstruction. J Comp Neurol 309: 40397 70, 1991.

Ferster D. A sense of direction. Nature 392: 433434, 1998.

Fransen JW, Borghuis BG. Temporally Diverse Excitation Generates Direction-Selective Responses in ON- and OFF-Type Retinal Starburst Amacrine Cells. Cell Rep 18: 13561365, 2017.

Fried SI, Mnch T a, Werblin FS. Directional selectivity is formed at multiple levels by laterally offset inhibition in the rabbit retina. Neuron 46: 11727, 2005.

Fried SI, Mnch TA, Werblin FS. Mechanisms and circuitry underlying directional selectivity in the retina. Nature 420: 4114, 2002.

Gavrikov KE, Dmitriev A V., Keyser KT, Mangel SC. Cation–chloride cotransporters mediate neural computation in the retina. Proc Natl Acad Sci U S A 100: 1604752, 2003.

Gavrikov KE, Nilson JE, Dmitriev A V, Zucker CL, Mangel SC. Dendritic compartmentalization of chloride cotransporters underlies directional responses of starburst amacrine cells in retina. Proc Natl Acad Sci U S A 103: 187938, 2006.

Grzywacz NM, Amthor FR, Merwine DK. Necessity of acetylcholine for retinal directionally selective responses to drifting gratings in rabbit. J Physiol: 57581, 1998a.

Grzywacz NM, Merwine DK, Amthor FR. Complementary roles of two excitatory pathways in retinal directional selectivity. Vis Neurosci 15: 111927, 1998b.

Hausselt SE, Euler T, Detwiler PB, Denk W. A dendrite-autonomous mechanism for direction selectivity in retinal starburst amacrine cells. PLoS Biol 5: e185, 2007.

Helmstaedter M, Briggman KL, Turaga SC, Jain V, Seung HS, Denk W. Connectomic reconstruction of the inner plexiform layer in the mouse retina. Nature 500: 16874, 2013.

Hillier D, Fiscella M, Drinnenberg A, Trenholm S, Rompani SB, Raics Z, Katona G, Juettner J, Hierlemann A, Rozsa B, Roska B. Causal evidence for retina-dependent and independent visual motion computations in mouse cortex. Nat Neurosci 20: 960968, 2017.

Hoggarth A, McLaughlin AJJ, Ronellenfitch K, Trenholm S, Vasandani R, Sethuramanujam S, Schwab D, Briggman KLL, Awatramani GBB. Specific Wiring of Distinct Amacrine Cells in the Directionally Selective Retinal Circuit Permits Independent Coding of Direction and Size. Neuron 86: 276291, 2015.

Holtmaat A, Caroni P. Functional and structural underpinnings of neuronal assembly formation in learning. Nat Neurosci 19: 15531562, 2016.

Hubel DH, Weisel TN. Receptive fields of single neurones in the cats striate cortex. J Physiol 148: 57491, 1959.

Huberman AD, Wei W, Elstrott J, Stafford BK, Feller MB, Barres BA. Genetic identification of an On-Off direction-selective retinal ganglion cell subtype reveals a layer-specific subcortical map of posterior motion. Neuron 62: 32734, 2009.

Kay JN, De la Huerta I, Kim I-J, Zhang Y, Yamagata M, Chu MW, Meister M, Sanes JR. Retinal ganglion cells with distinct directional preferences differ in molecular identity, structure, and central projections. J Neurosci 31: 775362, 2011.

Kim I-J, Zhang Y, Yamagata M, Meister M, Sanes JR. Molecular identification of a retinal cell type that responds to upward motion. Nature 452: 47882, 2008.

Kim JS, Greene MJ, Zlateski A, Lee K, Richardson M, Turaga SC, Purcaro M, Balkam M, Robinson A, Behabadi BF, Campos M, Denk W, Seung HS. Space-time wiring specificity supports direction selectivity in the retina. Nature 509: 3316, 2014.

Kim T, Soto F, Kerschensteiner D. An excitatory amacrine cell detects object motion and provides feature-selective input to ganglion cells in the mouse retina. Elife 4, 2015.

Kittila CA, Massey SC. Effect of ON pathway blockade on directional selectivity in

the rabbit retina. [Online]. J Neurophysiol 73: 70312, 1995.

Kittila CA, Massey SC. Pharmacology of directionally selective ganglion cells in the rabbit retina. [Online]. J Neurophysiol 77: 67589, 1997.

Koren D, Grove JCR, Wei W. Cross-compartmental Modulation of Dendritic Signals for Retinal Direction Selectivity. Neuron 95: 914927.e4, 2017.

Kosaka T, Tauchi M, Dahl JL. Cholinergic neurons containing GABA-like and/or glutamic acid decarboxylase-like immunoreactivities in various brain regions of the rat.

Kostadinov D, Sanes JR. Protocadherin-dependent dendritic self-avoidance regulates neural connectivity and circuit function. Elife 4, 2015.

Lee S, Chen L, Chen M, Ye M, Seal RP, Zhou ZJ. An unconventional glutamatergic circuit in the retina formed by vGluT3 amacrine cells. Neuron 84: 70815, 2014.

Lee S, Kim K, Zhou ZJ. Role of ACh-GABA cotransmission in detecting image motion and motion direction. Neuron 68: 115972, 2010.

Lee S, Zhang Y, Chen M, Zhou ZJ. Segregated Glycine-Glutamate Co-transmission from vGluT3 Amacrine Cells to Contrast-Suppressed and Contrast-Enhanced Retinal Circuits. Neuron 90: 2734, 2016.

Lee S, Zhou ZJ. The synaptic mechanism of direction selectivity in distal processes of starburst amacrine cells. Neuron 51: 78799, 2006.

Lipin MY, Taylor WR, Smith RG. Inhibitory input to the direction-selective ganglion cell is saturated at low contrast. J Neurophysiol 114: 92741, 2015.

Marshel JH, Kaye AP, Nauhaus I, Callaway EM. Anterior-Posterior Direction Opponency in the Superficial Mouse Lateral Geniculate Nucleus. Neuron 76: 713720, 2012.

Masland RH. The tasks of amacrine cells. [Online]. Vis Neurosci 29: 39, 2012.

Mauss AS, Vlasits A, Borst A, Feller M. Visual Circuits for Direction Selectivity. Annu Rev Neurosci 40: 211230, 2017.

Miller RF, Bloomfield SA. Electroanatomy of a unique amacrine cell in the rabbit retina.

Morrie RD, Feller MB. An Asymmetric Increase in Inhibitory Synapse Number Underlies the Development of a Direction Selective Circuit in the Retina. J Neurosci 35: 92816, 2015.

Morrie RD, Feller MB. Development of synaptic connectivity in the retinal direction selective circuit. Curr Opin Neurobiol 40: 4552, 2016.

Morrie RD, Feller MB. A Dense Starburst Plexus Is Critical for Generating Direction Selectivity. Curr Biol 28: 12041212.e5, 2018.

OMalley DM, Masland RH. Co-release of acetylcholine and gamma-aminobutyric acid by a retinal neuron. [Online]. Proc Natl Acad Sci U S A 86: 34148, 1989.

Oesch N, Euler T, Taylor WR. Direction-selective dendritic action potentials in rabbit retina. Neuron 47: 73950, 2005.

Oesch NW, Taylor WR. Tetrodotoxin-resistant sodium channels contribute to directional responses in starburst amacrine cells. PLoS One 5: e12447, 2010.

Oyster CW, Barlow HB, Takahashi E. Direction-selective units in rabbit retina: distribution of preferred directions. Science 155: 8412, 1967.

Ozaita A, Petit-Jacques J, Vlgyi B, Ho CS, Joho RH, Bloomfield SA, Rudy B. A unique role for Kv3 voltage-gated potassium channels in starburst amacrine cell signaling in mouse retina. J Neurosci 24: 733543, 2004.

Park SJH, Borghuis BG, Rahmani P, Zeng Q, Kim I-J, Demb JB. Function and Circuitry of VIP+ Interneurons in the Mouse Retina. J Neurosci 35: 10685700, 2015.

Park SJH, Kim I-J, Looger LL, Demb JB, Borghuis BG. Excitatory synaptic inputs to mouse on-off direction-selective retinal ganglion cells lack direction tuning. J Neurosci 34: 397681,2014.

Pei Z, Chen Q, Koren D, Giammarinaro B, Acaron Ledesma H, Wei W. Conditional Knock-Out of Vesicular GABA Transporter Gene from Starburst Amacrine Cells Re-

veals the 507 Contributions of Multiple Synaptic Mechanisms Underlying Direction Selectivity in the Retina. J Neurosci 35: 1321932, 2015.

Percival KA, Venkataramani S, Smith RG, Rowland Taylor W. Directional Excitatory Input to Direction-Selective Ganglion Cells in the Rabbit Retina. J. Comp. Neurol.

Piscopo DM, El-Danaf RN, Huberman AD, Niell CM. Diverse Visual Features Encoded in Mouse Lateral Geniculate Nucleus. J Neurosci 33: 46424656, 2013.

Poggio T, Reichardt W. Considerations on models of movement detection. [Online]. Kybernetik 13: 2237, 1973.

Poleg-Polsky A, Diamond JS. Imperfect space clamp permits electrotonic interactions between inhibitory and excitatory synaptic conductances, distorting voltage clamp recordings. PLoS One 6: e19463, 2011.

Poleg-Polsky A, Diamond JS. NMDA Receptors Multiplicatively Scale Visual Signals and Enhance Directional Motion Discrimination in Retinal Ganglion Cells. Neuron 89: 127790, 2016a.

Poleg-Polsky A, Diamond JS. Retinal Circuitry Balances Contrast Tuning of Excitation and Inhibition to Enable Reliable Computation of Direction Selectivity. J Neurosci 36: 586176, 2016b.

Poleg-Polsky A, Ding H, Diamond JS. Functional Compartmentalization within Starburst Amacrine Cell Dendrites in the Retina. Cell Rep 22: 28982908, 2018.

Rivlin-Etzion M, Wei W, Feller MBB. Visual Stimulation Reverses the Directional Preference of Direction-Selective Retinal Ganglion Cells. Neuron 76: 518525, 2012.

Rivlin-Etzion M, Zhou K, Wei W, Elstrott J, Nguyen PL, Barres BA, Huberman AD, Feller MB. Transgenic mice reveal unexpected diversity of on-off direction-selective retinal ganglion cell subtypes and brain structures involved in motion processing. J Neurosci 31: 87609, 2011.

Rosa JM, Morrie RD, Baertsch HC, Feller MB. Contributions of Rod and Cone

Pathways to Retinal Direction Selectivity Through Development. J Neurosci 36: 96839695, 2016.

Sabbah S, Gemmer JA, Bhatia-Lin A, Manoff G, Castro G, Siegel JK, Jeffery N, Berson DM. A retinal code for motion along the gravitational and body axes. Nature 546: 492497, 2017.

Sanes JR, Masland RH. The Types of Retinal Ganglion Cells: Current Status and Implications for Neuronal Classification. Annu Rev Neurosci 38: 221246, 2015.

Schachter MJ, Oesch N, Smith RG, Taylor WR. Dendritic spikes amplify the synaptic signal to enhance detection of motion in a simulation of the direction-selective ganglion cell. PLoS Comput Biol 6, 2010.

Sethuramanujam S, McLaughlin AJ, deRosenroll G, Hoggarth A, Schwab DJ, Awatramani GB. A Central Role for Mixed Acetylcholine/GABA Transmission in Direction Coding in the Retina. Neuron 90: 124356, 2016.

Sethuramanujam S, Yao X, deRosenroll G, Briggman KL, Field GD, Awatramani GB. Silent NMDA Synapses Enhance Motion Sensitivity in a Mature Retinal Circuit. Neuron 96: 546 10991111.e3, 2017.

Shi X, Barchini J, Ledesma HA, Koren D, Jin Y, Liu X, Wei W, Cang J. Retinal origin of direction selectivity in the superior colliculus. Nat Neurosci 20: 550558, 2017.

Sivyer B, Williams SR. Direction selectivity is computed by active dendritic integration in retinal ganglion cells. Nat Neurosci 16: 184856, 2013.

Stincic T, Smith RG, Taylor WR. Time course of EPSCs in ON-type starburst amacrine cells is independent of dendritic location. J Physiol 594: 568594, 2016.

Sun L, Han X, He S. Direction-Selective Circuitry in Rat Retina Develops Independently of GABAergic, Cholinergic and Action Potential Activity. PLoS One 6: e19477, 2011.

Taylor WR, Vaney DI. Diverse synaptic mechanisms generate direction selectivity in

the rabbit retina.

Trenholm S, Johnson K, Li X, Smith RG, Awatramani GB. Parallel mechanisms encode direction in the retina. Neuron 71: 68394, 2011.

Tukker JJ, Taylor WR, Smith RG. Direction selectivity in a model of the starburst amacrine cell. Vis Neurosci 21: 61125, 2004.

Vaney DI, Sivyer B, Taylor WR. Direction selectivity in the retina: symmetry and asymmetry in structure and function. Nat Rev Neurosci 13: 194208, 2012.

Vaney DI, Young HM. GABA-like immunoreactivity in cholinergic amacrine cells of the rabbit retina.

Velte TJ, Miller RF. Spiking and nonspiking models of starburst amacrine cells in the rabbit retina.

Vlasits AL, Morrie RD, Tran-Van-Minh A, Bleckert A, Gainer CF, DiGregorio DA, Feller MB. A Role for Synaptic Input Distribution in a Dendritic Computation of Motion Direction in the Retina. Neuron 89: 13171330, 2016.

Vlasits ALL, Bos R, Morrie RDD, Fortuny C, Flannery JGG, Feller MBB, Rivlin-Etzion M. Visual stimulation switches the polarity of excitatory input to starburst amacrine cells. Neuron 83: 117284, 2014.

Watanabe D, Inokawa H, Hashimoto K, Suzuki N, Kano M, Shigemoto R, Hirano T, Toyama K, Kaneko S, Yokoi M, Moriyoshi K, Suzuki M, Kobayashi K, Nagatsu T, Kreitman RJ, Pastan I, Nakanishi S. Ablation of cerebellar Golgi cells disrupts synaptic integration involving GABA inhibition and NMDA receptor activation in motor coordination.

Wei W, Hamby AM, Zhou K, Feller MB. Development of asymmetric inhibition underlying direction selectivity in the retina. Nature 469: 4026, 2011.

Yonehara K, Balint K, Noda M, Nagel G, Bamberg E, Roska B. Spatially asymmetric reorganization of inhibition establishes a motion-sensitive circuit. Nature 469: 40710, 2011.

Yonehara K, Farrow K, Ghanem A, Hillier D, Balint K, Teixeira M, Jttner J, Noda M, Neve RLL, Conzelmann K-K, Roska B. The first stage of cardinal direction selectivity is localized to the dendrites of retinal ganglion cells. Neuron 79: 107885, 2013.

Yonehara K, Shintani T, Suzuki R, Sakuta H, Takeuchi Y, Nakamura-Yonehara K, Noda M. Expression of SPIG1 reveals development of a retinal ganglion cell subtype projecting to the medial terminal nucleus in the mouse. PLoS One 3: e1533, 2008.

2

Using multi-photon imaging for targeted electrophysiological recording and live cell imaging of fluorescently labeled neurons from isolated retinas

This Chapter is a full reprint of Chen et al., Springer Nature Neuromethods Book Series, in which I was the primary author.The work is included with permission from all authors.

Relevant Publication

Qiang Chen, Wei Wei. (to appear in Springer Nature) "Using multi-Photon imaging for targeted electrophysiological recording and live cell imaging of fluorescently labeled neurons from isolated retinas". **Multiphoton Microscopy**.

2.1 Abstract

A central goal of neuroscience is to understand how neural computations are implemented by neural circuits. An excellent model system is the mammalian retina. Besides its important role in visual processing, the retina offers technical advantages for

circuit interrogation at the cellular and synaptic levels due to its experimental accessibility and well-defined cell types. Recent development of genetic and molecular tools in mice has made the mouse retina a preferred choice for studying retinal circuitry, since an increasing repertoire of cell types can be specifically labeled by fluorescent proteins. However, measuring the light response of fluorescently-tagged retinal neurons is challenging because excitation of fluorophores at visible wavelengths often leads to rapid photopigment bleaching that prevents subsequent recording of light responses from retinal neurons. One way to circumvent this problem is to use multiphoton excitation in the infrared range to visualize fluorescent-protein-expressing cells. In this chapter, we describe a detailed protocol for multiphoton targeted electrophysiological recording from fluorescently-labeled retinal neurons while preserving their sensitivity to visual stimulation. This technique also enables live imaging of the three-dimensional morphology of the recorded neurons. With the continued development of cell-specific markers in the mouse retina, this method is expected to be widely used for harnessing the power of genetic and molecular tools in retinal circuit analysis.

Keywords: Multiphoton Microscopy, Retina; Light Response, Fluorescence Proteins, Patch Clamp Recording.

2.2 Introduction

The retina, the neural tissue of the eye, belongs to the central nervous system. Visual processing in the retina is implemented by five major classes of retinal neurons that are organized into three cellular layers interconnected by two synaptic layers (Sanes and Masland, 2015) (Figure. 2.1). In the vertical pathway, visual inputs are relayed and transformed by photoreceptor-bipolar cell-ganglion cell connections. Importantly, this forward signaling is profoundly modified by lateral connections made

by horizontal and amacrine cells. The complexity of retinal circuitry is reflected in its diverse cell types (over 100 distinct types according to the current estimate (Demb and Singer, 2015; Sanes and Masland, 2015). Through precise wiring between specific neuronal types, visual inputs are processed in parallel by > 30 retinal circuits (Baden et al., 2016). Each circuit extracts a specific visual feature, which is represented as the spiking output of a retinal ganglion cell type (Gollisch and Meister, 2010). Together, the axons of > 30 types of retinal ganglion cells exit the retina at the optic disc and convey processed visual information to multiple brain targets such as thalamus, superior colliculus, accessory optic system and suprachiasmatic nucleus (Dhande et al., 2015). One well-known example of feature extraction in the retina is implemented by the direction-selective circuit (reviewed in (Vaney et al., 2012; Wei et al., 2011b)), which we use as an example to illustrate the method described in this chapter. The output neurons of the circuit, the direction-selective ganglion cells, fire action potentials maximally to motion in their preferred direction, but minimally to motion in the opposite, null direction. The direction-selective ganglion cells consist of multiple types that project their axons to distinct visual nuclei. The On direction selective ganglion cells innervate the accessory optic system and mediate the optokinetic reflex (Barlow et al., 1964; Barlow and Levick, 1965; Simpson, 1984), while the On-Off type mainly innervates the superior colliculus and the dorsal lateral geniculate nucleus, and is involved in motion processing in these nuclei and the primary visual cortex (Cruz-Martn et al., 2014; Hillier et al., 2017; Huberman et al., 2009; Shi et al., 2017). The diverse set of retinal circuits that perform parallel visual processing makes the retina an intriguing place to study synaptic, cellular and network level mechanisms of feature detection. Understanding retinal computations will have broad implications for the general principles of information processing by the brain. Technically, the retina is a highly accessible system for experimental manipulations and recording. Since the retina receives minimal feedback inputs from the rest of

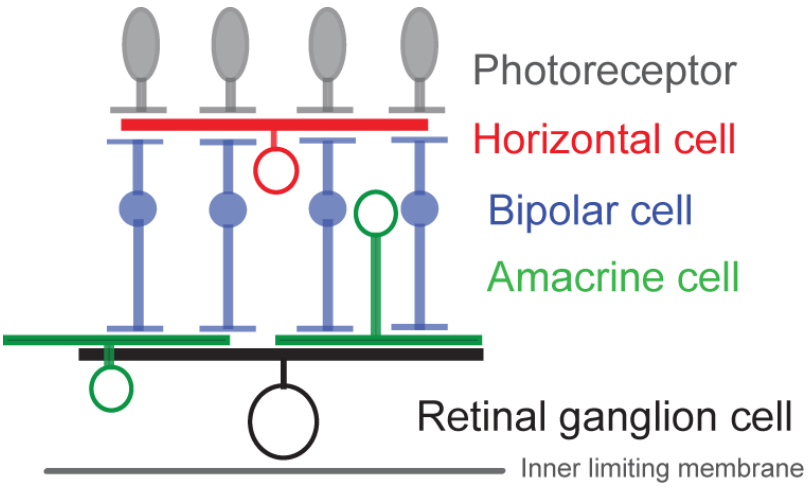

FIGURE 2.1: Schematic side view of the major cell types in the mammalian retina.

the brain (Zucker and Dowling, 1987), the neural circuitry in the isolated retina is largely intact. When protected from visible light, acutely isolated retina survives and remains light responsive for a sufficiently long period to enable electrophysiological experiments on visually evoked neuronal responses. For this purpose, retinal neurons are traditionally visualized using infrared optics and distinguished by morphological characteristics of their somas such as size, shape and retinal location (van Wyk et al., 2009). While a few cell types can be efficiently targeted by this approach, it poses a significant challenge for targeting the rest of the retinal cell types for circuit analysis. Recent progress in genetically engineered mouse lines and viral vectors offers an unparalleled opportunity to record from specific and sparse subpopulation of retinal neurons (Sanes and Masland, 2015). Selective labeling of one or several types of retinal neurons can be achieved by expressing a fluorescent protein directly under a cell type-specific promoter, or by using a binary system with the driver and reporter genes such as the Cre-loxP system (Zeng and Madisen, 2012). Genetic targeting leads to greatly improved efficiency of finding cells of interest. Importantly, stable expression of genetic markers offers the unique advantage of studying the early development of visual circuits even before the retina becomes light responsive (Wei

et al., 2011a; Yonehara et al., 2011).

While cell type-specific labeling greatly simplifies the initial targeting step, recording light-evoked responses from fluorescently-labeled retinal neurons is subject to the observer effect in which the process of observation affects the observed results. In this case, the visible light source used to excite fluorophores also potently stimulates the photoreceptors in the retina, and therefore contaminates the neurons response to the visual stimulus of interest. Even more problematic is that the visible light used to excite the fluorophores often bleaches the photoreceptors rapidly and prevents subsequent experiments using visual stimulation. For cells with bright fluorescence, this caveat can be alleviated by minimizing the intensity and duration of the excitation light exposure to the retina. However, this approach is not applicable to cells with low level of fluorescence.

Two-photon microscopy, thus, becomes a preferred choice for targeting retinal neurons labeled with green fluorescent protein (GFP) or other two-photon excitable fluorophores, because the infrared wavelengths used in two-photon excitation cause much weaker single-photon absorption for mammalian retinal photopigments. It is notable that the infrared laser used during two-photon imaging still causes activation of the photoreceptors, primarily due to two-photon excitation of the photopigments (Euler et al., 2009). However, for most practical purpose two-photon excitation of photoreceptors at typical laser intensity ($\sim$5 mw) does not cause a significant bleaching effect and therefore does not pose serious problems for subsequent recording experiments due to the following two factors. First, the imaging process for identifying a fluorescently labeled neuron is usually short in duration (e.g. $\sim$1-5 mins) . Second, the cells most suitable for electrophysiological recording are located in the retinal ganglion cell layer near the surface of the whole mount retina preparation. Due to the good optical sectioning of two-photon microscopy, two-photon excitation is spatially restricted to the illumination focal point at the ganglion cell layer, which is $\sim$200 μm above the

outer segments of the photoreceptors where the photopigments are located. Therefore, the activation and photobleaching of the photoreceptors is further minimized. In addition, the other general advantages of two-photon microscopy also apply to the isolated retina preparation, including good depth penetration and three-dimensional resolution, and minimized photodamage to the living tissue (Svoboda and Yasuda, 2006). Together, two-photon targeting of fluorescently labeled retinal neurons allows for the acquisition of both electrophysiological recordings of a cells light response and detailed live morphology of the cells dendritic arbors.

In this chapter, we describe the equipment and procedure to perform two-photon targeted recording and imaging of fluorescent-protein-expressing retinal neurons in whole-mount mouse retinas. The retina is first isolated under infrared illumination, and then transferred to a two-photon microscope for fluorescence imaging. The identified cells of interest are then subject to patch-clamp recording aided by infrared optics and an IR-sensitive camera while visual stimuli are presented to the retina through the microscope condenser. Inclusion of a dye in the internal solution during patch-clamp recording allows for subsequent live imaging of the recorded cell in three dimensions.

2.3 Materials

2.3.1 Reagents

- Transgenic mice expressing two-photon excitable fluorophores in retinal neurons (All procedures need to be performed in accordance with ethical and safety guidance of relevant institutions and authorities). When retinal orientation is important, for example, during investigation of direction-selective or orientation-selective circuits, or when the fluorescence labeling pattern is non-uniform across the retina, a transgenic mice line from a pigmented background

such as C57/BL6 is recommended, because they have more distinguishable landmarks on the choroid than albino strains.

- Ames medium (pH 7.36; Sigma, Cat. No. A1420-10X1L)
- Intracellular solution for patch-clamp recording, prepared according to requirements of experiments being performed (e.g. Cesium-based internal solution containing: 110 mM CsMeSO4, 2.8 mM NaCl, 4 mM EGTA, 5 mM TEA-Cl, 4 mM adenosine 5-triphosphate (magnesium salt), 0.3 mM guanosine 5-triphosphate (trisodium salt), 20 mM HEPES, 10 mM phosphocreatine (disodium salt), 5 mM N-Ethyllidocaine chloride (QX314), pH 7.25). Fluorescent dyes like Alexa Fluor 594 or 488 hydrazide (ThermoFisher Scienfitic) can be added to the internal solution to fill the recorded cells for subsequent two-photon imaging
- Isoflurane (e.g. Phoenix Pharmaceuticals, Cat. No. NDC 57319-507-05) for anaethesia

2.3.2 Equipment

Retina dissection

- Black mixed cellulose esters membrane filter paper (0.45 μm; Millipore, Cat.No. HABG01300) for mounting the isolated retina
- White filter paper (e.g. Whatman 1001090) for holding the eyeballs in step 3 of section 3.1
- Surgical razor blade (e.g. Feather Safety Razor Co., Cat. No. GRF-2976 #11)
- Pyrex petri dish (100 mm x15 mm; e.g. Fisher Scientific, Cat. No. 08-747C)

- Dissection tools (fine dissection scissors and forceps) (e.g. Roboz Surgical Instrument Inc.)
- Dissection microscope (e.g. Olympus SZ61)
- Infrared light source for the dissection microscope (e.g. CMVision IR30 illuminator)
- Red LED headlamp for ambient room illumination and during dissection (e.g. Energizer, model No. HD33AIEN)
- Two IR-sensitive CCD cameras (e.g. Watec, model no. WAT-902H) for visualization under infrared optics during retina dissection and patch-clamp recording respectively
- Two Video monitors (e.g. Sanyo, model no. DP1B41B) for visualization under infrared optics during retina dissection and patch-clamp recording respectively

Visual Stimulus

- White organic light-emitting display (OLED; Emagin Corporation, model no. 100100-01 with glass faceplate) for presenting visual stimuli
- The Design Reference Kit (Emagin Corporation) for connecting the OLED to a VGA port of a PC for visual stimuli
- Custom-made OLED holder for use with Thorlabs 30mm cage systems.
- Cage plate (Thorlabs, Cat. No. CP02)
- XY translating lens mount (Thorlabs, Cat. No. HPT1)
- Right-Angle Kinematic Mount for Elliptical Mirrors (Thorlabs, KCB2EC)

- Protected Silver-Coated Elliptical Mirrors (Thorlabs PFE20-P01)
- Cage assembly rods 8 (Thorlabs, Cat. No. ER8)
- Manual rotation base (Thorlabs, QRP02)
- Dual-port high performance video card for the OLED (Nvidia GeForce, 9500 GT 512 MB)
- Monitor for visual stimuli (e.g. Dell 1704FPT). Visual stimuli monitor for user observation and OLED for stimulus display are connected to a PC with dual-port video card and displayed in parallel or duplicate mode at a resolution of 800x600 pixels, refresh rate of 60 Hz. This allows the user to conveniently see the pattern of the visual stimulus shown on the OLED during experiments.

Electrophysiology

- Amplifier (Molecular Devices, model no. Multiclamp 700B)
- Analog-to-digital converter (Molecular Devices, Digidata 1440A)
- Micromanipulator (Sutter Instruments, MPC-200)
- Head-stage (Molecular Devices, 1-CV-7B)
- Borosilicate glass capillaries (1.5-mm outer and 1.10-mm inner diameters, 7.5-cm length; Sutter Instruments, Cat. No. BF150-110-7.5)
- Glass microelectrode puller (Narishinge PC-100)
- Custom made grounding wires for the head-stages

Two-Photon microscopy

- Two-photon microscope with dual channel external Multi-Alkali detectors and a translatable stage (We have verified this protocol with multiphoton systems from Bruker and Scientifica.)
- Femtosecond, wavelength Tunable IR Laser Sources (e.g. Coherent Chameleon Ultra II or Spectra-Physics Mai Tai)
- Water-immersion objectives (Olympus LUMPlan Fl/IR 60x/0.90NA Water Objective)
- 5x objectives for bright-field observation (Olympus MPlan N 5x/0.10NA Microscope Objective)
- Dichroic filter (D1)
- Dichroic filter (D2)
- Band-pass filter (BP1)
- Band-pass filter (BP2)
- (optional) Notch filter, placed in front of OLED for simultaneous visual stimulation with functional calcium imaging.

Other equipment

- Recording chamber (e.g. Warner Instruments, RC-26GLP)
- Perfusion pump (e.g. Watson Marlow 120S, Cat No. 14-284-202)
- In-line solution heater (Warner, model No. 64-0102) for warming solutions flowing into recording chamber. Check the temperature of bath with thermistor regularly to make sure bath temperature is stable

- Computers for two-photon imaging, electrophysiological recordings and visual stimulation
- Stand-alone breakout board for a parallel port cable (Winford Engineering, BRK25F-R-FT)
- MATLAB software with Psychophysics Toolbox installed (Mathworks Inc.)

2.4 Experimental Setup

Schematics of overall equipment layout are shown in Figure. 2.2

- Visual stimulation: the OLED is secured by a custom made plastic holder that fits into Thorlabs 30 mm cage system that can be swung in under the condenser for visual stimulation or out to allow infrared light illumination of the tissue for patch clamp recording (Figure. 2.2f). Images from the OLED are reflected by a silver mirror below the condenser mounted on the 30mm cage system, and projected and focused onto the photoreceptors through the condenser lens. In our setup, the area of retina stimulated by the OLED is 330 m in diameter. The size of stimulated area can be adjusted by adjusting the light path distance between OLED and condenser. Custom visual stimuli are generated using MATLAB and Psychophysics Toolbox (http://psychtoolbox.org) (Brainard 1997). There are alternative designs in which visual stimulation is delivered through the objective (Euler et al., 2009; Wei et al., 2010). In the current protocol, visual stimulation is delivered through the condenser since this configuration requires no custom modification for most commercial upright microscopes. The only requirement is that the distance between the bottom of the condenser and the transmitted light source is sufficiently large to accommodate the Thorlabs 30

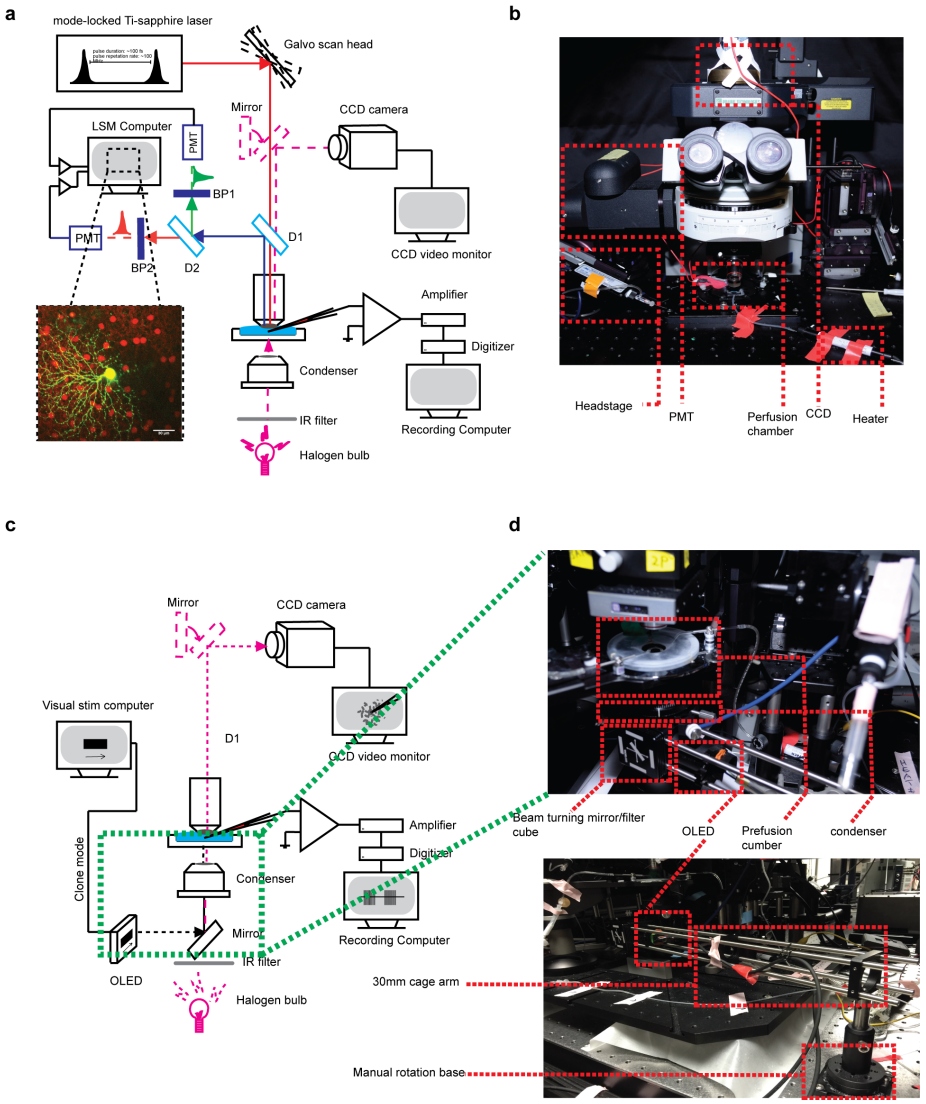

FIGURE 2.2: Schematics view of the setup for targeted electrophysiological recording of light responses from retinal neurons expressing fluorescent proteins.
(a). Schematic diagram of the two-photon microscope configured for targeted recording. Once a fluorescently labeled neuron is identified, the cell is targeted for recording aided by transmitted infrared (IR) illumination (cyan) and an IR-sensitive CCD camera. D1: dichroic filter (695 nm split); D2: dichroic filter (585 nm split); BP1: band pass filter (500-550 nm); BP2: band pass filter (600-660 nm).
(b). Example layout based on a Bruker Ultima two-photon system.
(c). Schematic diagram of the two-photon microscope configured for visual stimulation. Once a successful recording has been established, visual stimuli from the OLED are delivered to the retina through the condenser.
(d). Example layout of a visual stimulation module built around the Thorlabs 30 mm cage system.

mm cage system. If this distance in an existing microscope is not large enough (e.g. ~10 cm), the Thorlabs 16 mm cage system can be used, or the microscope stage can be raised.

- Synchronize visual stimuli with electrophysiological recording: The onset of the visual stimulus is accompanied by a Transistor-transistor logic (TTL) pulse. Details on generating TTL pulse triggers can be found at the MATLAB Psychophysics Toolbox website (`https://github.com/Psychtoolbox-3/Psychtoolbox-3/wiki/FAQ:-TTL-Triggers-in-Windows`). In short, a TTL pulse is generated by Psychophysics Toolbox in Matlab, then sent to the patch clamp devices through a parallel cable connected to the visual stimulation computer and a breakout card to trigger electrophysiological recording (Figure. 2.3).

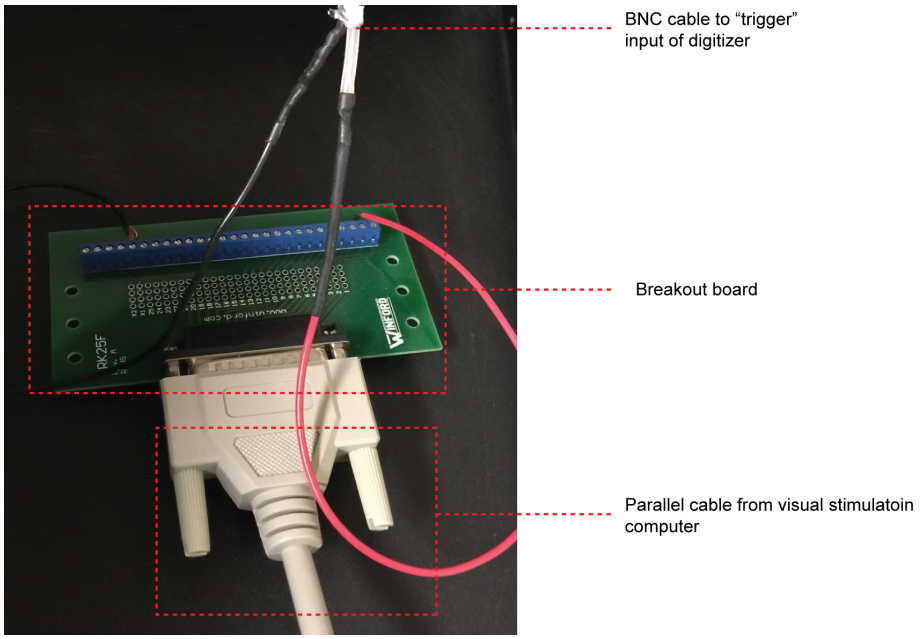

FIGURE 2.3: Example connection of a breakout board for TTL triggering.

- Alignment of OLED to the image forming center of the objective: First, the images on the OLED needs to be centered to the field of view through the objective. To do this, a whole-mount retina sample is placed into the recording

chamber perfused with oxygenated Ames solution. Then, focus the objective on the outer segment of the photoreceptors. Next, move the microscope stage in the X-Y plane so that the retina preparation is outside the field of view and an area containing clear unobstructed coverslip bottom of the imaging chamber is under the objective. Swing in the visual stimulus arm below the condenser and project a centered circular crosshair pattern on the OLED. Without moving the objective in the Z axis, adjust the condenser focus knob below the microscope stage until the crosshair patterns is focused under the objective. Next, without adjusting the condenser focusing screw, move the adjusting screws of the silver mirror mount in the visual stimulation arm so that the center of crosshair pattern in the OLED coincides with the cross-hair center of the eyepiece (imaging forming center of the objective). It is recommended that the alignment and focus of the visual stimulation is checked daily before experiments.

- Create a reference point to align the field of view under laser scanning with that under transmitted light illumination: Fill a glass electrode with a two-photon excitable dye such as Alexa Fluor 488 or Alexa Fluor 594. Focus the tip of the dye under the 60x objective. First, image the dye-filled pipette tip with the two-photon microscope, and position the tip in the center of the imaging window. Mark the center position on the monitor of the imaging computer with a piece of tape. Gentle positive pressure should be applied to the pipette so that the tip is clearly visible during imaging due to the constant flow of the dye out of the pipette. Next, stop laser scanning, and without moving the pipette position, visualize the pipette tip on the TV monitor using the IR-sensitive CCD camera under transmitted light illumination. Mark the position of the tip on the TV screen with another piece of tape. Now, a reference point has been created to represent the image forming center of the objective in both

the CCD video monitor and two-photon imaging monitor. It is important to maintain the two-photon imaging window in a fixed position on the imaging computer monitor. It is also necessary to image the fluorescently labeled neuron before and after recording and dye filling to verify the correct targeting.

2.5 Methods

2.5.1 Preparation of acutely isolated retina samples

1. Cut black membrane filter papers into pieces that fit into the recording chamber. Cut a hole (1mm x 2mm) at the center of the filter paper with a sharp razor blade. When the orientation of the retina is important, mark the filter paper with the razor blade so that the dorsal, ventral, nasal and temporal directions can be recognized.

2. Adapt mice in darkness for at least 1 hour before euthanization. Anaesthetize with isoflurane and then decapitate the mice. Enucleate the eyeballs rapidly under dim red-light illumination (All animal handling and euthanization procedures need to be performed accordingly to the ethical guidelines of the relevant institution and authorities).

3. Under infrared illumination, place the eyeball on a piece of white filter paper. Note the left and right eyeballs. Make an incision through the cornea with a sharp surgical blade or a 15 gauge needle.

4. Transfer the eyeball to a glass Petri dish filled with oxygenated (95% O_2 5% CO_2) Ames' medium . Remove the cornea, the lens and the vitreous from the eye under a dissection microscope under infrared illumination. Vitreous body needs to be removed completely for patch clamp recording.

5. Identify the dorsal/ventral side of retina according to the landmarks in the choroid (Figure. 2.4). Mark the dorsal/ventral axis by making small cuts at the periphery of the retina.

6. Carefully peel the pigmented epithelial layer, choroid and sclera from the retina using a pair of fine forceps. Cut the isolated retina into dorsal and ventral halves along the nasal-temporal axis.

7. Under dim red light, mount the isolated retina pieces onto filter paper prepared in step 1 with ganglion cell layer facing up. Make sure that the retina fully covers the hole in the middle of the filter paper. Note down the orientation of retina on the filter paper.

8. Keep the mounted retina in the continuously bubbled (95% O_2 5% CO_2) incubation chamber with Ames' medium in darkness at room temperature before transferring to the microscopes bath chamber for recording and imaging. To maintain the health of the tissue, transfer the retina to a new petri dish with freshly oxygenated Ames medium every 10 min during step 4-7.

2.5.2 Two-photon targeted recording of fluorescently labeled neurons

9. Place a retina sample with ganglion cell layer facing up into the microscope chamber continuously perfused with oxygenated Ames' medium at physiological temperature ($34 - 36\,^{\circ}\mathrm{C}$).

10. Check the condenser position so that the images from the OLED are focused on the outer segments of the photoreceptors in the filter paper hole. (See Experimental Setup)

11. Focus the 60x objective at the ganglion cell layer within the filter-paper hole with infrared optics and the CCD camera.

12. Switch the microscope to the laser scanning/imaging mode (Figure. 2.2a). Depending on the fluorescent probe expressed in the cells of interest, tune the wavelength of the infrared laser accordingly. Adjust the x-y position of the retina so that the labelled cell is positioned at the reference point (See Equipment Setup).

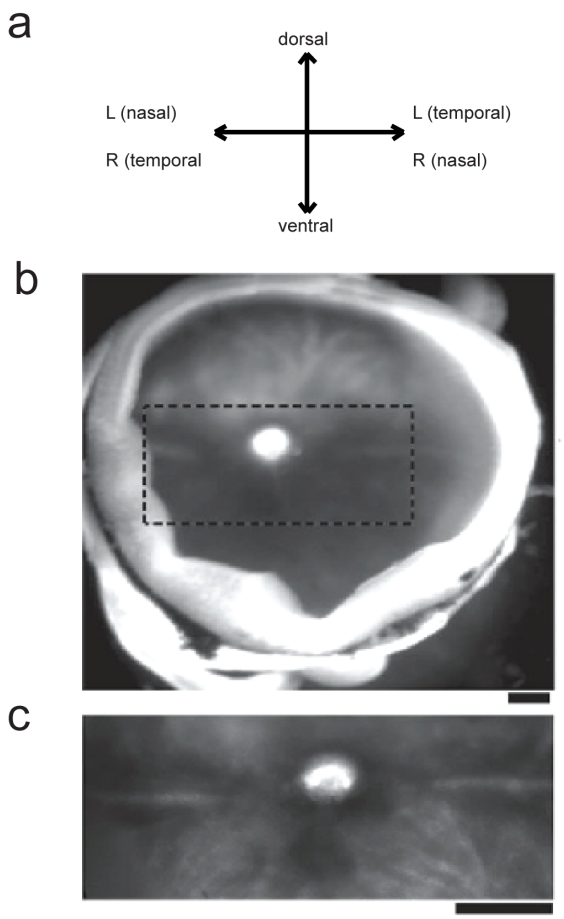

FIGURE 2.4**:** The landmarks in the choroid for marking the orientation of the retina.
Under a dissection microscope, a retina with the pigment epithelium attached is positioned with the ganglion cell layer facing up and dorsal side facing upward
(a, b). The nasal/temporal axis is aligned with a horizontal stripe running beneath the optic nerve, with a dark-appearing patch in the ventral side
(c). The nasal/temporal side is opposite for left and right eyes. Scale bars: 250μm (b, c).

13. Switch back to transmitted infrared illumination (Figure.2.2c) and use the CCD camera to visualize the targeted cell body at the reference point on the TV screen. Use a glass patch electrode to carefully remove the inner limiting membrane around the cell body, exposing the targeted cell while minimizing damages damage to the surrounding tissue.

14. Perform patch clamp recording from the target cell using a new glass pipette filled with appropriate internal solution and an intracellular dye.

2.5.3 Recording light responses from the targeted neuron

15. After the recording is established, turn off all transmitted light sources and swing in the OLED stimulus arm under the condenser. Allow the retina to adapt (e.g. ∼10s) to the background light intensity of the OLED before presenting visual stimuli.

16. Present visual stimuli to the retina and record the cell's light response.

17. At the end of the recording, acquire a Z stack of the dye-filled neuron using the two-photon microscope.

2.5.4 Representative results

We have used this protocol to obtain light responses and morphology of fluorescently labeled retinal neurons such as direction selective ganglion cells and starburst amacrine cells. The acute retina preparation remains healthy and light responsive for at least 8 hours when incubated in oxygenated Ames medium at room temperature. We have successfully targeted GFP-expressing neurons from a transgenic mouse line Drd4-GFP with low levels of GFP expression (Figure. 2.5) (Chen et al., 2016; Pei et al., 2015). Such low fluorescence levels are barely detectable with a standard CCD camera under full-field UV-illumination from xenon arc lamps. This method can be used in combination with pharmacology to address outstanding questions in retinal circuitry. It is important to note that the onset of the laser scanning at typical intensity (∼5mw) still activate the photoreceptors [20]. Despite using infrared wavelengths and the local nature of multiphoton excitation that heavily alleviate the photo-bleaching effects, it is good practice to use minimal laser power and laser exposure time when locating fluorescent-protein-expressing neurons.

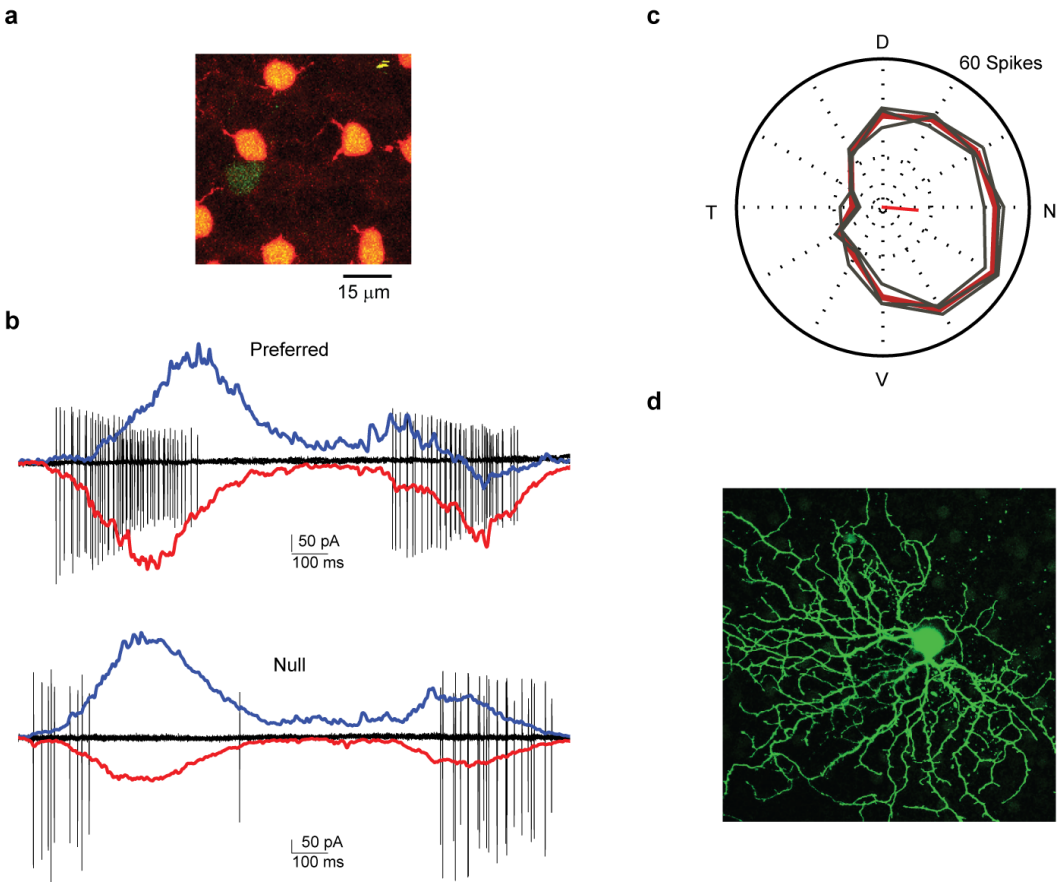

FIGURE 2.5: Example of two-photon imaging and targeted recording from a GFP-expressing On-Off direction selective ganglion cell.
(a). An image of a retina from a transgenic mouse line that labels a subtype of On-Off direction-selective ganglion cells with low level of GFP (green) and starburst amacrine cells with td-Tomato (red).
(b). Spiking (black), inward excitatory (red) and outward inhibitory (blue) postsynaptic currents of an On-Off direction selective ganglion cell evoked by a bar moving in the preferred and null directions. Spiking response is measured by loose-attached recording before breaking. Excitatory and inhibitory currents are measured by holding the cell at -60mv and 0mv respectively in the whole-cell configuration. On and off responses are evoked by the leading and trailing edges of the bright bar, respectively.
(c). Polar plot of the total spike count (3 repetitions, same cell as b.) as a function of bar direction. Black lines indicate individual repetitions and the red line indicates the mean response. The vector sum of spike counts is shown as the red line in the middle. D: dorsal, N: nasal; V: ventral; T: temporal.
(d). Top view (maximum intensity projection) of the dendritic arbors of the Alexa Fluor 488-filled direction-selective ganglion cell (recorded in b, c.).

2.6 Trouble shooting and further directions

To obtain high-quality electrophysiological recordings of visually evoked responses from retinal neurons, the multiphoton rig should be equipped with a Faraday cage to reduce electromagnetic interference. The power supply unit of the OLED is a major source of noise and should be positioned outside the Faraday cage. To obtain high-quality images of the labeled neurons, the visual stimulation module should be light-proofed by lens tubes or light-blocking fabric to minimize the level of background light during multiphoton imaging. Several factors contribute to the health and visual stimulation responsiveness of the isolated retina samples. The rate of circulation of oxygenated Ames medium is recommended to be greater than 10 ml/min. The bath temperature needs to be above 32 C to obtain good visual response. Before recording, the retina samples should be examined by the infrared optics and the CCD camera to ensure that the vitreous body is completely removed from the retina. Incomplete removal of the vitreous body can prevent successful electrophysiological recordings from healthy retinal neurons. In the present protocol, multiphoton imaging of the fluorescent proteins is performed first, followed by simultaneous electrophysiological recording and visual stimulation. Therefore, the white light from the OLED needs to be blocked from the retina before the start of multiphoton imaging. However, this setup can be easily modified for simultaneous multiphoton imaging and visual stimulation without major modification of the microscope hardware (Figure 2.6). A notch filter can be placed in front of the OLED screen so that the wavelengths permitted for detecting fluorescence at the PMTs are well separated from those of the visual stimuli. We have used this approach to record light-evoked calcium transients from retinal neurons expressing the genetically encoded calcium sensor GCaMP6 (Chen et al., 2016).

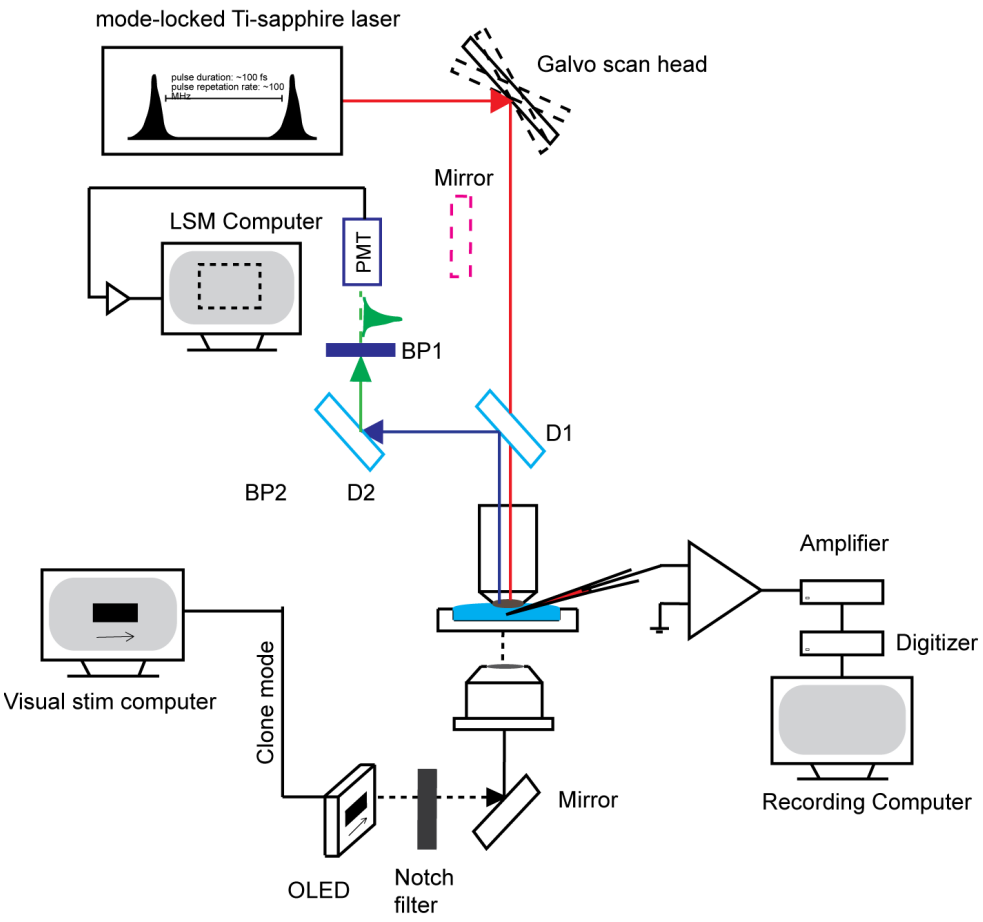

FIGURE 2.6: Schematic diagram of the two-photon microscope configured for simutaneous calcium imaging and visual stimulation. The microscope is configured at laser-scanning mode. A notch filter is placed in front of OLED to separate the wavelength of visual stimulation from those of the fluorescence detected at the PMT.

2.7 References

Baden, T., Berens, P., Franke, K., Roman Roson, M., Bethge, M., and Euler, T. (2016). The functional diversity of retinal ganglion cells in the mouse. Nature 529, 345-350.

Barlow, H.B., Hill, R.M., and Levick, W.R. (1964). Retinal Ganglion Cells Responding Selectively to Direction and Speed of Image Motion in the Rabbit. J Physiol 173, 377-407.

Barlow, H.B., and Levick, W.R. (1965). The mechanism of directionally selective units in rabbit's retina. J Physiol 178, 477-504.

Chen, Q., Pei, Z., Koren, D., and Wei, W. (2016). Stimulus-dependent recruitment of lateral inhibition underlies retinal direction selectivity. Elife 5, e21053.

Cruz-Martn, A., El-Danaf, R.N., Osakada, F., Sriram, B., Dhande, O.S., Nguyen, P.L., Callaway, E.M., Ghosh, A., and Huberman, A.D. (2014). A dedicated circuit linking direction selective retinal ganglion cells to primary visual cortex. Nature 507, 358.

Demb, J.B., and Singer, J.H. (2015). Functional circuitry of the retina. Annual Review of Vision Science 1, 263-289. Dhande, O.S., Stafford, B.K., Lim, J.-H.A., and Huberman, A.D. (2015). Contributions of retinal ganglion cells to subcortical visual processing and behaviors. Annual Review of Vision Science 1, 291-328.

Euler, T., Hausselt, S.E., Margolis, D.J., Breuninger, T., Castell, X., Detwiler, P.B., and Denk, W. (2009). Eyecup scope–optical recordings of light stimulus-evoked fluorescence signals in the retina. Pflugers Arch 457, 1393-1414.

Gollisch, T., and Meister, M. (2010). Eye smarter than scientists believed: neural computations in circuits of the retina. Neuron 65, 150-164.

Hillier, D., Fiscella, M., Drinnenberg, A., Trenholm, S., Rompani, S.B., Raics, Z., Katona, G., Juettner, J., Hierlemann, A., Rozsa, B., et al. (2017). Causal evidence for retina-dependent and -independent visual motion computations in mouse cortex. Nat Neurosci 20, 960-968.

Huberman, A.D., Wei, W., Elstrott, J., Stafford, B.K., Feller, M.B., and Barres, B.A. (2009). Genetic Identification of an On-Off Direction-Selective Retinal Ganglion Cell Subtype Reveals a Layer-Specific Subcortical Map of Posterior Motion. Neuron 62, 327-334.

Pei, Z., Chen, Q., Koren, D., Giammarinaro, B., Ledesma, H.A., and Wei, W. (2015). Conditional knock-out of vesicular GABA transporter gene from starburst amacrine

cells reveals the contributions of multiple synaptic mechanisms underlying direction selectivity in the retina. Journal of Neuroscience 35, 13219-13232.

Sanes, J.R., and Masland, R.H. (2015). The types of retinal ganglion cells: current status and implications for neuronal classification. Annual review of neuroscience 38, 221-246.

Shi, X., Barchini, J., Ledesma, H.A., Koren, D., Jin, Y., Liu, X., Wei, W., and Cang, J. (2017). Retinal origin of direction selectivity in the superior colliculus. Nature Neuroscience 20, 550-558.

Simpson, J.I. (1984). The accessory optic system. Annual review of neuroscience 7, 13-41.

Svoboda, K., and Yasuda, R. (2006). Principles of two-photon excitation microscopy and its applications to neuroscience. Neuron 50, 823-839.

van Wyk, M., Wassle, H., and Taylor, W.R. (2009). Receptive field properties of ON- and OFF-ganglion cells in the mouse retina. Vis Neurosci 26, 297-308.

Vaney, D.I., Sivyer, B., and Taylor, W.R. (2012). Direction selectivity in the retina: symmetry and asymmetry in structure and function. Nature reviews Neuroscience 13, 194.

Wei, W., Elstrott, J., and Feller, M.B. (2010). Two-photon targeted recording of GFP-expressing neurons for light responses and live-cell imaging in the mouse retina. Nat Protoc 5, 1347-1352.

Wei, W., Hamby, A.M., Zhou, K., and Feller, M.B. (2011a). Development of asymmetric inhibition underlying direction selectivity in the retina. Nature 469, 402-406.

Wei, W., Hamby, A.M., Zhou, K.L., and Feller, M.B. (2011b). Development of asymmetric inhibition underlying direction selectivity in the retina. Nature 469, 402-+.

Yonehara, K., Balint, K., Noda, M., Nagel, G., Bamberg, E., and Roska, B. (2011). Spatially asymmetric reorganization of inhibition establishes a motion-sensitive circuit. Nature 469, 407-410.

Zeng, H., and Madisen, L. (2012). Mouse transgenic approaches in optogenetics. Prog Brain Res 196, 193-213. Zucker, C.L., and Dowling, J.E. (1987). Centrifugal fibres synapse on dopaminergic interplexiform cells in the teleost retina. Nature 330, 166-168.

3

Stimulus-dependent recruitment of lateral inhibition underlies retinal direction selectivity

This Chapter is a full reprint of Chen et al., eLife, in which I was the primary author.The work is included with permission from all authors.

Relevant Publication

Qiang Chen, Zhe Pei, David Koren, and Wei Wei. 2016 "Stimulus-dependent recruitment of lateral inhibition underlies retinal direction selectivity." eLife 2016; 10.7554/elife.21053

For supplementary multimedia documents, please refer to `https://elifesciences.org/articles/21053`

3.1 Abstract

The dendrites of starburst amacrine cells (SACs) in the mammalian retina are preferentially activated by motion in the centrifugal direction, a property that is important for generating direction selectivity in direction selective ganglion cells (DSGCs). A candidate mechanism underlying the centrifugal direction selectivity of

SAC dendrites is synaptic inhibition onto SACs. Here we disrupted this inhibition by perturbing distinct sets of GABAergic inputs onto SACs removing either GABA release or GABA receptors from SACs. We found that lateral inhibition onto Off SACs from non-SAC amacrine cells is required for optimal direction selectivity of the Off pathway. In contrast, lateral inhibition onto On SACs is not necessary for direction selectivity of the On pathway when the moving object is on a homogenous background, but is required when the background is noisy. These results demonstrate that distinct sets of inhibitory mechanisms are recruited to generate direction selectivity under different visual conditions.

3.2 Introduction

Encoding of motion direction first appears in the inner plexiform layer (IPL) of mammalian retina (Barlow and Hill, 1963; Barlow and Levick, 1965; Oyster and Barlow, 1967), where positive- and negative-contrast motion stimuli are processed in anatomically distinct On and Off sublaminae. One of the main output neurons that signal motion direction from the retina to higher visual centers, the On-Off DSGC, has bistratified dendritic arbors that receive directionally tuned inhibition from On and Off subtypes of SACs at each of these sublamina (Figure 3.1a) (Famiglietti, 1983, 1992; Kittila and Massey, 1997; Taylor and Vaney, 2002). SACs are monostratified, axonless interneurons that release GABA and acetylcholine from varicosities at the distal ends of their dendritic arbors (Brecha et al., 1988; Famiglietti, 1991; Kosaka et al., 1988; OMalley and Masland, 1989; Vaney and Young, 1988). Generating directionally tuned GABAergic inhibition onto DSGCs requires two mechanisms. First, GABAergic inputs preferentially originate from SAC dendritic sectors that extend in the anti-preferred (null) direction of On-Off DSGCs (Figure 3.1b, Briggman et al., 2011; Fried et al., 2002; Lee et al., 2010; Wei et al., 2011). Second, the dendritic

sectors of SACs are electrotonically isolated and directionally tuned to motion in the centrifugal direction (from soma to dendritic tips) (Figure 3.1b, Euler et al., 2002). Since null-direction motion for a DSGC corresponds to centrifugal motion for its presynaptic SAC dendrites, maximal GABA release from SACs to DSGCs occurs during motion in the null direction (Figure 3.1b).

Along with providing inhibition to DSGCs, SACs at each sublamina receive GABAergic lateral inhibition from neighboring SACs (Ding et al., 2016; Kostadinov and Sanes, 2015; Lee and Zhou, 2006) and other wide-field amacrine cells (Ding et al., 2016; Lee and Zhou, 2006). The role of this lateral inhibition in establishing the centrifugal preference of SACs remains controversial (Ding et al., 2016; Euler et al., 2002; Hausselt et al., 2007; Lee and Zhou, 2006; Mnch and Werblin, 2006; Oesch and Taylor, 2010). Centrifugal direction selectivity has also been attributed to other mechanisms such as patterned distribution of voltage-gated channels (Euler et al., 2002; Hausselt et al., 2007; Oesch and Taylor, 2010) and chloride transporters (Gavrikov et al., 2006), segregation of excitatory inputs from distinct bipolar cell types (Kim et al., 2014; but see Stincic et al., 2016), and skewed distribution of glutamatergic inputs along SAC dendrites (Vlasits et al., 2016). However, the relative contributions of these synaptic and intrinsic mechanisms to SAC centrifugal preference is unclear. Furthermore, the role that synaptic inhibition onto SACs plays in the direction selectivity of DSGCs has not yet been experimentally demonstrated.

To address these outstanding questions, we perturbed GABAergic inhibition onto SACs using two types of SAC-specific genetic manipulations. The first one disrupted GABA release from SACs by conditionally knocking out the vesicular GABA transporter (Vgat) gene Slc32a1 in SACs. This selectively removed reciprocal SAC-SAC inhibition and allowed us to determine its contribution to the centrifugal direction selectivity of SACs. The second manipulation blocked all GABAergic inputs onto SACs by removing their functional GABA receptors. This enabled us to determine

the role that total GABAergic inhibition onto SACs plays in the direction selectivity of both SACs and On-Off DSGCs. Combining these genetic manipulations with pharmacology, we found that motion stimuli with different contrast and backgrounds recruit different sets of inhibitory mechanisms for the computation of motion direction.

3.3 Results

3.3.1 Direction selectivity of SAC dendrites persists in the absence of SAC-mediated GABA release during a simple moving bar stimulus

To eliminate reciprocal GABAergic inhibition among neighboring SACs, we used a conditional knockout (KO) mouse line in which Slc32a1 is selectively removed from SACs (Slc32a1 KO) to block GABA release from SACs. This line contains homozygous floxed Slc32a1 alleles (acronym: Slc32a1flox/flox) to replace the endogenous Slc32a1 gene, and a choline acetyltransferase (Chat)-IRES-Cre knockin allele for SAC-specific Cre expression (acronym: C). A floxed tdTomato transgene (acronym: T) was also included when SACs were targeted for electrophysiological recordings (Figure 13.1c). We have previously shown that these KO mice display disrupted GABAergic inhibition from SACs to DSGCs and no detectable developmental compensation (Pei et al., 2015). To confirm that GABAergic synapses between neighboring SACs are also lost in these mice, we performed paired recordings from neighboring SACs in the ganglion cell layer with intersoma distance of $50 \sim 100 \mu m$. Evoked GABAergic inhibitory postsynaptic currents (IPSCs) were measured from one SAC at holding potential of -80 mV while the other SAC was depolarized to 0 mV for 20 ms in voltage clamp configuration. We detected reciprocal inhibition between SACs

in 9 out of 9 pairs in the control group (Figure 3.1d, mean peak amplitude 16.4 $\pm$ 2.8 pA, 5 mice), consistent with previous studies (Kostadinov and Sanes, 2015; Lee and Zhou, 2006). We did not detect any evoked IPSCs in the KO group (Figure 3.1e, n = 9 pairs, 3 mice), indicating that reciprocal SAC-SAC inhibition is abolished in Slc32a1 KO mice.

Next, we examined centrifugal direction selectivity of SAC dendrites in these KO

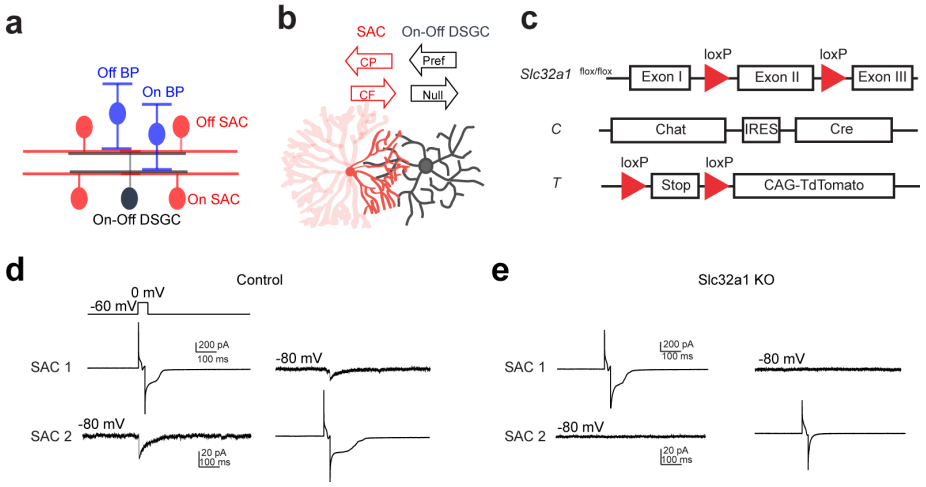

FIGURE 3.1: Genetic deletion of Slc32a1 from SACs eliminates reciprocal inhibition between SACs.
a. Schematic shows laminar organization of cell types involved in the direction selective circuit in the IPL.
b. Schematic shows the orientation of SAC and DSGC dendrites connected by GABAergic synapses. Black arrows indicate referred and null directions of DSGC. GABAergic inputs onto DSGC come from SAC dendritic quadrant (dark red) that extends to the null direction of the DSGC. Red arrows indicate centrifugal (CF) and centripetal (CP) direction of motion for the SAC quadrant. Maximal activation and GABA release occurs in the CF direction, while minimal activation occurs in the CP direction.
c. Schematic diagram shows transgenes involved in Slc32a1 KO mice.
d. Voltage clamp traces from reciprocal On SAC-SAC pairs in control mouse (CT) show IPSCs evoked in one SAC at -80 mV by depolarizing the other in the presence of glutamatergic and nicotinic receptor antagonists (see Experimental procedures).
e. As in d but for Slc32a1 KO mouse (Slc32a1 flox/flox CT).

mice using two-photon imaging of the calcium indicator GCaMP6. We imaged calcium transients in varicosities located in the furthest distal 20 μm of GCaMP6-expressing SAC dendrites while a bright bar moved against a homogeneous dark background (Figure 3.2a). We term this stimulus "simple moving bar stimulus. As expected, the leading edge of the bright bar evoked calcium transients in On SACs

and the trailing edge evoked responses in Off SACs (Figure 3.2b, and Videos 1 and 2). We used the peak amplitude of the calcium transients in varicosities as a measure of the strength of dendritic activation. We quantified direction selectivity of responses using the direction selectivity index (DSI, see Experimental methods) and the vector sum. In control mice, dendritic calcium signals in both On and Off SACs show strong directional tuning to motion in the centrifugal direction (Figures 3.2b and 3.2c).

In Slc32a1 KO mice, centrifugal direction selectivity (both DSI and vector sum) of On SACs is similar to that of control mice (Figure 3.2d). However, Off SACs exhibit a small, but statistically significant, increase in DSI and vector sum values (Figure 3.2f) due to decreased centripetal direction response (Figure 3.3). Adding the GABAA receptor antagonist SR95531 to Slc32a1 KO retinas reduces these direction selectivity parameters for both On and Off SACs (Figures 3.2d-g), indicating a role for GABAergic inhibition of SACs by non-SAC amacrine cells. Our results demonstrate that, for a simple moving bar stimulus, losing reciprocal SAC-SAC inhibition in Slc32a1 KO mice does not affect the direction selectivity of On SACs, and enhances the direction selectivity of Off SACs.

3.3.2 SAC-specific deletion of GABAA receptors

The GABAergic inhibition required for generating the centrifugal direction selectivity of On and Off SACs could come from two sources besides other SACs. The first is the GABAergic synapse onto presynaptic bipolar cells from other amacrine cell types (Hoggarth et al., 2015; Lee and Zhou, 2006). The second is direct GABAergic input onto SACs from non-SAC amacrine cells (Ding et al., 2016). To distinguish between these two possibilities, we examined the direction selectivity of SACs when GABAA receptors are removed from SACs but not from bipolar cells. If presynaptic inhibition

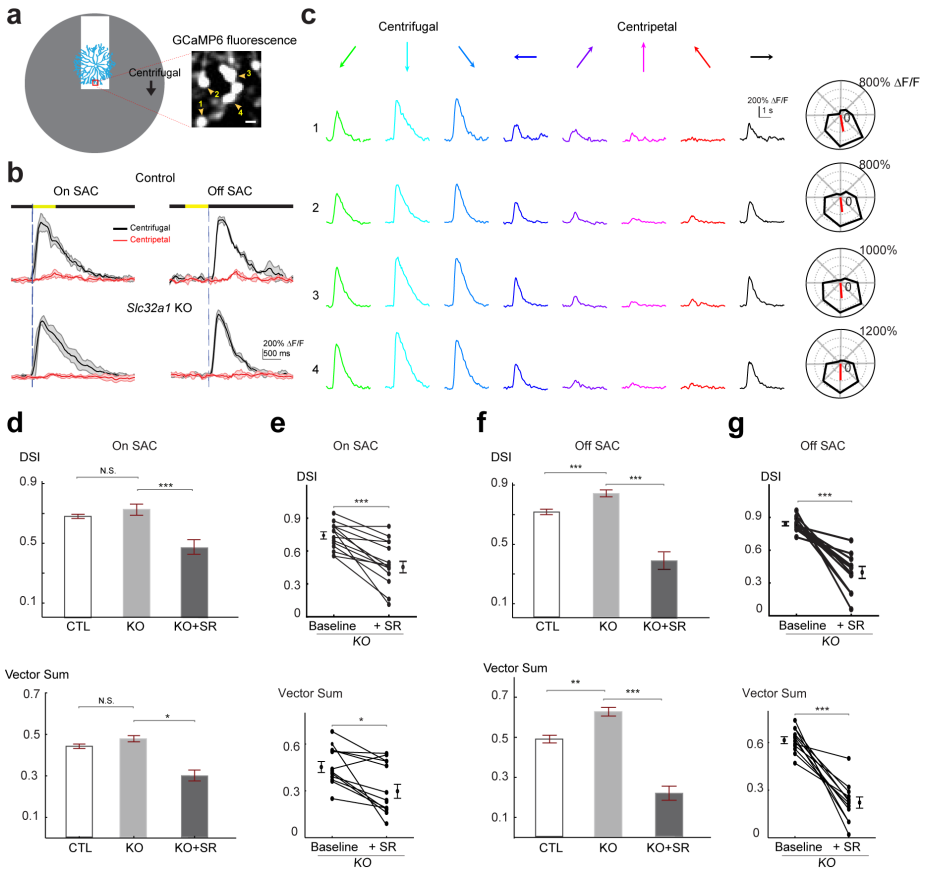

FIGURE 3.2: Centrifugal preference of SACs is not reduced in Slc32a1 KO mice.
a. Left: Schematic of simple moving bar stimulus used during calcium imaging of SAC dendrites. Red square indicates location of imaging window. Gray area indicates area within which the moving bar (white) was presented. For the varicosities in the imaging window, downward motion of the bar corresponds to centrifugal (CF) motion, and upward motion corresponds to centripetal (CP) motion. Right: maximal intensity projection of GCaMP6m fluorescence in distal varicosities of an On-SAC from a control (C) mouse infected with AAV-floxed GCaMP6m. Four example varicosities are labeled 1 - 4. Scale bar: 1 μm.
b. Example GCaMP6m fluorescence traces from varicosities of the On and Off SACs in control (C) and Slc32a1 KO (Slc32a1 flox/flox C) mice during CF and CP motion. Dark lines represent mean values and shaded areas represent standard deviations. Yellow bar at top indicates time window when the bar moved across the imaging area. Blue vertical lines indicate when leading edge reaches varicosities of On SAC and trailing edge reaches varicosities of Off SAC.
c. Example single sweeps of moving bar-evoked GCaMP6 fluorescence from varicosities 1-4 shown in A. Polar plots of mean peak amplitude on right show centrifugal tuning of all 4 varicosities. d. Summary bar graphs of DSI and vector sum values for On SACs in control (CTL) and Slc32a1 KO mice before and after adding SR95531.
e. Pairwise comparison of DSI and vector sum values of individual On-SACs before and after adding SR95531 in Slc32a1 KO mice.
f. As in D, summary bar graphs of DSI and vector sum values for Off-SACs.
g. As in E, pairwise comparison of DSI and VS values of individual Off-SACs.
See also Figure 2 - figure supplement 1 for cumulative probability distributions of peak fluorescence in On and Off SACs of control and Slc32a1 KO mice during CP and CF motion.

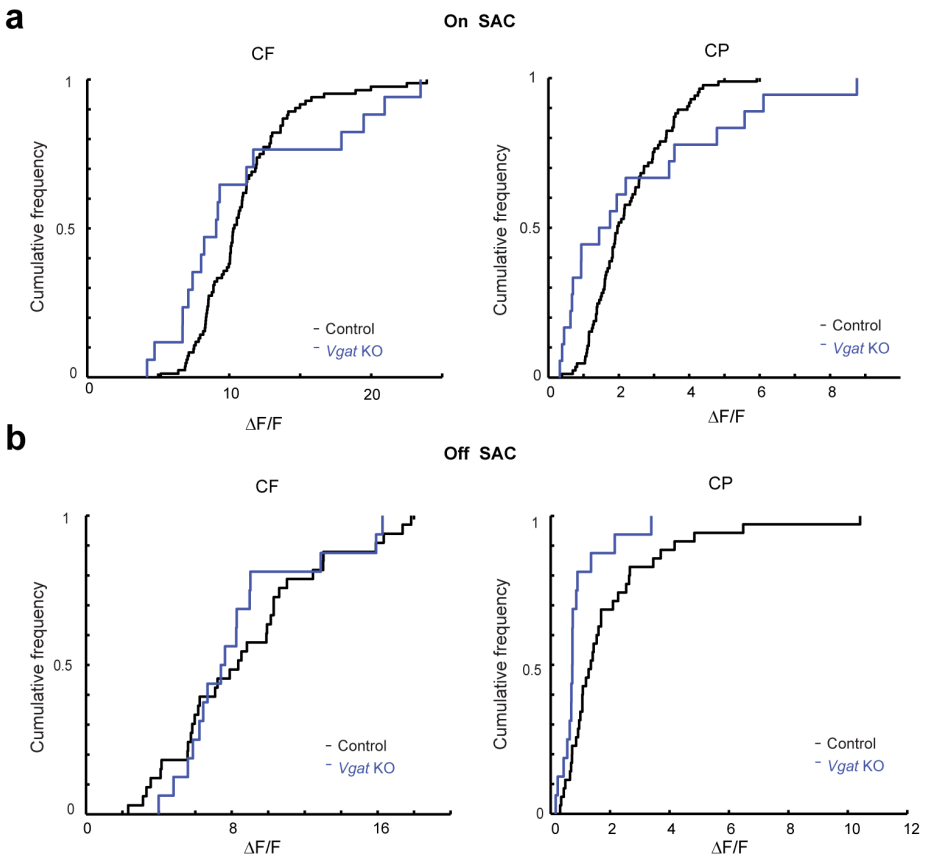

FIGURE 3.3: Centripetal response of Off SAC dendrites is selectively reduced in Slc32a1 KO mice.
a. Cumulative probability distributions of peak fluorescence in dendritic varicosities of On SACs during CF (left) and CP (right) motion in control and Slc32a1 KO mice.
b. As in a, cumulative probability distributions of peak fluorescence in dendritic varicosities of Off SACs.

from non-SAC amacrine cells onto bipolar cells is sufficient for direction selectivity, we would expect normal direction selectivity under this condition. In comparison, if non-SAC-mediated GABAergic inputs directly onto SACs are important, we would expect impaired direction selectivity.

We eliminated all direct GABAergic inhibition onto SACs by generating a conditional KO mouse line in which the $\alpha 2$ subunit of GABAA receptors, Gabra2, is selectively knocked out from SACs (Gabra2 KO mice, Figure 3A). Gabra2 expression colocalizes with On and Off SAC dendrites in the IPL (Brandsttter et al., 2009) and has been shown to be important for direction selectivity (Auferkorte et al., 2012). For targeted

recording from these KOs, we also labeled SACs and a subtype of On-Off DSGCs that prefer motion in the posterior direction (pDSGCs) (Huberman et al., 2009) with tdTomato and GFP, respectively (Figure 3.4a). To confirm loss of functional GABAA receptors in SACs of Gabra2 KO mice, we recorded their spontaneous IPSCs and found that they are eliminated (Figures 3.4b and 3.4c). We also performed paired recordings from neighboring SACs, and found that none of the pairs showed evoked IPSCs (Figure 3.4d, n = 10 pairs, 3 mice). Therefore, GABAergic inputs onto SACs are abolished in Gabra2 KO mice.

Although multiple studies have demonstrated that the emergence of retinal direction selectivity occurs independent of neural activity (Elstrott et al., 2008; Hamby et al., 2015; Sun et al., 2011; Wei et al., 2011), we needed to rule out potential developmental changes in this circuit in Gabra2 KO mice. Therefore, we examined other critical synapses involved in direction selectivity: the GABAergic and cholinergic synapses between SACs and DSGCs. Using paired voltage-clamp recording, we depolarized SACs and measured evoked GABAergic IPSCs and cholinergic excitatory postsynaptic currents (EPSCs) in pDSGCs. We targeted SAC-pDSGC pairs with overlapping dendritic arbors and intersoma distances of 60-80 μm. In control mice, SACs from the null side provide strong GABAergic inputs onto pDSGCs while SACs from the preferred side provide weak GABAergic inputs. In Gabra2 KOs, this asymmetric wiring pattern remains unchanged (Figures 3E and 3F). Similarly, cholinergic transmission in the KO is unaffected (Figures 3.4e and 3.4f). Thus our results show that GABAergic and cholinergic synapses from SACs to DSGCs are not altered in the Gabra2 KO mice. In addition, the amplitude of EPSCs in pDSGCs evoked by a bright flashing spot is similar between control and Gabra2 KO groups (Figure 3.4g), indicating that both cholinergic and glutamatergic synapses onto pDSGCs are unaltered.

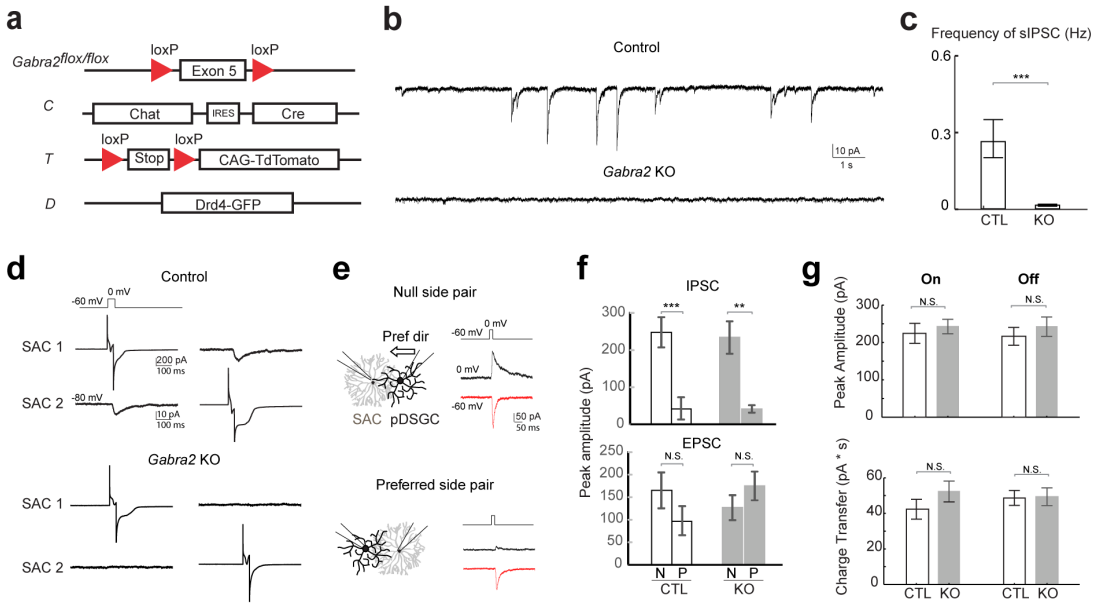

FIGURE 3.4: Genetic deletion of Gabra2 from SACs eliminates GABAergic inputs onto SACs without affecting the synapses between SACs and pDSGCs.
a.Schematic diagram shows transgenes involved in Gabra2 conditional KO mice. The KO mice carry homozygous floxed Gabra2 allele to replace the endogenous Gabra2 gene for Cre-dependent excision (acronym: Gabra2flox/flox), and Chat-IRES-Cre (C). The floxed tdTomato (T) and a Drd4-GFP transgene to label pDSGCs (D) were also included when SACs or pDSGCs were targeted for electrophysiological recordings.
b.Example traces of spontaneous IPSCs (sIPSCs) in On SACs from control (CT) and Gabra2 KO (Gabra2flox/flox CT) mice.
c.Summary bar graph of sIPSC frequency in control and KO groups. Control: 0.28 ± 0.07 Hz, n = 18 cells, 5 mice; KO: 0.02 ± 0.04 Hz, n = 16 cells, 4 mice. ***$p < 0.0005$.
d.Example evoked IPSC traces from reciprocal On SAC-SAC pairs in Control and Gabra2 KO mice.
e.Voltage clamp traces from null-side and preferred-side SAC-DSGC pairs in control (CTD) and KO (Gabra2flox/floxCTD) mice showing cholinergic EPSCs (red inward) and GABAergic IPSCs (black outward) evoked in pDSGCs by depolarizing SACs. Schematic on left shows soma locations of the null and preferred side pairs. Black arrows indicate the pDSGCs preferred direction.
f.Summary bar graphs of IPSC and EPSC peak amplitudes in pDSGCs evoked by null (N) and preferred (P) side SACs in control and KO groups.
g.Summary bar graphs of EPSC amplitudes and total charger transfer in pDSGCs evoked by onset and offset of a bright spot in control and KO mice.

3.3.3 Centrifugal direction selectivity of Off SACs is impaired in Gabra2 KO mice during the simple moving bar stimulus

How do SACs respond to visual motion when their direct ionotropic GABAergic inhibitory inputs are lost? To address this question, we measured centrifugal direction selectivity by monitoring GCaMP6 fluorescence in On and Off SACs of Gabra2 KO

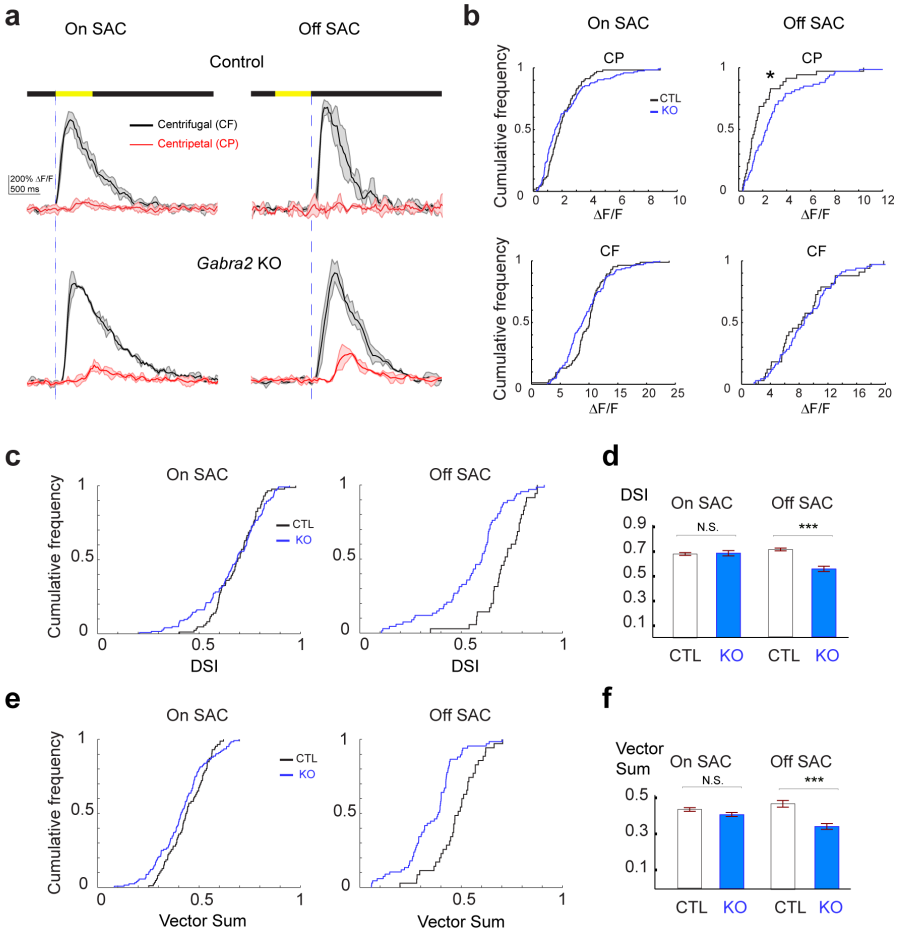

FIGURE 3.5: Centrifugal preference of Off, but not On, SACs is impaired in Gabra2 KO mice.
a.Example GCaMP6m fluorescence traces from varicosities of On (left) and Off (right) SACs in control (C) and KO (Gabra2flox/flox C) mice during CF and CP motion. Dark lines represent mean values and shaded areas represent standard deviations. Yellow bar at top indicates time window when the bar moved across the imaging area. Blue vertical lines indicate when leading edge reaches varicosities of On SAC and trailing edge reaches varicosities of Off SACs.
b.Cumulative probability distributions of peak fluorescence from dendritic varicosities in On (left) and Off (right) SACs of control and Gabra2 KO mice during CP and CF motion.
c.Cumulative probability distributions of DSI values from dendritic varicosities in On and Off SACs of control and KO mice.
d.Summary bar graph of DSI values from dendritic varicosities in On and Off SACs of control and KO mice: On SAC: Control 0.69 $\pm$ 0.01, KO 0.71 $\pm$ 0.02, p = 0.22; Off SAC: Control 0.72 $\pm$ 0.01, KO 0.55 $\pm$ 0.02, ***p $<$ 0.0005.
e.Cumulative probability distributions of vector sum values from dendritic varicosities in On and Off SACs of control and KO mice.
f.Summary bar graph of vector sum values from dendritic varicosities in On and Off SACs of control and KO mice.
See also Figure 3.6 for the effect of SR95531 on direction selectivity of On SACs in Gabra2 KO mice.

mice during the simple moving bar stimulus described above. We found that Off SACs in these KOs display a significant increase in centripetal-direction response (Figures 3.5a and 3.5b, Video 3), resulting in reduced direction selectivity (Figures 3.5c-f). Therefore, direct GABAergic inputs onto Off SACs from non-SAC amacrine cells are important for centrifugal direction selectivity. In contrast, we found that On SACs in the KOs exhibit centrifugal preference similar to those of control mice (Figure 3.5 Video 4), suggesting that direct GABAergic inputs are not required for direction selectivity in On SACs during the simple moving bar stimulus. Bath application of SR95531 reduced direction selectivity of On SACs in KOs (Figure 3.6), suggesting a role for presynaptic inhibition onto bipolar cells in generating direction selectivity.

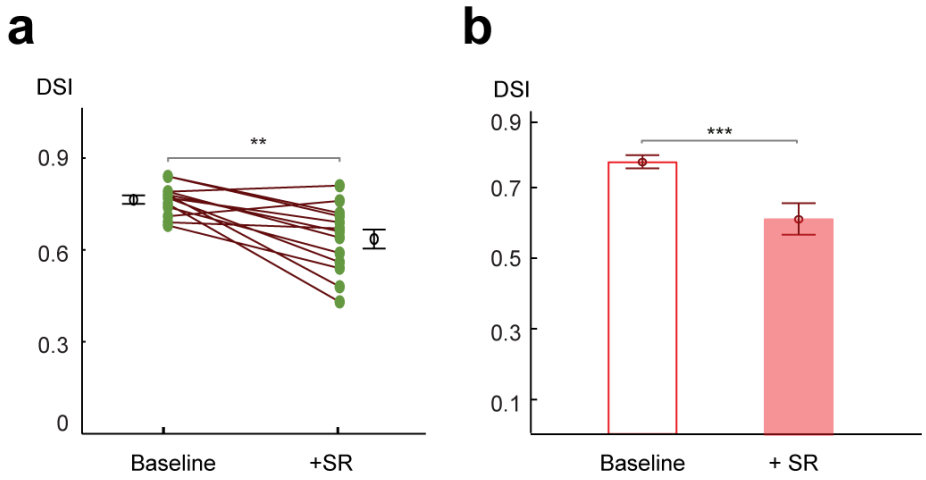

FIGURE 3.6: Centrifugal preference of On SACs is impaired in Gabra2 KO mice in the presence of SR95531.
a. Pairwise comparison of DSI values of individual On SACs before and after adding SR95531 in Gabra2 KO mice. Paired t-test ** $p<0.005$
b. Summary bar graph of DSI values. Error bars represent standard error of the mean (SEM).Unpaired t-test *** $p<0.0005$. Baseline: 0.76 ± 0.01; + SR: 0.63 ± 0.03; n=13 cells, 3 mice.

3.3.4 *Off inhibitory inputs onto On-Off DSGCs display impaired direction selectivity in Gabra2 KO mice*

Since centrifugal preference of Off SAC dendrites is selectively impaired in Gabra2 KO mice, we would expect that the Off component of inhibitory inputs onto DSGCs would also display reduced direction selectivity. We tested this hypothesis by performing whole-cell voltage clamp recordings in pDSGCs to measure light-evoked IPSCs during the simple moving bar stimulus. To quantify direction selectivity of the inhibitory inputs onto DSGCs, we calculated DSI and vector sum of the peak amplitude and total charge transfer of IPSCs in response to the simple moving bar stimulus. In control mice, both On and Off components of IPSCs are direction selective (Figure 3.7a-d). In Gabra2 KO mice, the Off component of IPSCs shows reduced selectivity (Figure 3.7c and 3.7d) but the On component does not (Figure 3.7a-b). Therefore, in the absence of GABAergic inputs onto SACs, the Off component of inhibitory inputs onto DSGCs displays impaired directional tuning.

3.3.5 *Off component of On-Off DSGC spiking activity shows impaired direction selectivity in Gabra2 KO mice*

To test if loss of lateral inhibition onto Off SACs impacts the ultimate output of the retinal direction selective circuit, we determined its effect on the spiking activity of DSGCs. We recorded the spiking activity of pDSGCs in loose-patch configuration, and compared the direction selectivity of the leading edge-evoked On response and the trailing edge-evoked Off response in control and Gabra2 KO mice during the simple moving bar stimulus. Consistent with the reduced directional tuning of IPSCs observed in the Off component, we found that the Off response of pDSGC spiking activity in Gabra2 KO mice shows less direction selectivity than that in control mice

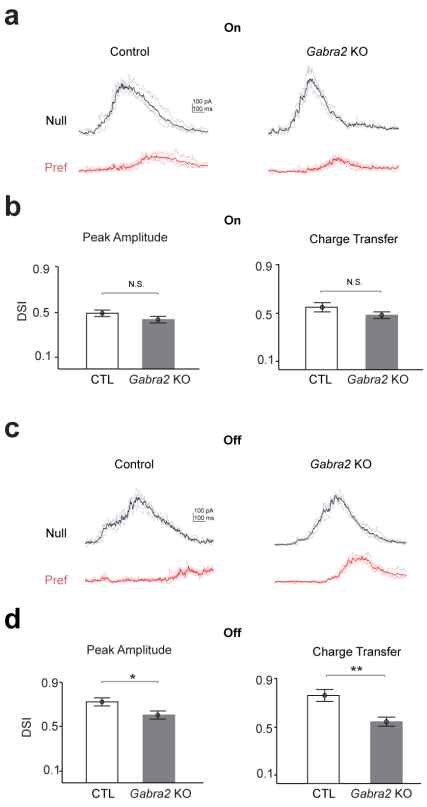

Figure 3.7: Off inhibitory inputs onto pDSGCs display impaired directional selectivity in Gabra2 KO mice.
a. Example IPSC traces of pDSGCs evoked by leading edge (On) of a bright bar moving in the preferred and null directions in control (CTD) and Gabra2 KO (Gabra2flox/flox CTD) mice.
b. Summary bar graphs of DSI values for peak amplitude and charge transfer of the On component of IPSCs in control and KO groups. Peak Amplitude: Control 0.49±0.03, KO 0.44 ± 0.03, p = 0.19; Charge Transfer: Control 0.53± 0.04, KO 0.49 ± 0.03, p = 0.16. Control n = 32 cells, 13 mice; KO n = 33 cells, 18 mice.
c. As in a, example IPSC traces of pDSGCs evoked by trailing edge (Off) of a bright moving bar.
d. As in b, summary bar graphs for the Off component of IPSCs in pDSGCs. Control 0.72 ± 0.03, KO 0.58 ± 0.03, *p = 0.01; Charge Transfer: Control 0.73 ± 0.03, KO 0.51 ± 0.03, **p < 0.005.

(Figures 3.8a and 3.8c). In contrast, the On responses in KOs display direction selectivity similar to that of controls (Figure 3.8a-b. To rule out the possibility that the Off response is influenced by prior activation of the On pathway, we reversed the contrast of the moving bar stimulus by presenting a dark bar against a bright background. We found that direction selectivity of the leading edge-evoked Off component in Gabra2 KOs was again less than that in controls (Figure 3.8d and 3.8f), while the trailing edge-evoked On response of KOs shows direction selectivity similar to controls (Figure 3.8d, 3.8e). Therefore, the Off component of pDSGC spiking activity becomes less directionally tuned in Gabra2 KO mice.

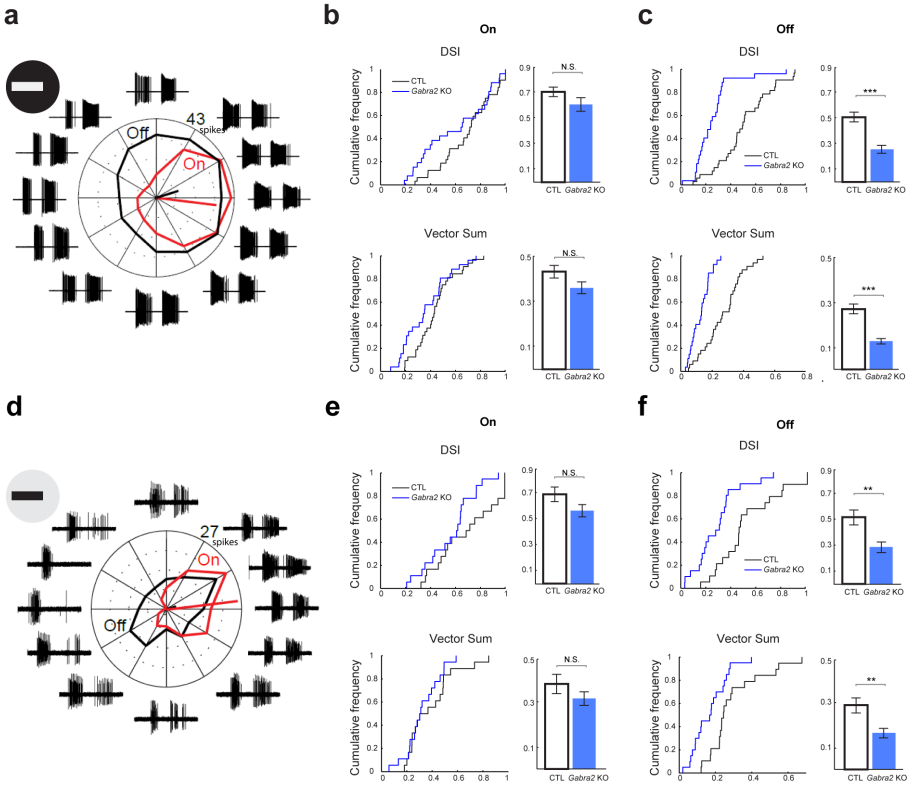

FIGURE 3.8: Off component of pDSGC spiking activity displays impaired directional tuning in Gabra2 KO mice.
a-c: Spiking response of pDSGCs to a bright moving bar.
a.Example loose-patch recordings and polar plot for a pDSGC in a Gabra2 KO (Gabra2flox/flox CTD) mouse in response to a bright bar moving in 12 directions. Trace for each direction is the overlay of three trials. The leading edge-evoked On and trailing edge-evoked Off components of the spiking activity can be clearly separated. Mean spike counts for On (red) and Off (black) responses are shown on the polar plot.
b.Cumulative distributions (left) and summary bar graphs (right) of DSI and vector sum values for On responses of pDSGCs during the bright moving bar stimulus.
c.As in b, DSI and vector sum for Off responses of pDSGCs during the bright moving bar stimulus.
d - f: Spiking response of pDSGCs to a dark moving bar.
d.As in a, example loose-patch recordings and polar plot for a pDSGC in a Gabra2 KO (Gabra2flox/flox CTD) mouse in response to a dark bar moving in 12 directions.
e.As in b, DSI and vector sum for On responses of pDSGCs during the dark moving bar stimulus.
f.As in c, DSI and vector sum for Off responses of pDSGCs during the dark moving bar stimulus.

3.3.6 Lateral inhibition in the On pathway is required for direction selectivity on a noisy background

In the experiments above, we used a simple moving bar stimulus and found that direction selectivity of the Off pathway requires lateral inhibition onto Off SACs,

but direction selectivity of the On pathway does not require direct GABAergic input onto On SACs. What, then, is the role of lateral inhibition in the On pathway? We hypothesized that our stimulus conditions did not optimally activate this inhibitory pathway. In particular, a noisy background may more effectively engage this inhibition and reveal its functional importance in direction selectivity. To test this idea, we measured the direction selectivity of pDSGCs in Gabra2 KO mice using a bright bar moving against a flickering checkerboard background. This flickering checkerboard provides "white noise" that is commonly used for mapping receptive fields in the spike-triggered average method (Chichilnisky, 2001). We set the brightness of this moving bar equal to that of our simple moving bar stimulus, and varied the brightness of the checker pattern from 0% to 100% of the moving bar intensity. In control mice, the pDSGC spiking response maintains direction selectivity over a wide range of checker intensities (Figures 3.9a-c). Consistent with the earlier finding that lateral inhibition is crucial for direction selectivity of the Off component (Figures 3.9c and 3.9e), the direction selectivity of the Off response in Gabra2 KO mice is reduced regardless of checker intensity (Figures 3.9a and 3.9c). Interestingly, however, replacing the gray background with a flickering checkerboard also significantly reduces the On direction selectivity in KO mice (Figures 3.9a and 3.9b), indicating a functional contribution of lateral inhibition during more complex stimuli.

The flickering checkerboard not only adds noise to the visual stimuli, but also changes the average background illuminance and therefore the effective contrast of the moving bar. To test if changing either ambient illuminance or contrast alone can mimic the effect of introducing the flickering checkerboard, we measured the direction selectivity of pDSGCs in Gabra2 KO mice using the simple moving bar stimulus with different contrast and background illuminance levels that lie in the upper and lower range of the flickering checkerboard stimuli. We found that, similar to the results with our original simple bar stimulus (Figure 3.8), the On component

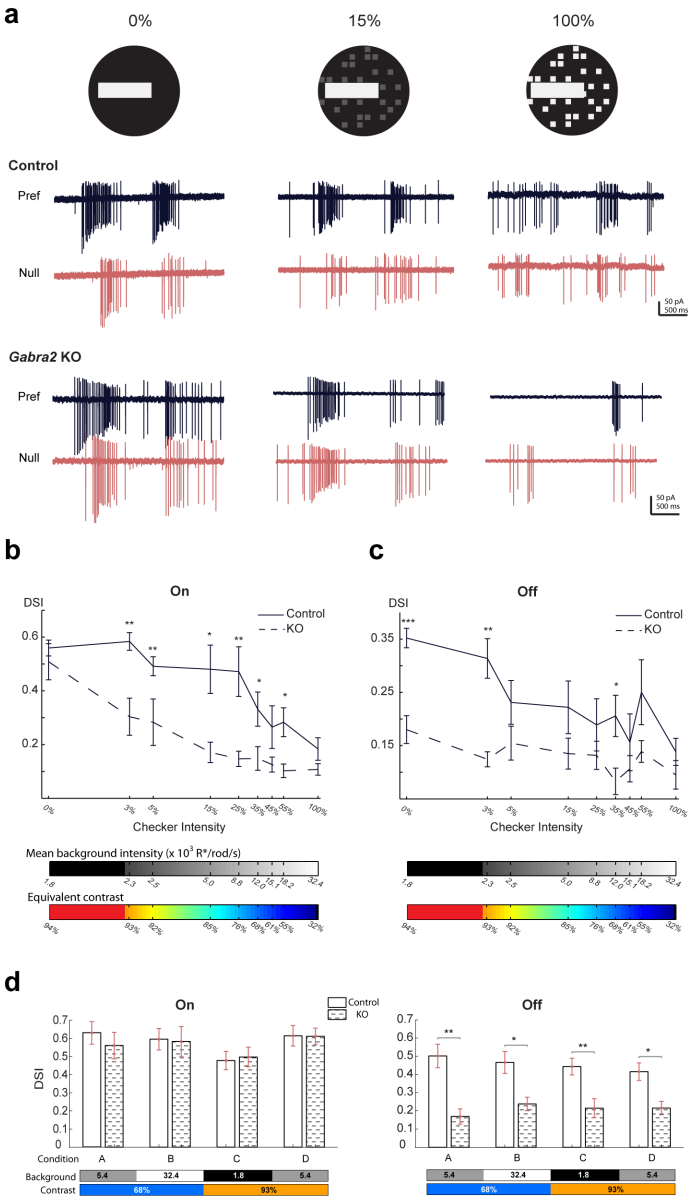

Figure 3.9: Direct inhibitory inputs onto On SACs are required for robust direction selectivity against noisy background.
a.Visual stimulus (top) is a bright bar moving on a checkered background with different checker intensities, and loose-patch recordings (bottom) show pDSGC responses in control (CTD) and Gabra2 KO (Gabra2flox/flox CTD) mice in preferred and null directions.
b.Summary plot of DSI values of the On component of pDSGC spiking activity evoked by a bright bar moving against a flickering checkerboard background. Checker intensity is expressed as the percentage of the brightness of the moving bar. Bars below plot indicate the mean background intensity of the flickering checkerboard (top) and the equivalent contrast of the moving bar stimulus (bottom). Control, n = 12 cells, 4 mice; Gabra2 KO, n = 18 cells, 4 mice.
c.As in b, summary plot of DSI of Off component of pDSGC spiking activity.
d.Summary bar graphs of DSI values from On and Off components of pDSGC spiking at different background illuminance and contrast levels during the simple moving bar stimulus against a homogeneous background. Bars below plots indicate the background intensity (x103 R*/rod/s) and contrast of the bar.

of the pDSGC's spiking response displays normal direction selectivity, while the Off component shows reduced direction selectivity at all illuminance and contrast levels tested (Figures 3.9d). Therefore, the impaired direction selectivity seen in the On pathway in Gabra2 KO mice with the flickering checkboard background is not due to changes in stimulus contrast or ambient illuminance. Instead, the noise introduced by the flickering checkerboard is important for the functional recruitment of lateral

inhibition in the On pathway.

3.4 Discussion

Here we used synapse-specific genetic manipulations to distinguish the effects on retinal direction selectivity of GABAergic inhibition originating from different sources. We found that distinct sets of inhibitory mechanisms are recruited, depending on the properties of the background and the positive versus negative contrast of the moving object. Optimal direction selectivity of a dark object, encoded by the Off pathway, requires lateral inhibition from non-SAC amacrine cells onto Off SACs. In contrast, direction selectivity of a bright object, encoded by the On pathway, does not require lateral inhibition onto On SACs when the moving bar stimulus lies on a homogeneous background, but does require it when the bar moves on a noisy background. Together, our results highlight the multiple levels of synaptic mechanisms that underlie direction selectivity under complex visual conditions.

3.4.1 Slc32a1 KO and Gabra2 KO mice display no detectable developmental compensations

Although using conditional KO mice offers the unique advantage of achieving cell type and synapse specificity, a major concern of this genetic approach is that neural circuits may potentially be altered due to developmental compensations. In our study, we selectively remove from SACs the two genes involved in GABAergic transmission, Slc32a1 and Gabra2, during the early postnatal period (Xu et al., 2016). Therefore, we must verify that aside from loss of SAC-mediated GABA release in Slc32a1 KO mice and loss of GABAA receptors in SACs in Gabra2 KO mice, the rest of the direction selectivity circuit is not altered. To address this issue, we examined

the other known synapse types that are involved in retinal direction selectivity, including the cholinergic and GABAergic synapses between SACs and DSGCs, as well as the glutamatergic inputs onto DSGCs from bipolar cells. We found that these synapses showed no detectable changes (Pei et al., 2015 and Figure 3.4), indicating that removing GABA release or GABA receptors from SACs does not lead to compensatory developmental changes at other synapses in the direction selective circuit. We cannot discount the possibility that developmental compensation has occurred at sites not examined in this study. However, our findings are consistent with multiple previous studies that demonstrate that the early development of retinal direction selectivity is highly resistant to changes in neural activity (Chan and Chiao, 2008; Elstrott et al., 2008; Hamby et al., 2015; Sun et al., 2011; Wei et al., 2011).

After direction selectivity is established, visual experience has been shown to play a role in refining the clustered distribution of preferred directions of On-Off DSGCs (Bos et al., 2016). In both Slc32a1 KO and Gabra2 KO mice, visually evoked responses are present in all retinal neurons including SACs and pDSGCs. Furthermore, pDSGCs in both KO lines remain tuned to the posterior direction (Pei et al., 2015; data not shown). Given that all known synaptic connections in the direction selective circuit and their strengths are preserved in our conditional KO mice, we consider these mouse lines valuable tools for circuit analysis and for testing existing models.

3.4.2 The role of lateral inhibition with a simple moving bar stimulus

The On pathway

During object motion in the centripetal direction, lateral inhibition is thought to selectively suppress SAC dendritic activation via inhibitory inputs from the surround (Lee and Zhou, 2006). A major candidate source for this lateral inhibition is

GABAergic input from neighboring SACs (Lee and Zhou, 2006). However, when a bar moves against a homogeneous dark background, we found that blocking GABA release or GABA receptors of On SACs does not affect their centrifugal preference. Therefore, under this stimulus condition, lateral inhibition is not necessary for centrifugal direction selectivity of On SACs, and other mechanisms (Hausselt et al., 2007; Kim et al., 2014; Oesch and Taylor, 2010; Vlasits et al., 2016) must act to maintain it.

The Off pathway

Unlike On SACs, Off SACs are sensitive to lateral inhibition during the simple bar stimulus. Removing all GABAergic inputs onto Off SACs in Gabra2 KO mice reduces centrifugal preference. As a result, the Off component of pDSGC inhibitory inputs and spiking responses shows significantly impaired direction selectivity. This effect does not stem from SAC-SAC inhibition, since loss of this inhibition in Slc32a1 KO mice does not reduce direction selectivity of Off SACs, but rather slightly enhances it by decreasing centripetal-direction response. This indicates that the centrifugal preference of Off SAC dendrites requires additional GABAergic inputs onto Off SACs from non-SAC amacrine cells. These cells are presumably the wide-field amacrine cells that synapse onto the proximal dendrites of Off SACs and contribute about 8% of the total number of inhibitory synapses onto Off SACs identified by connectomic reconstruction (Ding et al., 2016). Though these synapses represent a small fraction of the synaptic inputs onto Off SACs, they may be sufficiently strong and efficient for shunting glutamatergic excitatory inputs that are also clustered in the proximal SAC dendrites (Vlasits et al., 2016).

We still do not know what mechanism underlies the improved selectivity of Off SACs in Slc32a1 KO mice, and if this improvement detected by calcium imaging impacts the spiking output of On-Off DSGCs. One possibility is that Off SACs also provide

GABAergic inhibition to the above-mentioned non-SAC amacrine cells. In the absence of GABA release from SACs in Slc32a1 KO mice, these non-SAC amacrine cells might be disinhibited, thus providing stronger lateral inhibition to Off SACs to decrease their centripetal-direction response. Directly testing this hypothesis requires targeted recordings from pairs of Off SACs and non-SAC amacrine cells, an experiment that is currently hindered by lack of cell type-specific markers.

We have shown here that the direction selectivity of On and Off SACs is differentially affected in both Slc32a1 KO and Gabra2 KO mice. Thus, the direction selective circuitry is not merely mirrored in the On and Off layers of the IPL, but consists of distinct sets of mechanisms in each sublamina. Our study therefore adds to others that have demonstrated differences and interactions between the On and Off pathways of the direction selective circuit (Ackert et al., 2009; Taylor and Vaney, 2002; Vlasits et al., 2014) and of other retinal circuits (Geffen et al., 2007; Tikidji-Hamburyan et al., 2014). Moreover, our study shows that GABAergic inhibition onto SACs consists of multiple facets that are engaged differently during retinal processing of positive- and negative-contrast motion.

3.4.3 The role of lateral inhibition during a moving bar stimulus against a noisy background

Lateral inhibition plays an important role in feature selection in multiple sensory systems. One elaborated form, the reciprocal inhibition between inhibitory neurons, has been described in multiple brain areas such as retina, thalamus, midbrain and cortex (Lee and Zhou, 2006; Machens et al., 2005; Miller and Wang, 2006; Papadopoulou et al., 2011). In sensory and cognitive systems, lateral inhibition motifs have been implicated in selecting the target feature in an environment when other "competi-

tor" features are present (Mysore and Knudsen, 2012; Sharpee, 2012). In the visual system, moving objects in natural scenes have backgrounds that are rarely homogeneous and stationary, but rather are spatially and temporally noisy. These can serve as "competitor" stimuli that pose challenges to the direction selective circuit for reliably detecting motion direction. We postulate that lateral inhibition onto On SACs functions to safeguard direction selectivity against a noisy environment. A noisy background increases activation of bipolar cells, which in turn provides stronger glutamatergic drive to the downstream amacrine cells including SACs. Under this condition, the lateral inhibitory network may be in a more 'primed" state to be efficiently recruited by the motion stimuli and to exert its function. In contrast, amacrine cells involved in lateral inhibition are less activated when bipolar cells adapt to the gray background, and thus the moving bar alone may not be sufficient to significantly recruit lateral inhibition in the On pathway. Consistent with this hypothesis, direction selectivity of the On response of DSGCs in Gabra2 KO mice is normal when the background is homogeneous but deteriorates as soon as white noise is introduced into the background. This findings represent an intriguing example in which additional neural mechanisms are recruited when the visual stimulus more closely resembles natural viewing conditions, but simpler visual stimuli involving only the feature of interest may not reveal the functional significance of these mechanisms (David et al., 2004; Felsen and Dan, 2005; Felsen et al., 2005; Turner and Rieke, 2016). A notable analogy has been reported in the visual cortex: a prominent inhibitory component in the receptive field of visual cortical neurons is uniquely revealed by more complex natural stimuli but is not observed with synthetic sinusoidal gratings (David et al., 2004).

3.4.4 Comparison to previous pharmacological results using GABA receptor antagonist

The role of lateral inhibition onto SACs in direction selectivity has been exclusively studied in On SACs using bath application of the GABAA receptor antagonist SR95531 with variable results (Ding et al., 2016; Euler et al., 2002; Gavrikov et al., 2006; Hausselt et al., 2007; Lee and Zhou, 2006; Oesch and Taylor, 2010; Vlasits et al., 2016). This variability may be due to a number of factors, such as species differences, conditions of visual stimulation, somatic recordings versus calcium imaging at the dendrites, and locations of varicosities along SAC dendrites. Furthermore, the effect of the antagonist cannot be attributed to specific type(s) of GABAergic synapses since GABAA receptors are extensively expressed in amacrine cells and bipolar cells in the IPL. Here, we combined pharmacology with the genetic dissection of the GABAergic circuitry to determine the synaptic loci that participate in direction selectivity. This approach allowed us to assign functional roles to different inhibitory synaptic components, and to identify a new component in the functional wiring diagram of the direction selective circuit: inhibitory inputs from non-SAC amacrine cells onto Off SACs.

Pharmacological experiments cannot establish the ultimate effect that lateral inhibition onto SACs has on the spiking output of DSGCs because SR95531 disrupts SAC-DSGC inhibition. However, by genetically eliminating GABAA receptors but not neurotransmitter release from SACs in Gabra2 KO mice, we preserved the critical synaptic connections between SACs and DSGCs, and determined the role that GABAergic inputs onto SACs play in the spiking output of DSGCs. We found that the direction selectivity of On-Off DSGC spiking decreases when SAC centrifugal preference is reduced. Therefore, the inhibitory mechanisms contributing to the centrifugal preference of SACs that we have studied here are functionally relevant for

determining the signals that are relayed from the retina to the brain.

3.5 Materials and Methods

3.5.1 Mice

The Gabra2flox/flox mouse line was a generous gift from Dr. Uwe Rudolph at Harvard Medical School. Slc32a1flox/flox mice, Chat-IRES-Cre mice and floxed td-Tomato mice were acquired from Jackson Laboratory. Drd4GFP mice were originally developed by MMRRC (http://www.mmrrc.org/strains/231/0231.html) in the Swiss Webster background, and were subsequently backcrossed to C57BL/6 background. All strains were backcrossed to the C57BL/6 background in our laboratory, and crossed to each other to create the lines used in this study. Mice of both sexes between postnatal days 18-35 were used for paired recording experiments, and those between postnatal days 24-35 were used for light response experiments. All procedures to maintain and use mice were in accordance with the University of Chicago Institutional Animal Care and Use Committee (Protocol number ACUP 72247) and in conformance with the NIH Guide for the Care and Use of Laboratory Animals and the Public Health Service Policy.

3.5.2 Preparation of isolated retina

Mice were anaesthetized with isoflurane and decapitated after dark adaptation. Under infrared illumination, retinas were isolated from the pigment epithelium at room temperature in oxygenated Ames medium (Sigma) for visual stimulation experiments or in artificial cerebrospinal fluid (ACSF) containing 119.0mM NaCl, 26.2mM NaHCO3, 11mM D-glucose, 2.5mM KCl, 1.0mM K2HPO4, 2.5mM CaCl2, and 1.3mM MgCl2 for dual patch clamp recording. Isolated retinas were then cut into

dorsal or ventral halves and mounted ganglion-cell-layer-up on top of a 1mm2 hole in a small piece of filter paper (Millipore). The orientation of the preferred direction (posterior) of Drd4-GFP positive neurons was noted for each piece. Retinas were kept in darkness at room temperature in Ames medium or ACSF bubbled with $95\%O_2$ $5\%CO_2$ until use (07h).

3.5.3 Whole-cell voltage-clamp recording

Recording electrodes of $3{\sim}5M\Omega$ were filled with a cesium-based internal solution containing 110mM CsMeSO4, 2.8mM NaCl, 4mM EGTA, 5mM TEA-Cl, 4mM adenosine 5-triphosphate (magnesium salt), 0.3mM guanosine 5-triphosphate (trisodium salt), 20mM HEPES, 10mM phosphocreatine (disodium salt), 5 mM N-Ethyllidocaine chloride (QX314), 0.025mM Alexa 488 (for SACs) and 0.025mM Alexa 594 (for pDSGCs), pH 7.25. tdTomato-labeled SACs and GFP-labeled pDSGCs were identified with epifluorescence imaging (X-Cite) or two-photon microscopy (Bruker Nano Surface Division, WI) under a water immersion objective (60x, Olympus LUMPlanFl/IR). Data were acquired using PCLAMP 10 recording software and a Multiclamp 700B amplifier (Molecular Devices), low-pass filtered at 4kHz and digitized at a sampling rate of 10kHz. Light-evoked responses were recorded at a bath temperature of $34-36\,^{\circ}\mathrm{C}$. Spontaneous IPSCs in SACs and paired SAC-SAC and SAC-pDSGC recordings were obtained at room temperature.

During paired SAC-pDSGC recordings, the evoked IPSCs and EPSCs in pDSGCs were isolated by holding the cells at reversal potentials for these conductances (0 mV for GABAergic, -60 mV for cholinergic) in the presence of 0.05mM D-AP5 and 0.05mM DNQX disodium salt. The reversal potentials were calculated and then experimentally confirmed by obtaining current-voltage (I-V) relationships of pharmacologically isolated GABAergic and cholinergic currents in pDSGCs. To measure

spontaneous IPSCs in SACs and evoked IPSCs in SAC-SAC paired recordings, 0.008 mM DHβE, 0.05mM D-AP5 and 0.05mM DNQX disodium salt were bath applied to the retinas to block NMDA-, AMPA/kainite- and nicotinic receptors. Since depolarizing SACs to 0 mV caused poorly controlled voltage-gated conductances at the beginning of the depolarizing step, we clamped the postsynaptic SACs at -80 mV to measure inward chloride currents while all excitatory channels were pharmacologically blocked. Reported potentials have been corrected for the liquid junction potential ($\sim$9 mV).

3.5.4 Analysis of whole-cell voltage clamp data

Light-evoked IPSCs in pDSGCs were isolated by holding cells at 0 mV. Three repetitions of raw synaptic traces were recorded and averaged to obtain the mean response for each stimulus condition. The peak amplitude and total charge transfer of IPSCs evoked by the leading and trailing edges of the moving bar were used to calculate the direction selective index (DSI) and vector sum. DSI is defined as $\left|\frac{(P-N)}{(P+N)}\right|$, where P is the peak amplitude or charge transfer of IPSCs in the preferred direction, and N is that in the null direction.

3.5.5 Visual stimulation

A white organic light-emitting display (OLEDXL, eMagin; 800600 pixel resolution, 60-Hz refresh rate) was controlled by an Intel Core Duo computer with a Windows 7 operating system and was presented to the retina at a resolution of 1.1 μm/pixel. Moving bar stimuli were generated by MATLAB and the Psychophysics Toolbox (Brainard, 1997), and projected through the condenser lens of the two-photon microscope onto the photoreceptor layer. For the flashing spot stimulus in Figure 3.4g, we used 10 repetitions of a 110 μm radius white spot (2s black, 2s white, 2s black) to

test On and Off responses. For the simple moving bar stimulus, a positive-contrast bar (110 μm wide, 385 μm long) moved along the long axis in 8 or 12 pseudo-randomly chosen directions at a speed of 440 μm/sec over a 660 μm -diameter field on the retina; and three to five trials were recorded for each direction. The percent stimulus contrast was calculated as $\frac{(L_{stimulus} L_{background}}{(L_{stimulus} + L_{background}}$. Unless otherwise noted (i.e., Figure 3.9d), the intensity of the moving bar was 6.3 x 104 isomerizations (R*)/rod/s, lying in the photopic range, and the background intensity was ∼1800 R*/rod/s, lying at the lower end of the photopic range. Individual checker size was 55 x 55 μm with each checkers intensity equal to either the background (0) or a white value (expressed as a percentage of the moving bar intensity) drawn from a binomial distribution. Checker pattern was updated at 15 Hz.

3.5.6 Two-photon calcium imaging of GCaMP6 fluorescence in SACs

Genetically encoded calcium indicator CCaMP6m was expressed in sparse populations of On and Off SACs by intravitreal injection of an AAV vector carrying floxed GCaMP6m (University of Pennsylvania Vector Core) into control (C) and KO mice ($Gabra2_{flox/flox}C$ and $Slc32a1_{flox/flox}$C). GCaMP6 fluorescence of isolated retinas in oxygenated Ames at $34-36\,^{\circ}$C was imaged in a customized two-photon laser scanning fluorescence microscope (Bruker). GCaMP6 was excited by a Ti:sapphire laser (Coherent, Chameleon Ultra II) tuned to 920 nm, and the laser power was adjusted to avoid saturation of the fluorescent signal. Onset of laser scanning induces a transient On response in On SACs that adapts to the baseline in ∼3s. Therefore, to ensure complete adaptation of this laser-induced response and a stable baseline, visual stimuli were given after 10s of continuous laser scanning. To separate the visual stimulus from GCaMP6 fluorescence, a band-pass filter (Semrock) was placed on the OLED to pass blue light peaked at 470 nm, while two notched filters (Bruker) were placed

before the photomultiplier tubes to block light of the same wavelength. Imaging was performed in regions of retina that contain sparsely labeled SAC varicosities so that individual varicosities could be resolved and the orientation of the dendrites relative to the soma could be determined. The objective was a water immersion objective (60x, Olympus LUMPlanFl/IR). Time series of each imaging window ($\sim$20 x 20 μm) were collected at 30-40 Hz.

3.5.7 Imaging analysis

Analysis was performed using ImageJ and MATLAB. Circular regions of interest (ROIs) corresponding to individual varicosities and a background region with no GCaMP6 expression were manually selected for each imaging window in ImageJ. The fluorescent time course of each ROI was determined by averaging all pixels within the ROI. The fluorescence of the background region was subtracted from the raw fluorescent signals of the ROIs in the same imaging window at each time frame. The resulting fluorescence measurements were then used to calculate the visually evoked responses in varicosities. The relative fluorescence change in each varicosity was taken as $\delta F = \frac{F-F_0}{F_0}$, where F is the peak amplitude of fluorescence and F_0 is the baseline fluorescence level. Mean δF was obtained by averaging 3-5 trials for each direction. To assess direction selectivity of SAC distal dendrites, we used the vector sum or direction selectivity index (DSI), defined as $\left|\frac{\delta F_{cf}-\delta F_{cp}}{\delta F_{cf}+\delta F_{cp}}\right|$, where δF_{cf} is the relative fluorescence change in centrifugal motion and δF_{cp} is that in centripetal motion. For statistical analysis, we compared variance across varicosities on the dendrites of the same SAC versus variance across varicosities of different SACs. Since the latter was larger, we averaged DSI and vector sum values of all the varicosities belonging to one SAC to get a single data point, and took N in the statistical analysis to be the number of cells, which approximately equals the number of imaging windows.

3.5.8 Two-photon targeted loose-attached recording of GFP-positive neurons for light response

The two-photon targeted recording of light responses was performed as in (Pei et al., 2015). Briefly, the retinas were perfused with oxygenated Ames at $34 - 36\,^{\circ}\mathrm{C}$. Cells were visualized with infrared light (¿900 nm) and an IR-sensitive video camera (Watec). Drd4-GFP-positive cells were identified using a two-photon microscope (Bruker Nano Surface Division) and a Ti:sapphire laser (Coherent Chameleon Ultra II) tuned to 920 nm. An electrode of 35M was filled with Ames medium for loose patch recordings of spikes. Then the electrode was carefully removed, and a new electrode filled with cesium-based internal solution and 25 μm Alexa 594 was used to fill the recorded cell. An image stack of the Alexa-488 filled pDSGC was acquired with the two-photon microscope at z intervals of 1.5 μm and was resampled three times for each z-plane using a 60x objective (Olympus LUMPlanFl/IR 60x/0.90W). Images were acquired to cover the entire dendritic field of the cell to verify the bistratified dendritic arbor and the cofasciculation with tdTomato-expressing SACs. Rarely, we encountered Drd4-GFP positive neurons that did not show the above two characteristics in both control and knockout groups. These mislabeled cells are not included in the analysis.

Data were analyzed using custom protocols in MATLAB. The number of spikes evoked by the leading (On) and trailing (Off) edges of the bar were counted using MATLAB and averaged across trials in each direction. Spiking DSI is defined as $\frac{N-pref-N_{null}}{/}N - pref + N_{null}$, where N is the number of spikes evoked by the leading or trailing edge of the moving bar.

3.5.9 Statistical analysis

Grouped data with error bars are presented as mean±SEM and tested for normality. For Figures 3.2, 3.4, 3.7 and 3.9, statistical differences were examined using one-way analysis of variance and post hoc comparisons using Students t-test with Bonferroni correction. For Figures 3.5 and 3.8, a two-sample KolmogorovSmirnov test was used and multiple comparisons were corrected by Bonferroni correction.

Author contributions

Q.C. conducted the experiments in all Figures and the data analysis. Z.P. and D.K. and W.W. conducted experiments in Figure 3.4. Q.C. and W.W. designed the experiments and wrote the paper.

Acknowledgements

We thank Chen Zhang for managing mouse colony and intravitreal injections, Dr. Uwe Rudolph from Harvard Medical School for the generous gift of the Gabra2flox/flox mouse line, and the Genetically-Encoded Neuronal Indicator and Effector (GENIE) Project and the Janelia Research Campus of the Howard Hughes Medical Institute GENIE Program and the Janelia Research Campus, specifically Vivek Jayaraman, Ph.D., Douglas S. Kim, Ph.D., Loren L. Looger, Ph.D., Karel Svoboda, Ph.D. for the AAV-GCaMP6 vectors. This work was supported by NIH R01 EY024016, E. Matilda Ziegler Foundation Grant, Whitehall Grant, Sloan Research Fellowship, Karl Kirchgessner Foundation Grant and Brinson Foundation Award. The authors declare no competing financial interests.

3.6 References

Ackert, J.M., Farajian, R., Vlgyi, B., and Bloomfield, S.A. (2009). GABA blockade unmasks an OFF response in ON direction selective ganglion cells in the mammalian

retina. J. Physiol. 587, 44814495.

Auferkorte, O.N., Baden, T., Kaushalya, S.K., Zabouri, N., Rudolph, U., Haverkamp, S., and Euler, T. (2012). GABA(A) receptors containing the 2 subunit are critical for direction-selective inhibition in the retina. PLoS One 7, e35109.

Barlow, H.B., and Hill, R.M. (1963). Selective sensitivity to direction of movement in ganglion cells of the rabbit retina. Science 139, 412414.

Barlow, H.B., and Levick, W.R. (1965). The mechanism of directionally selective units in rabbits retina. J. Physiol. 178, 477504.

Bos, R., Gainer, C., and Feller, M.B. (2016). Role for Visual Experience in the Development of Direction-Selective Circuits. Curr. Biol. 26, 13671375.

Brainard, D.H. (1997). The Psychophysics Toolbox. Spat. Vis. 10, 433436.

Brandsttter, J.H., Greferath, U., Euler, T., and Wssle, H. (2009). Co-stratification of GABAA receptors with the directionally selective circuitry of the rat retina. Vis. Neurosci. 12, 345.

Brecha, N., Johnson, D., Peichl, L., and Wssle, H. (1988). Cholinergic amacrine cells of the rabbit retina contain glutamate decarboxylase and gamma-aminobutyrate immunoreactivity. Proc. Natl. Acad. Sci. U. S. A. 85, 61876191.

Briggman, K.L., Helmstaedter, M., and Denk, W. (2011). Wiring specificity in the direction-selectivity circuit of the retina. Nature 471, 183188.

Chan, Y.-C., and Chiao, C.-C. (2008). Effect of visual experience on the maturation of ON-OFF direction selective ganglion cells in the rabbit retina. Vision Res. 48, 24662475.

Chichilnisky, E.J. (2001). A simple white noise analysis of neuronal light. 12, 199213.

David, S. V., Vinje, W.E., and Gallant, J.L. (2004). Natural Stimulus Statistics Alter the Receptive Field Structure of V1 Neurons. J. Neurosci. 24, 69917006.

Ding, H., Smith, R.G., Poleg-Polsky, A., Diamond, J.S., and Briggman, K.L. (2016). Species-specific wiring for direction selectivity in the mammalian retina. Nature 535,

105110.

Elstrott, J., Anishchenko, A., Greschner, M., Sher, A., Litke, A.M., Chichilnisky, E.J., and Feller, M.B. (2008). Direction selectivity in the retina is established independent of visual experience and cholinergic retinal waves. Neuron 58, 499506.

Euler, T., Detwiler, P.B., and Denk, W. (2002). Directionally selective calcium signals in dendrites of starburst amacrine cells. Nature 418, 845852.

Famiglietti, E. V (1983). Starburst amacrine cells and cholinergic neurons: mirror-symmetric on and off amacrine cells of rabbit retina. Brain Res. 261, 138144.

Famiglietti, E. V (1991). Synaptic organization of starburst amacrine cells in rabbit retina: analysis of serial thin sections by electron microscopy and graphic reconstruction. J. Comp. Neurol. 309, 4070.

Famiglietti, E. V. (1992). Dendritic Co-stratification of ON and ON-OFF directionally selective ganglion cells with starburst amacrine cells in rabbit retina. J. Comp. Neurol. 324, 322335.

Felsen, G., and Dan, Y. (2005). A natural approach to studying vision. Nat. Neurosci. 8, 16431646.

Felsen, G., Touryan, J., Han, F., and Dan, Y. (2005). Cortical Sensitivity to Visual Features in Natural Scenes. PLoS Biol. 3, e342.

Fried, S.I., Mnch, T. a, and Werblin, F.S. (2002). Mechanisms and circuitry underlying directional selectivity in the retina. Nature 420, 411414.

Gavrikov, K.E., Nilson, J.E., Dmitriev, A. V, Zucker, C.L., and Mangel, S.C. (2006). Dendritic compartmentalization of chloride cotransporters underlies directional responses of starburst amacrine cells in retina. Proc. Natl. Acad. Sci. U. S. A. 103, 1879318798.

Geffen, M.N., de Vries, S.E.J., and Meister, M. (2007). Retinal ganglion cells can rapidly change polarity from Off to On. PLoS Biol. 5, e65.

Hamby, A.M., Rosa, J.M., Hsu, C.-H., and Feller, M.B. (2015). CaV3.2 KO mice

have altered retinal waves but normal direction selectivity. Vis. Neurosci. 32, E003.

Hausselt, S.E., Euler, T., Detwiler, P.B., and Denk, W. (2007). A dendrite-autonomous mechanism for direction selectivity in retinal starburst amacrine cells. PLoS Biol. 5, e185.

Hoggarth, A., McLaughlin, A.J., Ronellenfitch, K., Trenholm, S., Vasandani, R., Sethuramanujam, S., Schwab, D., Briggman, K.L., and Awatramani, G.B. (2015). Specific wiring of distinct amacrine cells in the directionally selective retinal circuit permits independent coding of direction and size. Neuron 86, 276291.

Huberman, A.D., Wei, W., Elstrott, J., Stafford, B.K., Feller, M.B., and Barres, B.A. (2009). Genetic identification of an On-Off direction-selective retinal ganglion cell subtype reveals a layer-specific subcortical map of posterior motion. Neuron 62, 327334.

Kim, J.S., Greene, M.J., Zlateski, A., Lee, K., Richardson, M., Turaga, S.C., Purcaro, M., Balkam, M., Robinson, A., Behabadi, B.F., et al. (2014). Space-time wiring specificity supports direction selectivity in the retina. Nature 509, 331336.

Kittila, C.A., and Massey, S.C. (1997). Pharmacology of directionally selective ganglion cells in the rabbit retina. J. Neurophysiol. 77, 675689.

Kosaka, T., Tauchi, M., and Dahl, J.L. (1988). Cholinergic neurons containing GABA-like and/or glutamic acid decarboxylase-like immunoreactivities in various brain regions of the rat. Exp. Brain Res. 70, 605617.

Kostadinov, D., and Sanes, J.R. (2015). Protocadherin-dependent dendritic self-avoidance regulates neural connectivity and circuit function. Elife 4.

Lee, S., and Zhou, Z.J. (2006). The synaptic mechanism of direction selectivity in distal processes of starburst amacrine cells. Neuron 51, 787799.

Lee, S., Kim, K., and Zhou, Z.J. (2010). Role of ACh-GABA cotransmission in detecting image motion and motion direction. Neuron 68, 11591172.

Machens, C.K., Romo, R., and Brody, C.D. (2005). Flexible control of mutual inhi-

bition: a neural model of two-interval discrimination. Science 307, 11211124.

Miller, P., and Wang, X.-J. (2006). Inhibitory control by an integral feedback signal in prefrontal cortex: a model of discrimination between sequential stimuli. Proc. Natl. Acad. Sci. U. S. A. 103, 201206.

Mnch, T.A., and Werblin, F.S. (2006). Symmetric interactions within a homogeneous starburst cell network can lead to robust asymmetries in dendrites of starburst amacrine cells. J. Neurophysiol. 96, 471477.

Mysore, S.P., and Knudsen, E.I. (2012). Reciprocal inhibition of inhibition: a circuit motif for flexible categorization in stimulus selection. Neuron 73, 193205.

OMalley, D.M., and Masland, R.H. (1989). Co-release of acetylcholine and gamma-aminobutyric acid by a retinal neuron. Proc. Natl. Acad. Sci. U. S. A. 86, 34143418.

Oesch, N.W., and Taylor, W.R. (2010). Tetrodotoxin-resistant sodium channels contribute to directional responses in starburst amacrine cells. PLoS One 5, e12447.

Oyster, C.W., and Barlow, H.B. (1967). Direction-selective units in rabbit retina: distribution of preferred directions. Science 155, 841842.

Papadopoulou, M., Cassenaer, S., Nowotny, T., and Laurent, G. (2011). Normalization for sparse encoding of odors by a wide-field interneuron. Science 332, 721725.

Pei, Z., Chen, Q., Koren, D., Giammarinaro, B., Acaron Ledesma, H., and Wei, W. (2015). Conditional Knock-Out of Vesicular GABA Transporter Gene from Starburst Amacrine Cells Reveals the Contributions of Multiple Synaptic Mechanisms Underlying Direction Selectivity in the Retina. J. Neurosci. 35, 1321913232.

Sharpee, T.O. (2012). Adaptive switches in midbrain circuits. Neuron 73, 67.

Stincic, T., Smith, R.G., and Taylor, W.R. (2016). Time course of EPSCs in ON-type starburst amacrine cells is independent of dendritic location. J. Physiol.

Sun, L., Han, X., and He, S. (2011). Direction-Selective Circuitry in Rat Retina Develops Independently of GABAergic, Cholinergic and Action Potential Activity. PLoS One 6, e19477.

Taylor, W.R., and Vaney, D.I. (2002). Diverse synaptic mechanisms generate direction selectivity in the rabbit retina. J. Neurosci. 22, 77127720.

Tikidji-Hamburyan, A., Reinhard, K., Seitter, H., Hovhannisyan, A., Procyk, C.A., Allen, A.E., Schenk, M., Lucas, R.J., and Mnch, T.A. (2014). Retinal output changes qualitatively with every change in ambient illuminance. Nat. Neurosci. 18, 6674.

Turner, M.H., and Rieke, F. (2016). Synaptic Rectification Controls Nonlinear Spatial Integration of Natural Visual Inputs. Neuron 90, 12571271.

Vaney, D.I., and Young, H.M. (1988). GABA-like immunoreactivity in cholinergic amacrine cells of the rabbit retina. Brain Res. 438, 369373.

Vlasits, A.L., Bos, R., Morrie, R.D., Fortuny, C., Flannery, J.G., Feller, M.B., and Rivlin-Etzion, M. (2014). Visual stimulation switches the polarity of excitatory input to starburst amacrine cells. Neuron 83, 11721184.

Vlasits, A.L., Morrie, R.D., Tran-Van-Minh, A., Bleckert, A., Gainer, C.F., DiGregorio, D.A., and Feller, M.B. (2016). A Role for Synaptic Input Distribution in a Dendritic Computation of Motion Direction in the Retina. Neuron 89, 13171330.

Wei, W., Hamby, A.M., Zhou, K., and Feller, M.B. (2011). Development of asymmetric inhibition underlying direction selectivity in the retina. Nature 469, 402406.

Xu, H.-P., Burbridge, T.J., Ye, M., Chen, M., Ge, X., Zhou, Z.J., and Crair, M.C. (2016). Retinal Wave Patterns Are Governed by Mutual Excitation among Starburst Amacrine Cells and Drive the Refinement and Maintenance of Visual Circuits. J. Neurosci. 36, 38713886

4

Mutual inhibition prevents noise induced synaptic short-term depression for robust motion computation in mouse retina

4.1 Abstract

In mammalian retina, starburst amacrine cells (SACs) are critical for generating direction selectivity of On-Off direction-selective ganglion cells (DSGCs) by providing DSGCs with directionally tuned inhibition. The neurotransmission of SACs is shaped by diverse synaptic inputs from bipolar and amacrine cells. Previously, we found that GABAergic inhibition onto On SACs is important for preserving direction selectivity in the presence of background noise. Here, we study the underlying mechanisms of this noise resilience using a combination of multiphoton calcium imaging, patch clamp recording, genetic circuitry manipulation, and computational modeling. We found that the null-direction spiking of DSGCs in noisy background is enhanced in a conditional knockout mouse that lacks the $GABA_A$ receptors in SACs (*gabra2* KO). This aberrant null-direction response is associated with reduction of motion-evoked inhibitory inputs onto DSGCs in *gabra2* KO mice due to noise-induced short-term

synaptic depression at SAC-DSGC GABAergic synapses. Our results indicate that the amacrine cell (AC)-SAC-DSGC serial inhibition does not serve the conventional dis-inhibition role during noise processing. Instead, the visual noise in the background generates network dynamics that results in distinct algorithmic operations of these canonical circuit motifs for noise resilience for retinal direction selectivity.

4.2 Introduction

The capability to detect the most relevant signal, in the presence of competing noise, is crucial for the survival of animals. Natural environment is rich in noisy and often conflicting signals. How are neural circuits shaped to process sensory information encountered in natural environments? Our understanding of sensory processing has been enriched by the use of simple artificial stimuli. However, growing evidence from multiple studies highlights the importance of incorporating more naturalistic features into experimental stimuli to reveal the functional relevance of certain neural motifs (David, 2004; Felsen and Dan, 2005; Im and Fried, 2016; Sethuramanujam et al., 2016). Previous work documented that retina maintains its capability to compute motion direction in the presence of spatial or temporal noise (Chen et al., 2016; Poleg-Polsky and Diamond, 2016).

In the retina, direction selectivity is computed by the retinal direction-selective circuit. Output of this circuit is carried downstream by direction-selective ganglion cells (DSGCs) in the form of action potentials. DSGCs fires maximally to motion in certain direction (preferred direction), minimally to motion in the opposite direction (null direction) (Barlow and Hill, 1963; Barlow and Levick, 1965; Barlow et al., 1964). The asymmetric firing is generated predominantly by the direction-selective inhibition DSGCs receive from starburst amacrine cells (SACs) (Fried et al., 2002). SACs are a class of axon-less interneurons that release GABA and acetylcholine (Ach)

at distal dendrites (Euler et al., 2002; Famiglietti, 1991). One prominent feature of SACs is that they mutually inhibit each other through GABAergic synapses (Chen et al., 2016; Kostadinov and Sanes, 2015; Lee and Zhou, 2006).

Recent studies revealed that mutual inhibition regulates escaping behavior in motor system (Koyama and Pujala, 2018), and selection of most salient signal among many conflicting stimuli in auditory system (Mysore and Knudsen, 2012). In the visual system, we deployed a synapse-specific approach to study the functional role of mutual inhibition by disrupting either the GABA release or GABA reception selectively in SACs. Removal of mutual inhibition, along with GABAergic inhibition from non-SAC amacrine cells, affects direction selectivity of DSGCs in the On pathway, only during the presence of noise in the background (Chen et al., 2016). Here, we investigated how mutual inhibition generates noise resilience, using retinal direction-selective circuit as a model system. We combined electro-physiological recording, genetic manipulation, functional calcium imaging, and computational modeling, and demonstrated that mutual inhibition maintains the fidelity of retinal direction-selective circuit by preventing noise induced short-term depression in SACs.

4.3 Results

4.3.1 Removal of lateral inhibition onto SACs increases the null-direction spiking of DSGCs in noisy background

Previously we generated a conditional knock-out mouse line, Gabra2 KO, in which the $\alpha 2$ subunit of GABAA receptors (Gabra2) was selectively removed from SACs (Chen, 2016). As a result, all direct GABAergic inhibitions onto SACs are eliminated. We first determined how removal of inhibition onto SACs affects the ultimate retinal output in DSGCs. We performed loose-attach recording of pDSGCs while presenting

moving bar against either homogeneous or noisy backgrounds. The noisy background was generated from a randomly flickering checkerboard, with size of each flicker roughly matches the receptive field size of bipolar cells (Chichilnisky, 2011, Franke 2017). We found that direction selectivity of On pathway, evoked by leading edge of the bar was impaired only in the presence of noise (Chen, 2016; and Figure. 4.1a-b). This reduction in direction selectivity is mainly due to increase of spiking in response to null direction motion (Figure. 4.1c-d).

4.3.2 The EPSC onto pDSGC is glutamertagic in noisy background

The onset of bar-evoked spiking is delayed in noisy background (Figure. 4.2a). In homogeneous background, spikes are elicited when the leading edge of prefer direction moving bar is $\sim 130\ \mu m$ away from the soma. While in noisy background, the bar is $\sim 70\ \mu m$ from the soma when the first action potential is elicited in control and Gabra2 KO mice. DSGCs receive cholinergic excitation beyond its dendritic field from SACs and glutamatergic excitation within its dendritic field from bipolar cells. The relative delay of spiking onset, suggested changes in composition of excitatory post-synaptic currents (EPSCs) onto pDSGC. To test this hypothesis, we performed whole-cell voltage clamp recording in pDSGCs. No significant difference in total EPSCs onto pDSGCs was detected (4.9). Next, we isolated glutamatergic component of EPSCs by bath application of cholinergic receptors antagonist DhβE (Figure. 4.2c). In homogeneous background, bath application of DhβE reduced the EPSC amplitudes by 35%. However, in noisy background, the EPSC amplitudes are similar before and after DhβE application for the same cells (Figure. 4.2d), suggesting the absence of cholinergic component in EPSC. This change of EPSC compositions from a combination of cholinergic and glutamatergic to mostly glutamatergic agrees with the delayed onset of spiking in pDSGC.

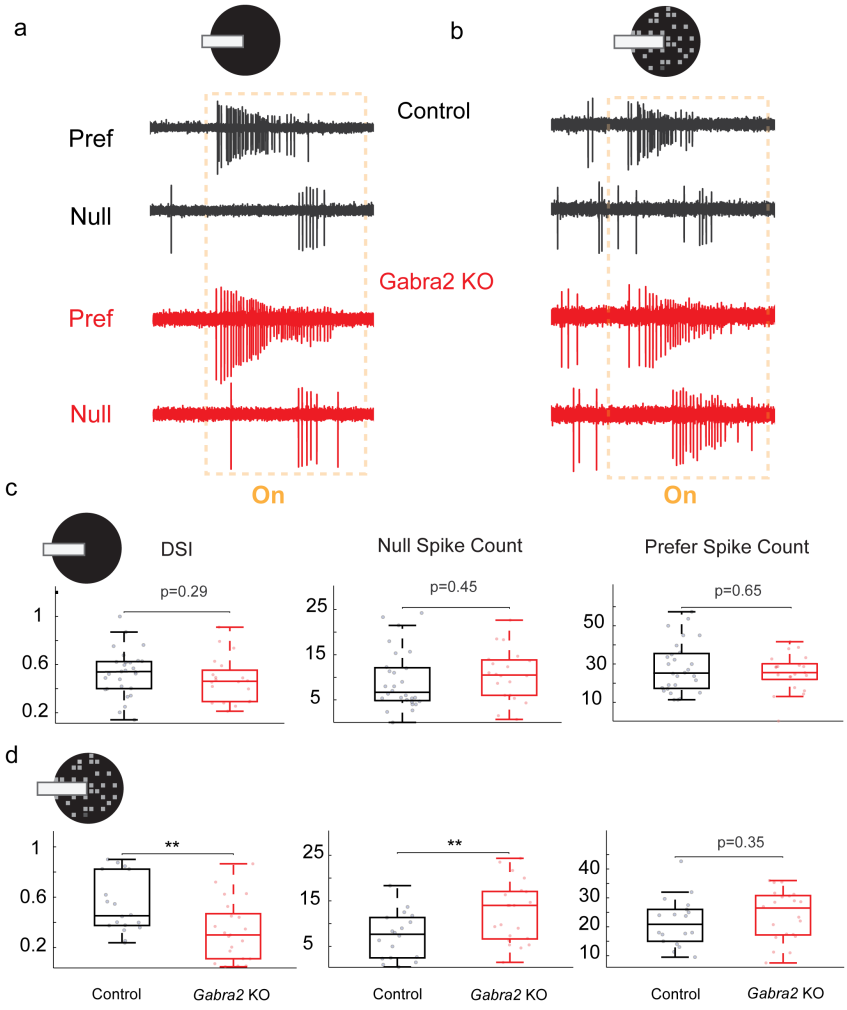

FIGURE 4.1: Lateral inhibition onto SACs minimizes null-direction DSGC spiking in noisy background.
A-B. Example loose-attach recording of pDSGCs in control (black) and Gabra2 KO (red) mouse, evoked by leading edge of moving bar against homogeneous (left) or noise background. Noise is generated as randomly flickering checker board (each checker is 55 μm x 55 μm, drew from binominal distribution, refreshed at 15Hz).
C. Summary of pDSGCs direction selectivity index (DSI) of spikes, null motion spike counts and prefer motion spike counts in homogeneous background.
D. Summary of pDSGCs DSI of spikes, null motion spike counts and prefer motion spike counts in noisy background.

4.3.3 Lateral inhibition onto SACs maintains strength of GABAergic inhibition onto DSGCs in noisy background

Next, we characterized the inhibitory inputs onto pDSGCs. We calculated the peak amplitude (Figure. 4.3c-d), as well as total charge transfer of inhibitory post-synaptic

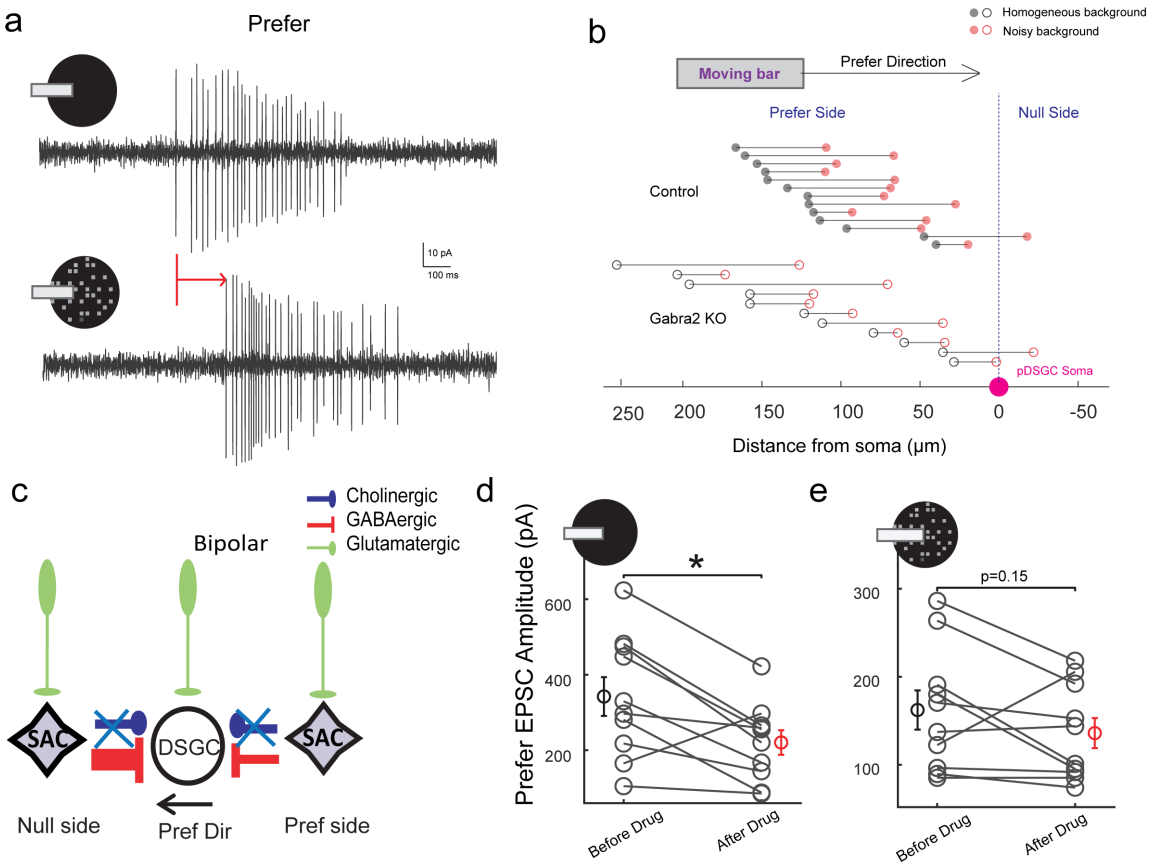

FIGURE 4.2: Excitatory drive onto pDSGC in noisy background is mostly Glutamatergic.
a.Example loose-attach recording of control mice pDSGC evoked by leading edge of moving bar in homogeneous and noisy backgrounds. Red arrow indicates the delay of onset of spiking response in noisy background.
b.Locations of leading edge of prefer direction moving bar relative to the soma (pink) of pDSGC at first spike onset time point in control (filled dots) and Gabra2 KO (hollow dots):
Control homogeneous background 127.6 $\pm$11.5 μm, control noisy background 73.0 $\pm$12.8 μm; Gabra2 KO homogeneous background 126.8 $\pm$ 21.5 μm, Gabra2 KO noisy background 74.0 $\pm$ 17.7 μm.
c.Schematic shows the side view of action loci of cholinergic receptors antagonist DhβE and identified synaptic inputs onto DSGCs. The preferred direction of DSGC is represented by black arrow.
d.Summary plot of prefer of EPSC amplitude evoked by leading edge of bar moving against homogeneous background before and after application of 0.08 μM cholinergic receptor antagonist DhβE in control mice:
Before drug 342.3$\pm$51.2 pA, after drug 220.5 $\pm$ 32.6 pA
e.Summary plot of prefer of EPSC amplitude evoked by leading edge of bar moving against noisy background before and after application of 0.08 M DhβE in control mice:
Before drug 162.2$\pm$22.3 pA, after drug 136.0$\pm$ 17.1 pA

currents (IPSCs) (Figure. 4.3 e-f), evoked by moving bar. In control group, the strength of IPSCs onto pDSGCs was not affected in noisy background compared

with that of homogeneous background (Figure. 4.3a, upper panel). In noisy background, IPSCs onto pDSGCs were significantly reduced (Figure. 4.3b) in Gabra2 KO. Together, our data suggested that removal of lateral inhibition onto SACs increases pDSGCs spiking activities by reducing IPSCs strength from SACs.

4.3.4 Lateral inhibition suppresses flickering noise induced response

In retina direction-selective circuit, AC, SAC, and DSGC form serial inhibition. The finding that disinhibiting SACs resulted in net decrease of inhibition onto DSGCs is unexcpected. The disinhibition paradigm assumes that the neurotransmission in the circuit is rather static. To identify the underlying mechanism of reduced inhibition in noisy condition, we might need to take into account the dynamic properties of neurotransmission. Since SACs release neurotransmitters in voltage-dependent manner, we first determined the SACs membrane potential kinetics during visual stimulation. We achieved this by performing whole-cell current clamp recording of SACs, using K_+ based internal. To delineate the contribution from other SACs versus non-SAC amacrine cells, we also incorporated recording from another conditional KO mice line: Vgat KO. In Vgat , the vesicular GABA transporter is selectively deleted from SACs (Pei, 2015). As a result, SACs no longer receive reciprocal inhibition from surrounding SACs while still receive inhibition from other amacrine cells.

In homogeneous background, moving bar first activated lateral inhibition that hyperpolarized the SACs when approaching soma of SAC from the surround (Figure. 4.4a-b). Then moving bar activated the excitatory center and depolarized the cell. Consistent with previous characterizations Gabra2 and Vgat KO lines, the motion-evoked surround suppression was significantly reduced in these KOs. We did not find significant difference between Gabra2 KO and Vgat KO, suggesting that surround suppression onto SACs is dominated by inhibition from surrounding SACs. Both

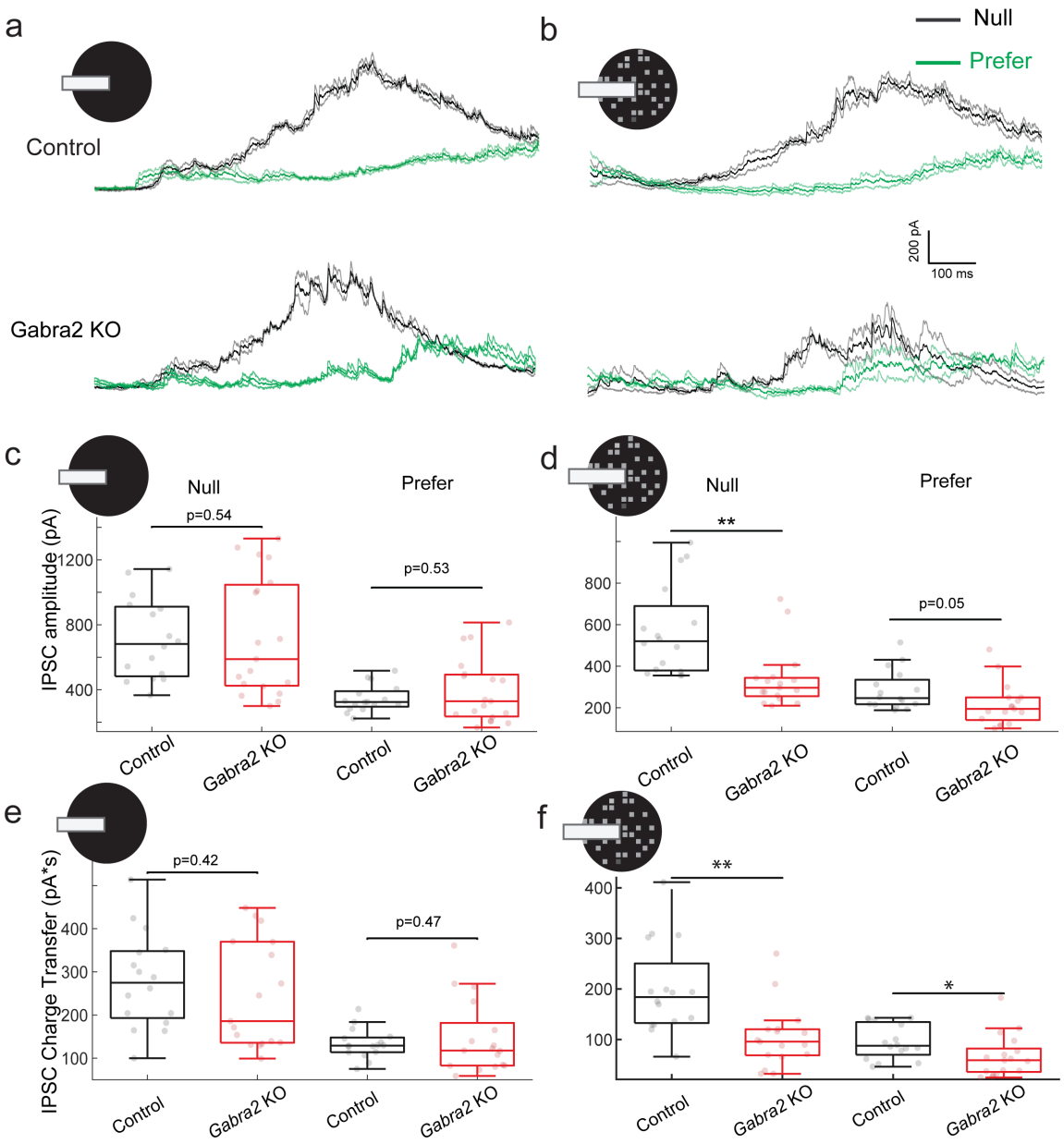

FIGURE 4.3: Reduced IPSCs onto DSGCs in Gabra2 KO in noisy background.
a.Example IPSC traces of pDSGCs evoked by moving bar against homogeneous background, in control (upper panel) and Gabra2 KO (lower panel) mice.
b.Example IPSC traces of pDSGCs evoked by moving bar against noisy background, in control (upper panel) and Gabra2 KO (lower panel) mice.
c.Summary plots of IPSC amplitudes of pDSGCs, in response to moving bar against homogeneous background.
d.Summary plots of IPSC amplitudes of pDSGCs, in response to moving bar against noisy background.
e.Summary plots of IPSC charge transfer of pDSGCs, in response to moving bar against homogeneous background.
f.Summary plots of IPSC charge transfer of pDSGCs, in response to moving bar against noisy background.

control and KOs showed similar level of bar evoked depolarization, indicating that removing inhibition onto SACs does not affect the activation of SAC receptive center. In noisy background, when moving bar reached the immediate surround of SACs dendritic field, in control mice, motion-evoked surround suppression silenced the flicker induced response. Silencing of flicker-induced responses was absent in Gabra2 and Vgat KOs (Figure. 4.4c-d). Taken together, moving stimulus recruits lateral inhibition that silences the noise induced response in control mice. Meanwhile, the similar response profile of Gabra2 and Vgat KOs suggest the silencing of noise is mediated mostly by SAC-SAC inhibition.

4.3.5 SAC-DSGC synapse exhibits short-term depression

How does suppression of flicker response by lateral inhibition in SACs affect SAC-DSGC transmission? Previously, it has been reported that SAC shows paired-pulse depression throughout development in mouse retina (Morre, 2015; but see Lee, 2010 in rabbit retina). We hypothesized that lateral inhibition maintains fidelity of neurotransmission by protecting SAC-DSGC synapse from short-term depression. To test this hypothesis, we first demonstrated that in mature retina, SAC-DSGC synapse exhibits similar short-term plasticity as during development. We performed paired-pulse recording between SAC and pDSGC pairs in control mice aged between postnatal 24 days and 60 days. We included all SAC-pDSGC pairs with overlapping dendritic arborization (inter-soma distance of 30-100 μm) with SACs located on the null side of pDSGC. SACs were depolarized by a pair of brief (20ms) voltage step of 60mv, with randomized intervals ranging from 50ms to 1600ms. SAC-DSGC synapse showed depression at shorter time interval, while recovers around interval of 1s (Figure. 4.5) within the time window that are subject to surround inhibition. So our data demonstrated the short-term plasticity in SAC-DSGC synapse in mature retina.

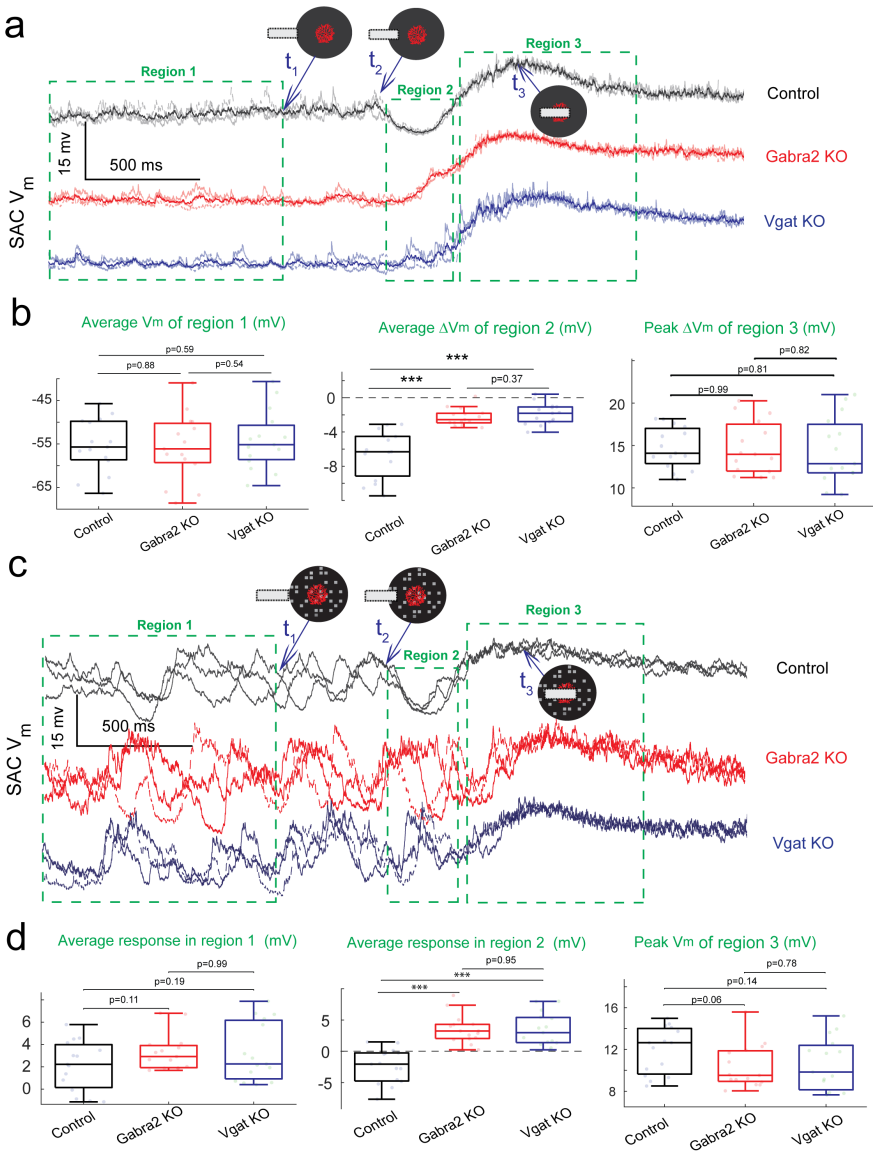

FIGURE 4.4: Lateral inhibition onto SACs shapes SACs membrane kinetics.
a.Example current-clamp recording of SACs in response to moving bar against homogeneous background: Top panel, schematics showing the location of moving bar (gray) relative to SAC (red); distance of leading edge of bar to SAC soma at t1, t2 is 330 μm, 110μm respectively.
Bottom panel, example membrane potential traces (3 sweeps, mean response depicted in thickened line) of SACs; Region 1 depicts the 1s time window recording without presentation of visual stimulus; Region 2 depicts the time window showing bar-evoke suppression; Region 3 depicts the time window of bar evoked depolarization
Region 2 is determined as $V_m < V_r - 2\tau_1$, in which V_r is the resting membrane potential computed from region 1, τ_1 is the standard deviation of membrane potential in region 1.
b.Summary plots of SACs membrane responses shown in a. Resting membrane potential, computed as average of membrane potential (liquid junction potential ~15mv corrected) in region 1
c.Example current-clamp recording of SACs in response to moving bar against noisy background
d.Summary plots of SACs membrane responses shown in c.

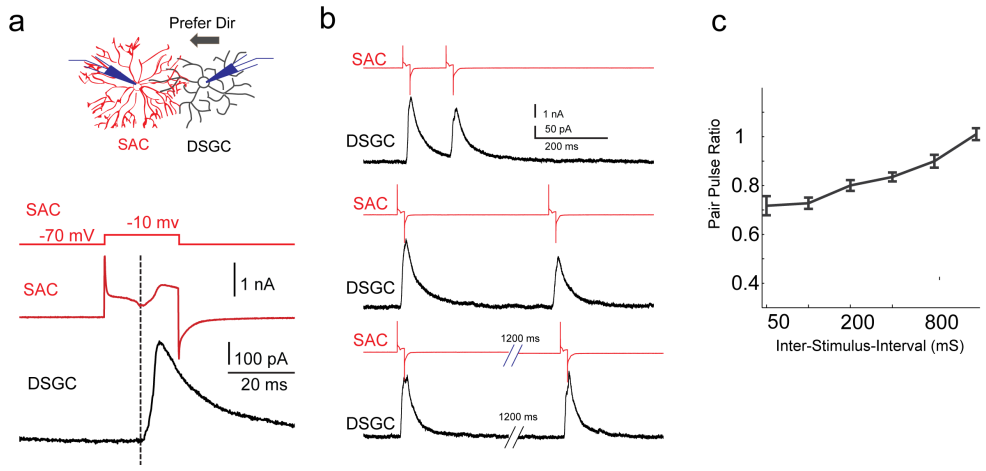

FIGURE 4.5: SAC-DSGC synapse shows paired-pulse depression
a.Voltage clamp recording from null-side SAC-pDSGC pairs in control mice showing GABAergic (black) IPSCs recorded in pDSGC by depolarizing SACs. Dashed line indicates the onset of IPSC onto pDSGC.
b.Example traces from paired-pulse protocol recording of SAC-pDSGC pair. SACs (red) were depolarized at varying timing intervals (200ms, 400ms, 1600ms). Black traces indicate the response of postsynaptic pDSGCs held at 0mv.
c.Summary (3 mice, 17 pairs) of pair-pulse depression ratio as a function of timing intervals (50,100,200,400,800,1600ms). x-axis is plot on log scale.

4.3.6 Flicker-evoked SAC activation in KO mice triggers short-term depression at SAC-DSGC GABAergic synapse, and reduces motion-evoked DSGC IPSCs

Next, we investigated the functional relevance of short-term depression during noisy visual stimulation. The experiment was designed as following: first, we mimic motion-evoked SAC membrane depolarization in paired voltage-clamp SAC-DSGC recording in control mice. Then we compared motion-evoked IPSCs onto pDSGCs when SACs are depolarized by V_m waveform recorded in noisy background in control or KO mice.

SACs release GABA in voltage dependent manner at distal dendritic tips. Thus, to mimic motion-evoked SAC GABA release through somatic depolarization, we de-

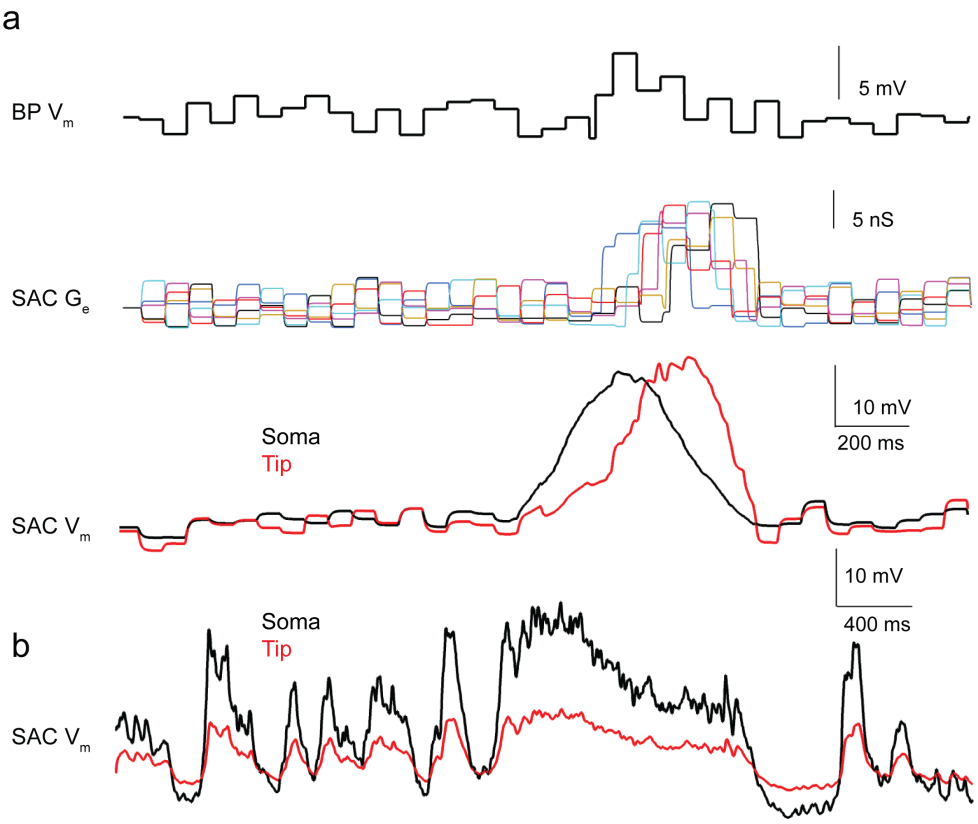

FIGURE 4.6: Modelling of dendritic attenuation of SACs.
a.Simulated SAC membrane potential kinetics at the soma versus that of the dendritic tip in response to moving bar stimuli
Upper panel: Simulated bipolar cell (BP) membrane response to moving bar;
Middle panel: Excitatory conductance (Ge) changes driven by individual BP inputs (color coded);
Lower panel: SAC membrane potential Vm response at the soma (black) or the dendritic tip (red) evoked by moving bar stimulus
b.Simulated SAC membrane potential controlled by somatic voltage clamp at the soma (black) versus the dendritic tip (red).

termined the dendritic attenuation when membrane depolarization propagates from dendritic tip towards the soma in somatic current-clamp recordings, as well as the attenuation of controlling membrane potential from soma to distal dendrites during voltage-clamp experiments. A compartmental model of the cell using morphology constructed from confocal imaging was generated with Neuron-C simulator. The excitatory inputs onto SACs was simulated as a semi-randomly spaced array of bipolar cells. Each bipolar cell receives inputs from a cone photoreceptor through inverse synapse. Unit response of photoreceptors corresponds to physiological measurement,

with realistic saturation and adaptation functions. No attenuation of motion-evoked postsynaptic potential (PSP) was observed at the soma compared with distal dendrites (Figure. 4.6a), suggesting the distal dendrites of SACs was depolarized similarly as the soma during visual stimulation. However, prominent attenuation of membrane potential exists from soma to distal dendrites in voltage clamp experiment (Figure. 4.6b). To depolarize distal dendrites of SACs to the same degree as during visual stimulation in voltage clamp experiments, we compensated the soma-to-tip attenuation by scaling the holding membrane potential waveform of SACs (Figure. 4.7a upper panel). To test the hypothesis that flicker induced response would suppress following bar-evoked response, we compared IPSCs evoked by Gabra2 KO or control waveforms of SACs. The control waveform was created by replacing the holding potential waveform immediately before (Figure. 4.7a, window 2) bar-evoked depolarization (Figure. 4.7a, window 3) in Gabra2 KO with the average membrane response from control mice which exhibits silencing of flicker-induced response by surround inhibition. The flicker induced response in SAC-DSGC pair was similar to response evoked by visual stimulation (Figure. 4.7a). However, the presence of flicker-induced response in Gabra2 KO mice, strongly suppress the following bar-evoked inhibition (Figure. 4.7a, lower panel; Figure. 4.7b, and 4.10). Therefore, our data suggested that silencing of flicker induced response by lateral inhibition onto SACs reduces the motion-evoked IPSCs onto DSGCs. Short-term depression induced at SAC-DSGC synapse in KOs recapitulated the reduction of IPSCs onto pDSGC during visual stimulation in Gabra2 KO (Figure. 4.3).

In noisy background, SAC dendritic varicosities in KO mice remain direction selective but show reduced response Next, we directly examined the effects of lateral inhibition on SAC GABA release during noisy visual stimulation by performing two-photon calcium imaging. We imaged GCaMP6 fluorescence signal in the distal 20 $30\mu m$ sector of SAC dendritic arbors evoked by a bar moving against homogeneous dark or noisy

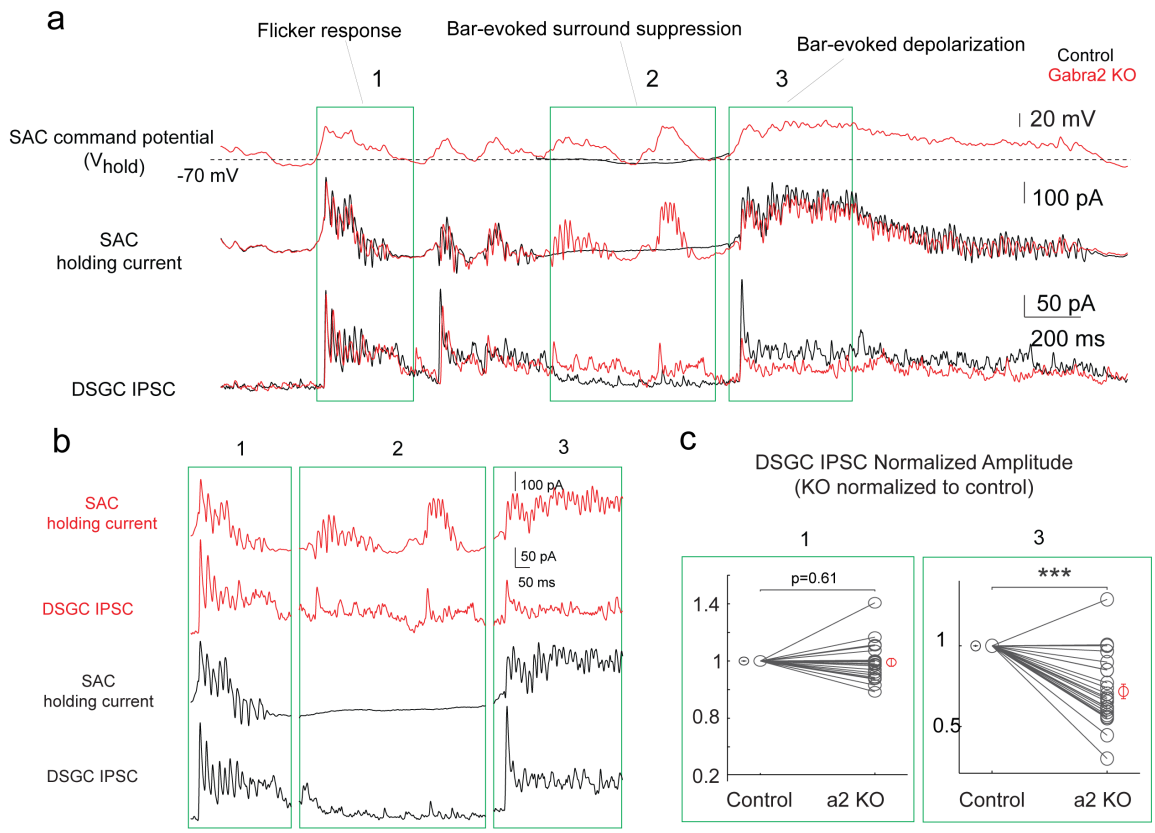

FIGURE 4.7: Flicker induced response in KO suppresses bar evoked DSGC IPSCs.
a.Example traces of SAC-DSGC paired recording
Top panel, waveform of holding membrane potential of SACs in voltage-clamp experiment, control waveform (black) generated from Gabra2 KO waveform (red) by replacing flicker induced response in region 2 (300ms) with mean response of control mice during visual stimulation at same time window;
Middle panel, holding current of SACs during voltage-clamp experiments;
Bottom panel, evoked IPSCs onto DSGC by depolarizing SACs to mimic motion-evoked response.
b.Expanded view of regions 1-3 in a.
c.Left: Summary plots of IPSCs (Response in Gabra2 KO is normalized to that of control) in regions 1 of DSGCs response. (8 mice, 23 pairs)
Right: Summary plots of IPSCs (Response in Gabra2 KO is normalized to that of control) in regions 3 of DSGCs response

backgrounds. Then we quantified the direction selectivity of SAC varicosities as well as the amplitude of fluorescence signal. The tuning of calcium transients was not affected comparing Gabra2 KO or Vgat KO to control mice, in either homogeneous or noisy background (Figure. 4.8). However, in the presence of noisy background, the amplitude of bar-evoked calcium signal is significantly reduced. Our data indicates that lateral inhibition might prevent the inactivation of calcium conductance

to regulate short-term plasticity in SACs GABA release.

4.4 Discussion

Here, we took a genetic approach and demonstrated that SAC-SAC-DSGC chain inhibition does not serve conventional disinhibition role for noise processing. SAC-DSGC synapse exhibits use-dependent short-term depression. In the presence of noise, noise-induced response could potentially suppress the following signal-evoked response. To maintain the fidelity of neurotransmission for robust direction selectivity, mutual inhibition motif among SACs is activated.

4.4.1 Role of excitation during bar moving against noisy background

In noisy background, the amplitude and total charge transfer of EPSCs onto pDSGC are similar in control and Gabra2 KO mice. Since DSGCs receive glutamatergic excitation from bipolar cells and cholinergic excitation from SACs. Further pharmacological blockade to isolate individual components of EPSCs showed that the EPSCs onto pDSGC are mediated by bipolar glutamatergic inputs, instead of cholinergic inputs from SACs, in noise condition. This finding is consistent with the delayed onset of spiking in noisy background. Bipolar cells adapt to homogeneous luminance or contrast changes rapidly ($\sim$0.1s, Baccus 2002). As a result, SACs are less activated when bipolar cells adapt to homogeneous background, therefore the mutual inhibition motif is less recruited in homogeneous condition. Non-homogeneous background stimuli, however, prevents the fast adaption of bipolar cells and increases the activation of SACs. In fact, current clamp recording from SACs shown strong responses to flicker-only stimulation, indicates robust activation of presynaptic bipolar cells. SACs are known to release both Ach and GABA onto DSGCs, the finding that in noisy background, SACs-DSGC transmission is mostly GABAergic is consistent

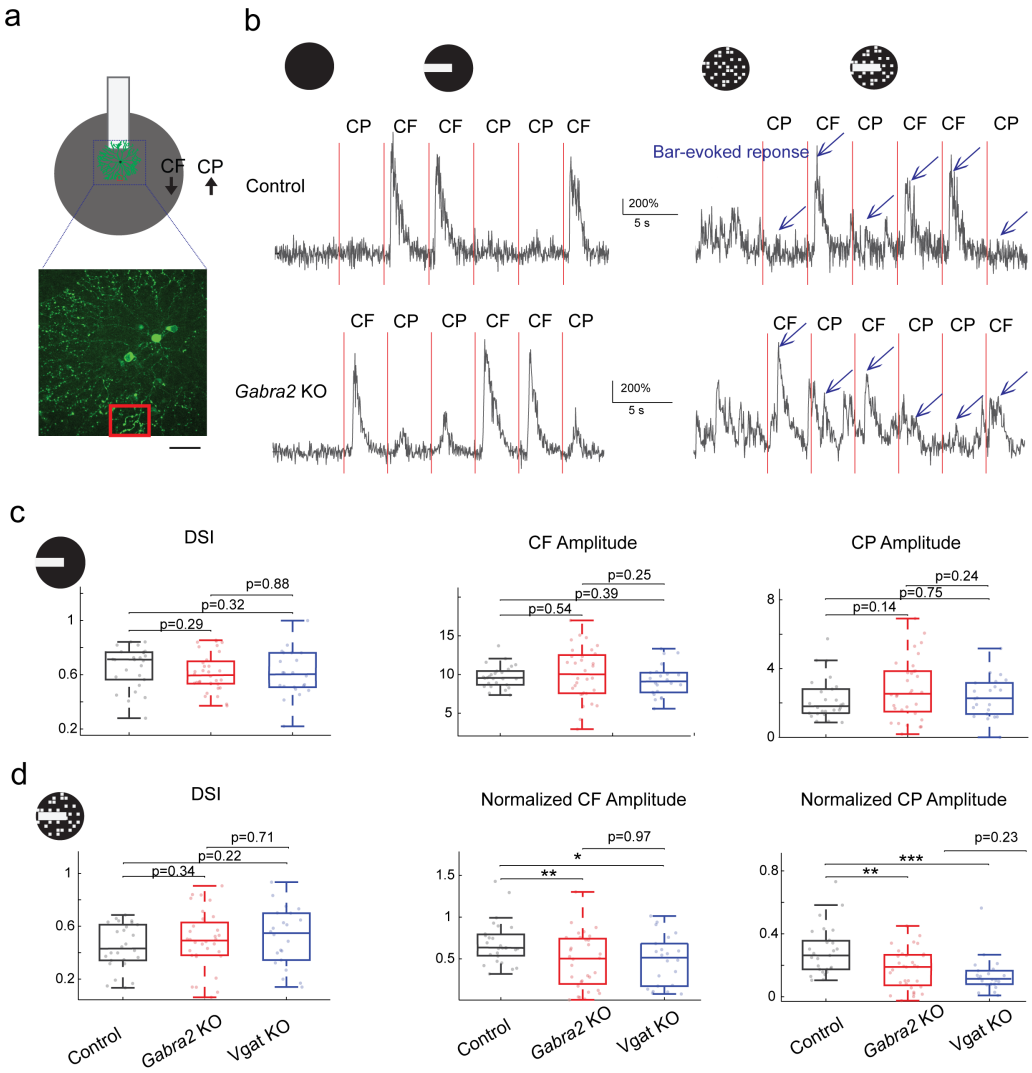

FIGURE 4.8: Reduced calcium response of SAC varicosities in KOs during noisy stimuli.
A. Upper panel: schematic of bar moving against backgrounds used during calcium imaging of SAC distal varicosities. Red square indicates the imaging window. For varicosities in the imaging window, upward motion corresponds the null (centripetal, acronym CP) direction and downward motion is the preferred (centrifugal, acronym CF) direction;
Lower panel: maximal intensity projection of GCaMP6m fluorescence of SAC dendrites from control mice. Scale bar: 30 μm.
B. Example GCaMP6m fluorescence traces from control and Gabra2 KO mice during backgrounds only or bar moving against backgrounds stimulation. Blue arrow indicates the bar evoked response. Red line indicates the time point that bar starts to move towards the imaging regions from surround ($330\mu m$)
C. Summary graph for DSI, centrifugal amplitude, centripetal amplitude of fluorescence signal in response to moving bar against homogeneous background in control and Gabra2 KO and vgat KO mice.
D. Summary graph for DSI, centrifugal amplitudes, centripetal amplitudes of fluorescence signal in response to moving bar against noisy background in control and Gabra2 KO and vgat KO mice. Fluorescence amplitudes are normalized to CF response evoked by bar against homogeneous background for the same varicosities.

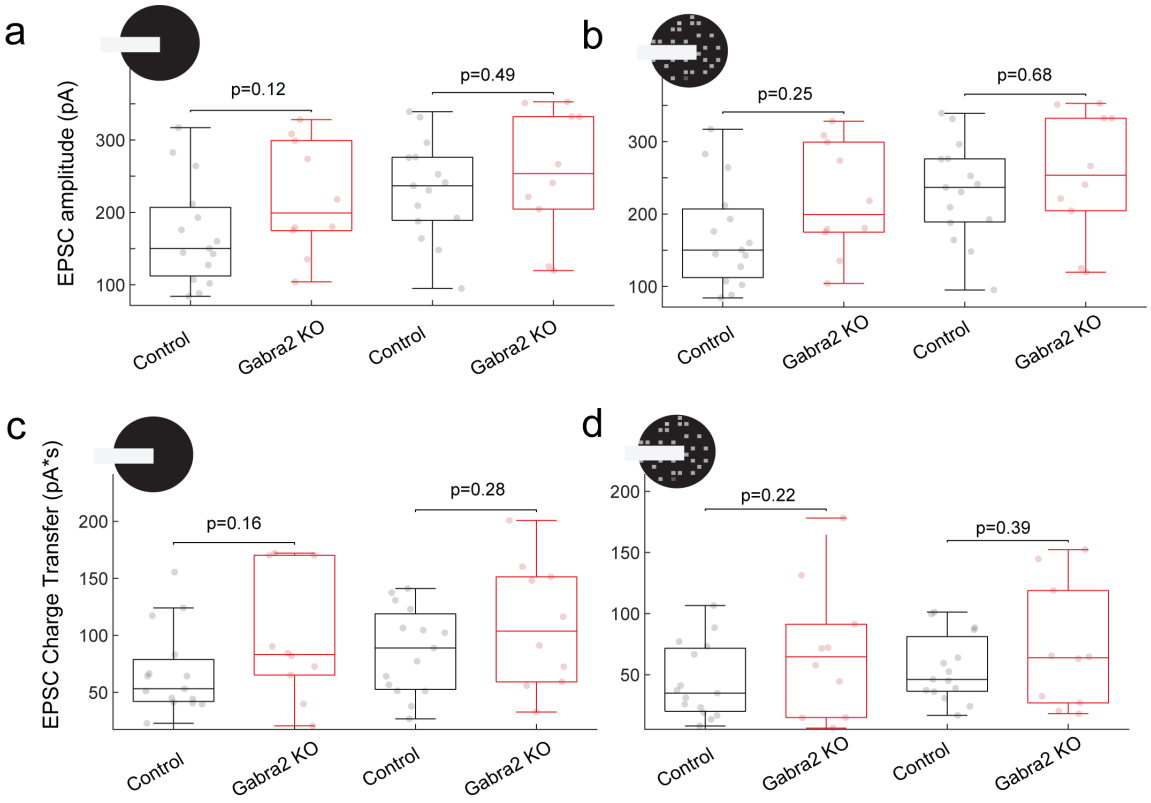

FIGURE 4.9: EPSCs onto pDSGC are not affected in Gabra2 KO during noisy stimulus. a-b. Summary plots of EPSC amplitudes of pDSGCs, in response to moving bar against homogeneous or noisy background, in control (black) or Gabra2 KO (red) mice.
c-d. Summary plots of EPSC charge transfer of pDSGCs, in response to moving bar against homogeneous or noisy background, in control (black) or Gabra2 KO (red) mice.

with previous finding that GABA and Ach release is differentially regulated in SAC, as Ach requires higher $[Ca_{2+}]$ for release (Lee 2010).

4.4.2 Functional role of use-dependent short-term depression in SACs

SACs undergo paired-pulse depression for GABA and Ach release. However, the functional significance of the short-term depression is less clear. While, use-dependent depression in photoreceptors and bipolar terminals has been suggested as cellular mechanism for adaptation during luminance or contrast changes (Demb 2008). Recent study proposed that short-term depression in amacrine cells contributes to sensitization, which compensates for information loss during adaptation (Kastner 2013).

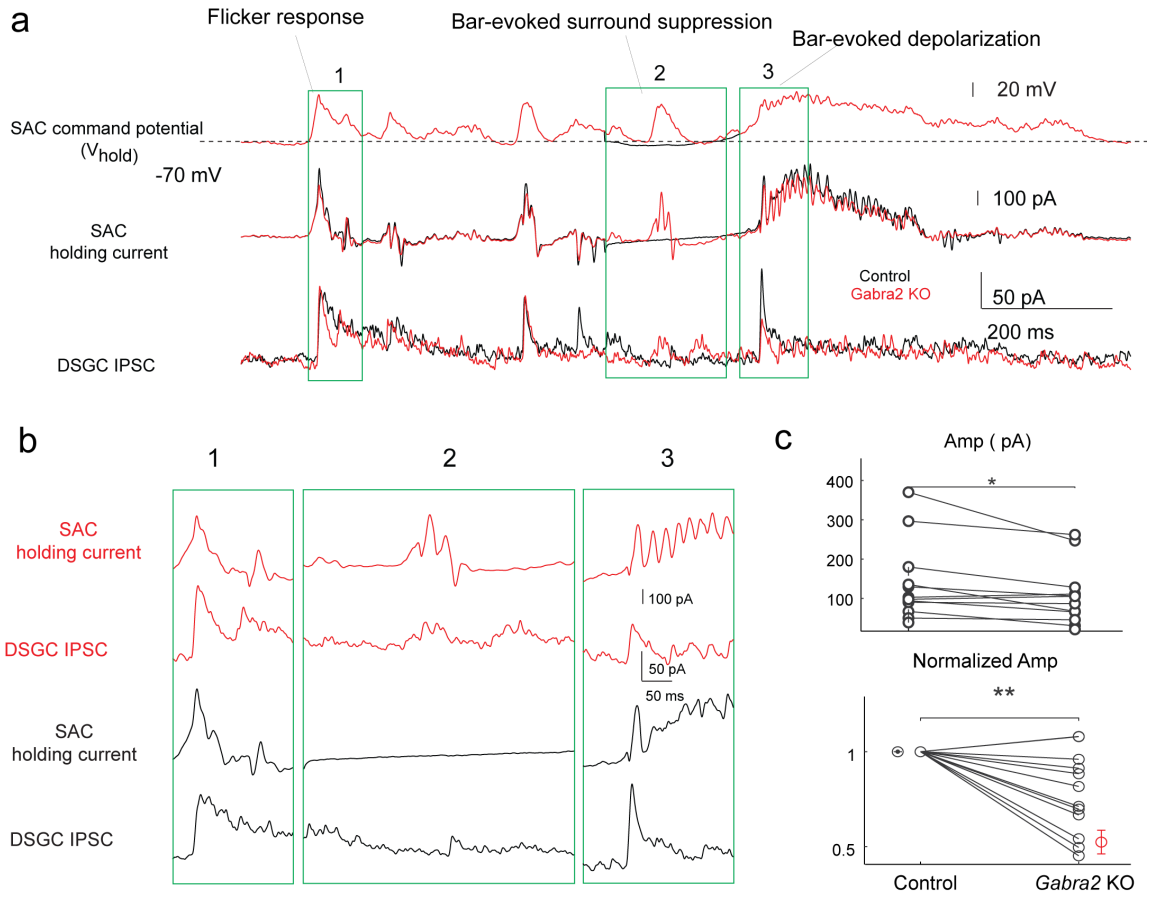

FIGURE 4.10**:** Flicker response in KO suppresses bar evoked DSGC IPSCs using different SACs membrane waveform.
a.Example traces of SAC-DSGC paired recording using a different waveform than Figure. 4.6
Top panel, waveform of holding membrane potential of SACs in voltage-clamp experiment, control waveform (black) generated from Gabra2 KO waveform (red) by replacing flicker response in region 2 (300ms) with mean response of control mice during visual stimulation at same time window;
Middle panel, holding current of SACs during voltage-clamp experiments;
Bottom panel, evoked IPSCs onto DSGC by depolarizing SACs to mimic motion-evoked response.
b.Expanded view of regions 1-3 in a.
c.Left: Summary plots of IPSCs response amplitudes in region 3.
Control 143.8±23.9 pA, KO 110.6 ±16.9 pA,
Right: Summary plots of normalized IPSC amplitudes (Response in Gabra2 KO is normalized to that of control)

However, in the scenario of multiple conflicting stimuli, competing stimuli-induced short-term depression in SACs results in more null direction spiking in DSGCs, which impairs the fidelity of direction selectivity. Given only the inhibitory inputs onto DSGCs are affected by noise induced short-term depression in noisy background. Taken together, these findings imply that for the short-term depression to sensitize the direction selective circuit, while maintain the fidelity of direction selectivity, a fine balance of excitation/inhibition should be maintained .

4.5 Materials and Methods

4.5.1 Animals

The C57BL/6 wild-type (WT) or transgenic mice of either sex were used in this study. The $Gabra2^{flox/flox}$ mouse line was a generous gift from Dr. Uwe Rudolph at Harvard Medical School. Loxp flanked Slc32a1 ($vgat^{flox/flox}$) mice, Chat-IRES-Cre mice and floxed tdTomato mice were originally acquired from the Jackson Laboratory. Drd4GFP mice were initially developed by MMRRC in the Swiss Webster background, and were subsequently backcrossed to C57BL/6 background. All strains in our laboratory were crossed to C57BL/6 background and crossed with each other to create the lines used in the study. Mice of both sexes aging from postnatal 21 to 60 days were used in the experiments. All procedures to maintain and use mice were in accordance with the University of Chicago Institutional Animal Care and Use Committee (Protocol number ACUP 72247) and in conformance with the NIH Guide for the Care and Use of Laboratory Animals and the Public Health Service Policy.

4.5.2 Whole-mount retina preparation

The procedures of isolating the retina from pigment epithelium has been previously described (Wei, 2010). In short, mice were dark adapted for at least 45 minutes, anaesthetized with isoflurane, then decapitated. The retina was then isolated under infrared illumination at room temperature in oxygenated $95\%O_2$ $5\%CO_2$ Ames medium (Sigma-Aldrich, St. Louis, MO). Isolated retinas were then cut into dorsal or ventral pieces and mounted on top of a 1mm2 hole in small piece of filter paper (Millipore, Billerica, MA) with ganglion-cell-layer up. The orientation of prefer direction (posterior) of Drd4-GFP positive cells was labelled for each piece. Retinas were kept in darkness at room temperature in oxygenated Ames medium until use (0-8 hrs).

4.5.3 Visual stimulation

A white organic light-emitting display (OLEDXL, eMagin, Bellevue, WA; 800 x 600 pixel resolution, 60 Hz refresh rate) was controlled by an Intel Core Duo computer with Windows 7 operating system and presented to the retina at 1.1 m/pixel resolution. Moving stimulus were generated by MATLAB and Psychophysics Toolbox (Brainard, 1997), and focused through the condenser lens of microscope to the photoreceptor layer. Positive contrast bar (220 μm wide, 440 μm long) moved along long axis and was presented in 8 or 12 pseudo-randomly chosen directions at a speed of 440 μm/sec over a 660 m-diameter field on the retina. Three to five trials were recorded for each moving direction. The intensity of the moving bar was $\sim 6.3 \cdot 10^4$ isomerization (R*)/rod/s, in the photopic range. For homogeneous background, the intensity of background is 1800 R*/rod/s, lying at the lower end of photopic range. For noisy background, the noise was generated as randomly flickering checker. Individual checker was 55 μmx55 μm in size, with intensity at either background (0)

or $\sim 1 \cdot 10^4$ R*/rod/s drawn from a binomial distribution. The checker pattern was refreshed at 15 Hz.

4.5.4 Two-photon guided recording of fluorescence-positive neurons for light response

The retinas were perfused with oxygenated Ames at $34 - 36\,^{\circ}$C during recordings. Drd4-GFP positive pDSGCs or td-Tomato positive SACs were identified using a two-photon microscope (Bruker Nano Surface Division) and a Ti: sapphire laser (Coherent Chameleon Ultra II) tuned to 920 nm. Then cells were visualized with infrared light (>900 nm) and an IR-sensitive video camera (Watec). The inner limiting membrane was removed by an empty glass electrode to expose the targeted cell. For loose-attach recording of spikes, an electrode of 3-5 MΩ was filled with filtered Ames medium. For voltage-clamp whole cell recording, recording electrode was filled with a cesium-based internal solution containing 110 mM CsMeSO4, 2.8 mM NaCl, 4 mM EGTA, 5 mM TEA-Cl, 4 mM adenosine 5-triphosphate (magnesium salt), 0.3 mM guanosine 5-triphosphate (trisodium salt), 20 mM HEPES, 10 mM phosphocreatine (disodium salt), 5 mM N-Ethyllidocaine chloride (QX314), 0.025 mM Alexa 488 (for SACs) and 0.025 mM Alexa 594 (for pDSGCs), pH 7.25. Light evoked IPSCs and EPSCs onto pDSGCs were isolated by holding at 0 mv and -60 mv respectively. For current-clamp whole cell recording, recording electrode was filled with a K+ based internal containing 120 mM KMeSO4, 10 mM KCl, 0.07 mM CaCl22H2O, 10 mM HEPES, 0.1 mM EGTA, 2 mM adenosine 5-triphosphate (magnesium salt), 0.4 mM guanosine 5-triphosphate (trisodium salt), 10 mM phosphocreatine (disodium salt). Data were acquired using Multiclamp 700B amplifier, and Digidata 1500A or Digidata 1400B digitizer (Molecular Devices, Sunnyvale, CA) and PClamp 10 software. The data was low-pass filtered at 4 kHz, and digitized at sampling rate of 10 kHz.

4.6 Neuron-C simulation of SACs

The NeuronC simulator generated a compartmental model of the cell using the morphology reconstructed from a confocal stack (Smith, 1992). The electrotonic length of the compartments was set to a short increment (¡0.02λ) to preserve accuracy. SBACs receive tonic excitatory input under steady background illumination that produces an inward current of 2040 pA at 70 mV. We modelled the excitatory input as an array of bipolar cells (n = 140170; density 7500 mm^2; semirandom regularity mean/SD = 8). Each bipolar cell was simulated as a single compartment, and made a synapse onto the closest dendrite of the SBAC if it was within a criterion distance (typically $\approx$ 15 μm). In order to model the experimental responses, an electrode comprising a series resistor and a capacitor was connected to the soma of the model. A fourth order Bessel filter was simulated to reproduce the lowpass filter in the recording system. The first step was to obtain estimates of the surface membrane resistivity (R_m), the cytoplasmic resistivity (R_i), the specific membrane capacitance (C_m), the electrode series resistance (R_s) and the electrode capacitance (C_e).

4.6.1 First spike latency detection

To compute the latency of first spike onset, a binless algorithm was adapted (Chase and Young, 2007). This algorithm is used to distinguish bar-evoked spikes from spontaneous spikes, under the assumption that spontaneous firing follows Poisson statistics. In short, spikes from N sweeps are collapsed into one single sweep. The probability of observing at least n spikes in time window t_n by chance is given by:

$P_{t_n}(\geqslant n) = 1 - \sum_{m=0}^{n-1} \frac{(N\lambda t_n)^m \cdot e^{-N\lambda t_n}}{m!}$

Where λ is the spontaneous firing rate of the neuron, computed from a 500 ms time window before onset of stimulus. The first time at which the probabilities exceeds a threshold of 10^{-6}s marked as the latency of neuron to the leading edge of moving

bar. Then the spike latency t was converted to distance d from soma by: $d = r - vt$; Where r is the moving radius, v is speed of moving bar.

4.6.2 Dual whole-cell patch-clamp recording

Dual whole-cell voltage clamp recording between SACs and pDSGCs was performed in oxygenated Ames medium at $34 - 36\,^{\circ}$C in the presence a cocktail of 0.05 mM D-AP5, 0.02 mM DNQX disodium salt, and 0.005 mM L-AP4. Neurons were visualized with transmitted visible light from a halogen bulb. The prefer direction of pDSGCs was noted using methods described before (Wei 2010) for each piece. tdTomato positive SACs and Drd4-positive pDSGCs were identified with epifluorescence imaging (X-Cite) under a water immersion 60x objective. SACs located on the null side of pDSGC with overlapping dendritic area (inter-soma distance 30-100 μm) were selected for paired recording with pDSGC. Evoked IPSCs onto pDSGCs were isolated by holding pDSGC at 0mv. For paired recording between SACs and pDSGCs to mimic light evoked response in pDSGC, holding waveforms of SACs were selected from exemplary current-clamp recording of SACs during visual stimulation. The waveform was scaled 4 times to compensate for dendritic attenuation to mimic the membrane kinetics at SACs distal tip during somatic voltage-clamp. Only recordings with series resistances $< 20\text{M}\Omega$, and ratio of membrane resistance to series resistance > 10 were included.

4.6.3 Two-photon calcium imaging of GCaMP6 fluorescence in SACs

The procedures have been described previously (Chen, 2016). Genetically encoded calcium indicator GCaMP6m was expressed sparsely in On SACs by intravitreal injection of AAV vector carrying floxed GCaMP6m (University of Pennsylvania Vector Core) into control, Gabra2 KO, or vgat KO mice retina. Isolated retina was perfused with oxygenated Ames medium at $34-36\,^{\circ}$C during the experiments. GCaMP6

fluorescence was imaged in two-photon laser scanning microscope (Bruker Nano Surface Division), excited by Ti: Sapphire laser (Coherent, Chameleon Ultra II, Santa Clara, CA) tuned to 920 nm. The laser power was adjusted to excite fluorescent signal while avoid saturation. Visual stimulus was presented as described above through condenser lens to photoreceptor layer. To separate visual stimulus from fluorescence signal, a customized band-pass filter (Semrock, Rochester, MA) was placed between top of condenser lens to pass blue light peaked at 470 nm, while two notched band-pass filters peaked at 525 nm and 630 nm were placed in front of photomultiplier tubes to pick up green and red light respectively. Imaging window (20 μm x 20 μm) was selected from regions of the retina that contains sparsely labelled SAC varicosities so that individual varicosities could be resolved and orientation of dendrites relative to the soma could be determined. Time series of each imaging window were collected at 30∼50 Hz sampling rate. Onset of laser scanning induces a fluorescence transit that adapts to the baseline after ∼3s. So visual stimuli and were given after at least 6s of continuous laser scanning.

4.6.4 Calcium imaging analysis

Analysis of calcium signal was performed offline in ImageJ and customized scripts in MATLAB. Elliptical regions of interest (ROI) were manually selected corresponding to SAC varicosities and background region. The fluorescence time course of each ROI was computed as the average pixel intensity within the ROI for each frame. The fluorescence of background was then subtracted from signals of the ROIs within the same imaging window at each frame. The result fluorescence was then used to compute the relative fluorescent for each varicosity, was taken as $\delta F = \frac{F-F_0}{F_0}$, where F is the peak amplitude of fluorescence and F_0 is the baseline fluorescence intensity before visual stimulation. The stimulus onset was triggered by TTL voltage pulse

generated by Psychophysics Toolbox in MATLAB. The voltage pulse was recorded by Prairie View software and subsequently used to clip the fluorescence time series into individual sweeps. These recording sweeps were then sorted for motion direction for further analysis. The peak amplitude of fluorescence change was computed as local maximum of a 1.5s time window following onset of moving stimulus. To assess direction selectivity of SAC distal dendrites, we used the vector sum or direction selectivity index (DSI), defined as $\left|\frac{\delta F_{cf}-\delta F_{cp}}{\delta F_{cf}+\delta F_{cp}}\right|$, where δF_{cf} is the relative fluorescence change in centrifugal motion and δF_{cp} is that in centripetal motion.

4.6.5 Statistical Analysis

Grouped data in Figure 4.1-3,7 were presented in boxplot, with the central mark indicates the median and the lower and upper edges of the box indicates 25%, and 75% of the data respectively. Grouped data in Figure 4,6 were presented as mean ± S.E.M. Statistical test was performed for each grouped data using metrics noted for each figure in MATLAB.

4.7 References

Baccus, S.A., and Meister, M. (2002). Fast and slow contrast adaptation in retinal circuitry. Neuron 36, 909919.

Barlow, H.B., and Hill, R.M. (1963). Selective Sensitivity to Direction of Movement in Ganglion Cells of the Rabbit Retina. Science (80-.). 139, 412412.

Barlow, H.B., and Levick, W.R. (1965). The mechanism of directionally selective units in rabbits retina. J. Physiol. 178, 477504.

Barlow, H.B., Hill, R.M., and Levick, W.R. (1964). Retinal ganglion cells responding selectively to direction and speed of image motion in the rabbit. J. Physiol. 173,

377407.

Chase, S.M., and Young, E.D. (2007). First-spike latency information in single neurons increases when referenced to population onset. PNAS 104, 51755180.

Chen, Q., Pei, Z., Koren, D., and Wei, W. (2016). Stimulus-dependent recruitment of lateral inhibition underlies retinal direction selectivity. Elife 5.

Chichilnisky, E.J. (2001). A simple white noise analysis of neuronal light responses. Network 12, 199213.

David, S. V. (2004). Natural Stimulus Statistics Alter the Receptive Field Structure of V1 Neurons. J. Neurosci. 24, 69917006.

Demb, J.B. (2008). Functional circuitry of visual adaptation in the retina. In Journal of Physiology, pp. 43774384. Euler, T., Detwiler, P.B., and Denk, W. (2002). Directionally selective calcium signals in dendrites of starburst amacrine cells. Nature 418, 845852.

Famiglietti, E. (1991). Synaptic organization of starburst amacrine cells in rabbit retina: analysis of serial thin sections by electron microscopy and graphic reconstruction. J. Comp. Neurol. 309, 4070.

Felsen, G., and Dan, Y. (2005). A natural approach to studying vision. Nat. Neurosci. 8, 16431646.

Franke, K., Berens, P., Schubert, T., Bethge, M., Euler, T., and Baden, T. (2017). Inhibition decorrelates visual feature representations in the inner retina. Nature 542, 439444.

Fried, S.I., Mnch, T.A., and Werblin, F.S. (2002). Mechanisms and circuitry underlying directional selectivity in the retina. Nature 420, 411414.

Gold, J.I., and Shadlen, M.N. (2007). The Neural Basis of Decision Making. Annu. Rev. Neurosci. 30, 535574. Im, M., and Fried, S.I. (2016). Directionally selective retinal ganglion cells suppress luminance responses during natural viewing. Sci. Rep. 6.

Kastner, D.B., and Baccus, S.A. (2013). Spatial segregation of adaptation and predictive sensitization in retinal ganglion cells. Neuron 79, 541554.

Kostadinov, D., and Sanes, J.R. (2015). Protocadherin-dependent dendritic self-avoidance regulates neural connectivity and circuit function. Elife 4.

Koyama, M., and Pujala, A. (2018). Mutual inhibition of lateral inhibition: a network motif for an elementary computation in the brain. Curr. Opin. Neurobiol. 49, 6974.

Lee, S., and Zhou, Z.J. (2006). The Synaptic Mechanism of Direction Selectivity in Distal Processes of Starburst Amacrine Cells. Neuron 51, 787799.

Lee, S., Kim, K., and Zhou, Z.J. (2010). Role of ACh-GABA Cotransmission in Detecting Image Motion and Motion Direction. Neuron 68, 11591172.

Machens, C.K., Romo, R., and Brody, C.D. (2005). Flexible control of mutual inhibition: A neural model of two-interval discrimination. Science (80-.). 307, 11211124.

Morrie, R.D., and Feller, M.B. (2015). An Asymmetric Increase in Inhibitory Synapse Number Underlies the Development of a Direction Selective Circuit in the Retina. J. Neurosci. 35, 92819286.

Mysore, S.P., and Knudsen, E.I. (2012). Reciprocal Inhibition of Inhibition: A Circuit Motif for Flexible Categorization in Stimulus Selection. Neuron 73, 193205.

Poleg-Polsky, A., and Diamond, J.S. (2016). NMDA Receptors Multiplicatively Scale Visual Signals and Enhance Directional Motion Discrimination in Retinal Ganglion Cells. Neuron 89, 12771290.

Sethuramanujam, S., McLaughlin, A.J., deRosenroll, G., Hoggarth, A., Schwab, D.J., and Awatramani, G.B. (2016). A Central Role for Mixed Acetylcholine/GABA Transmission in Direction Coding in the Retina. Neuron 90, 12431256. Sharpee, T.O. (2012). Adaptive Switches in Midbrain Circuits. Neuron 73, 67.

Stincic, T., Smith, R.G., and Taylor, W.R. (2016). Time course of EPSCs in ON-type starburst amacrine cells is independent of dendritic location. J. Physiol. 594,

56855694.

Smith, R.G. (1992). NeuronC: a computational language for investigating functional architecture of neural circuits. J. Neurosci. Methods 43, 83108.

Taylor, W.R., and Vaney, D.I. (2002). Diverse synaptic mechanisms generate direction selectivity in the rabbit retina. J. Neurosci. 22, 77127720.

Tukker, J.J., Taylor, W.R., and Smith, R.G. (2004). Direction selectivity in a model of the starburst amacrine cell. Vis. Neurosci. 21, 611625.

5

Synaptic and circuitry mediation of fine-time scale excitation-inhibition covariation for robust retinal direction selectivity

5.1 Abstract

Direction-selective retinal ganglion cells (DSGCs) encode motion direction by firing maximally to certain direction of motion (prefer direction) and minimally to motion in the opposite (null) direction. The silence towards null stimuli depends on the veto of excitation by inhibition onto DSGCs. While noise could contaminate the reliability of this vetoing process, correlated noise, however, could allow inhibitory fluctuation to cancel excitatory fluctuation in a timely manner. Such covariation of excitation and inhibition could arise from shared origins of excitation and inhibition in the circuitry. Both theoretical and experimental works have demonstrated the importance of this covariation for retinal direction selectivity. Less is known about the implementation and regulation of covariation of noise. In this work, we adopted a protocol to record inhibitory and excitatory fluctuation simultaneously. By combining genetic perturbation and pharmacology, we dissected the functional substrates

of synaptic covariation in retinal direction-selective circuit.

5.2 Introduction

The notion that computing of motion direction first arises in the retina starts since Hartlines work (Hartline, 1938). Since then, retinal direction-selective circuit has emerges one of the preferred model systems for understanding circuit-function relationship (Mauss et al., 2017). The output neurons of the circuit, direction-selective ganglion cells (DSRGCs) encode preferred motion direction by firing maximally while remains relative silent towards null direction motion (Barlow and Hill, 1963; Barlow and Levick, 1965; Barlow et al., 1964). The silencing of spikes towards null motion is generated by vetoing of excitation by strong inhibition DSGC receives (Fried et al., 2002; Taylor and Vaney, 2002). However, fluctuation from synaptic or stimulus noises could generate unwanted spikes in the null direction. Recently, it has been reported that retinal direction selective circuit exhibits stimulus dependent covariation between excitation and inhibition, in which the covariation is maximal in the null direction (Brinkman et al., 2016; Cafaro and Rieke, 2010). Theoretical studies indicated that the covariation could arise from shared origins of excitation and inhibition (Brinkman et al., 2016). In the retinal direction selective circuit, there are two major sources of covariation: first, starburst amacrine cells (SACs) release both Acetylcholine (Ach) and GABA onto DSGCs (Lee et al., 2010); second, same subpopulation of bipolar cells drives DSGC directly through glutamatergic synapse and indirectly inhibits DSGC through SACs, thus forming a feedforward motif (Figure. 5.1). Less is known about the relative contribution of neurotransmitter release versus feedforward motif for the covariation of excitation and inhibition.

In chapter 4, we reported the synaptic and circuitry mechanisms underlying robust retinal direction selectivity in noisy environment. In particular, we found that DS-

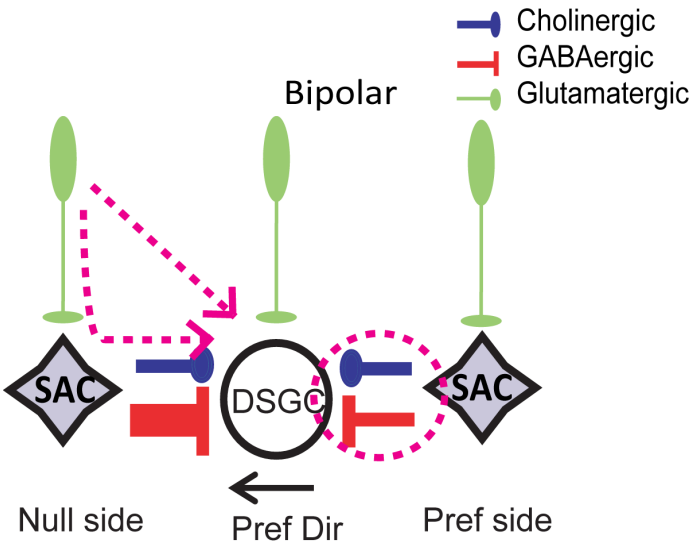

FIGURE 5.1: Schematic showing shared origins (highlighted by pink color) of excitation and inhibition inputs onto DSGCs. Pink arrow indicates feedforward motif from bipolar cells (green). Pink circle highlights the co-release of Ach and GABA from SACs.

GCs veto unwanted spikes towards conflicting stimuli to remain direction selective. Here we further investigated how covariation of excitation and inhibition contributed to noise resilience of retinal direction selectivity.

5.3 Results

5.3.1 Pulse-train protocol capture find-time scale stimulus dependent synaptic covariation

To understand the covariation between excitatory and inhibitory synaptic inputs, we first adopted a protocol previously reported to record excitation and inhibition simultaneously (Cafaro and Rieke, 2010; Zylberberg et al., 2016). In short, whole-cell voltage clamp recording was established on DSGCs while stimulating the cell with visual stimuli. The holding potential was alternated every 5ms between the inhibition and excitation reversal potential (Figure 5.1a). Then EPSC and IPSC are interpolated from the recording (from last data point before next voltage change) for

each trial (Figure. 5.1b). Residual traces, which reveals the fluctuating noise, were then calculated by subtracting the mean excitatory or inhibitory conductance evoked by the same stimulus (Figure 5.1c). Lastly, the covariation between excitatory and inhibitory inputs was computed as cross-correlation between the residual excitatory and inhibitory conductances. We successfully applied the protocol to capture the stimulus dependency of synaptic covariation, in which the covariation evoked by null direction motion is much stronger than that of prefer direction (Figure. 5.2d-e). Additional control experiments were performed on the same cells by recording EPSCs and IPSCs separately and compared with extracted currents using pulse-train protocol (Figure 5.2 f-g). The stimulus dependent covariation structure was only captured by pulse-train protocol.

5.3.2 Synaptic fluctuation is less correlated without lateral inhibition onto SACs in noisy background

In chapter 3, we found that lateral inhibition onto On SACs is important for direction selectivity only in the presence of noise background. More specifically, without lateral inhibition onto SACs, DSGCs fire more action potential towards null stimuli, thus direction selectivity is impaired. Lateral inhibition onto SAC could affect correlated synaptic fluctuation in three possible ways:

- First, SACs release both Ach and GABA through voltage-dependent vesicular mechanism. Previously it has been reported that Ach and GABA release by SAC are differentially regulated, with Ach release requires higher $[Ca^{2+}]$ and membrane potential threshold(Lee et al., 2010). Lateral inhibition could potentially affect the co-transmission from SACs that regulated the correlated synaptic fluctuation and result in impairment of vetoing unwanted response.

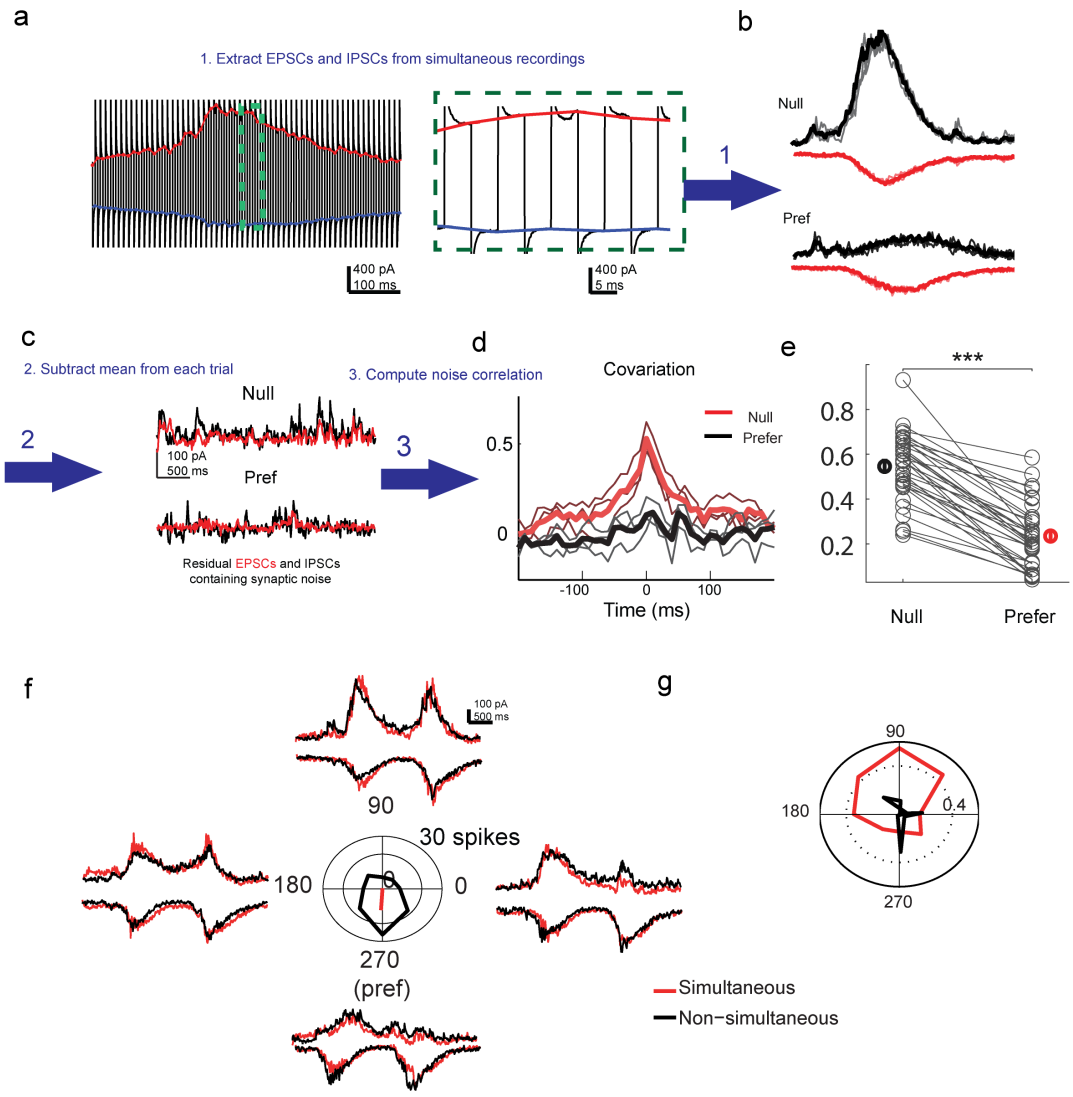

FIGURE 5.2: Pulse train protocol capture synaptic fluctuations.
a-d.Example traces show the process of extracting residual EPSCs (red) and IPSCs (black) through pulse train protocol, and computing of EPSC-IPSC covariation.
e.Summary plots shows stimulus dependent covariation for the same cells in control mice.
f.Example traces of pulse-train extracted IPSCs and EPSCs, in comparison with non-simultaneously recorded currents.
f.Tuning plot of covariation for the cells in f.

- Second, a common GABAergic inhibition from wide-field amacrine cells (WACs) onto bipolar terminal and SACs could serve to correlate glutamatergic and GABAergic inputs.

- Thirdly, theoretical models have predicted that synaptic gains are correlated with strength of covariation(Zylberberg et al., 2016). Lateral inhibition could indirectly affect covariation through regulating synaptic transmission strength.

Given the multiple ways synaptic fluctuation covariation could be affected by lateral inhibition onto SACs and ultimately impact directional output of DSGCs. We first applied the pulse train-protocol to examine how covariation has been affected. As in chapter 4, a conditional knock-out mice line, Gabra2 KO, was used in which the $\alpha 2$ subunit of GABAA receptor was knocked out(Chen et al., 2016). As a result, SACs no longer receive lateral inhibition from neighboring SACs and non-SAC amacrine cells. Since lateral inhibition affects directional spiking particularly in the null direction and covariation of synaptic fluctuation is much stronger in response to null motion, we focused on the analysis of synaptic inputs properties evoked by null motion. In no noise condition, neither the directional tuning (characterized by direction selectivity index, see methods), or amplitudes of IPSCs or covariation was affected in the Gabra2 KO (Figure. 5.3a). However, in noise condition, covariation is significantly reduced in knockouts compared with control group (Figure. 5.3b). Meanwhile, the amplitude of IPSCs was reduced, consistent with finding in chapter 4 using non-simultaneous recording. Both the reduction of covariation and synaptic gains are consistent with increased spiking in the null direction. Together, these data indicate a role of synaptic covariation for noise resilience.

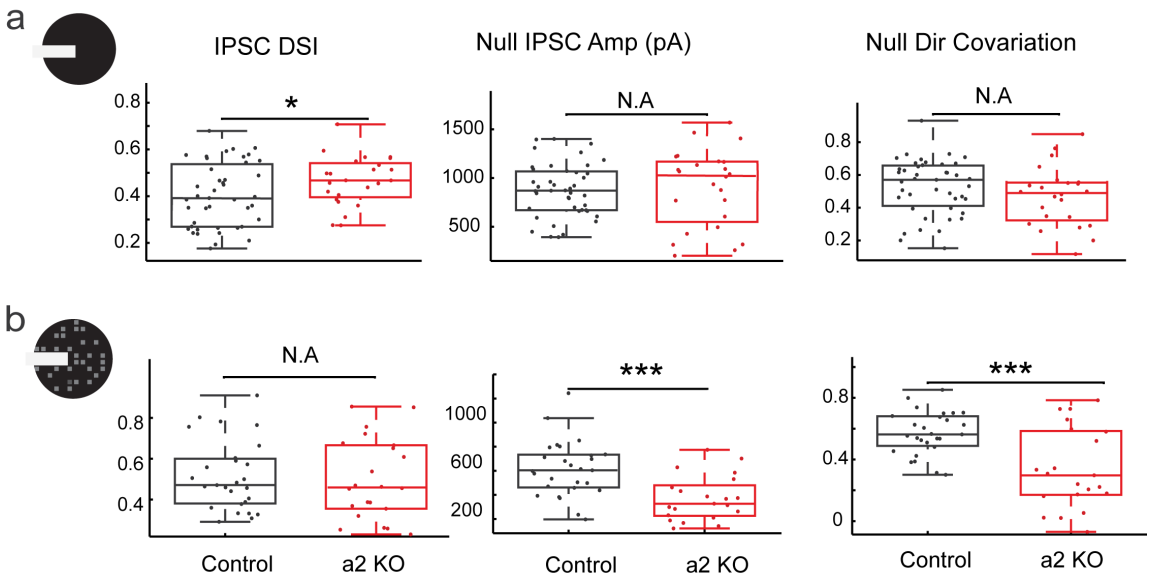

FIGURE 5.3: In noisy background, Covariation between IPSCs and EPSCs onto DSGC is reduced in Gabra2 KOs
a.Summary boxplots of DSGCs IPSC DSI, amplitude and IPSC-EPSC covariation, in response to moving bar against homogeneous background.
b.Summary boxplots of DSGCs IPSC DSI, amplitude and IPSC-EPSC covariation, in response to moving bar against noise background.
* p<0.05, ** p<0.005, *** p<0.0005, two-sampled student t-test
Control: 13 mice, 43 cells; Gabra2 KO: 9 mice, 24 cells

5.3.3 Covariation in noisy background arises from glutamatergic and GABAergic pathways

As discussed above, synaptic covariation onto DSGCs could come from multiple sources. One of the origins of covariation is from Ach and GABA co-transmission (Figure. 5.4a). We used pharmacological blockage to remove cholinergic inputs onto DSGCs by bath applying cholinergic receptors antagonist DhβE. As a result, the covariation from corelease mechanism is removed. We found that while cholinergic EPSC is a prominent component of excitation onto DSGCs in no noise condition, the EPSCs onto DSGCs is mostly glutamatergic (5.4 b-d, see also chapter 4). So, further blockage of cholinergic excitation in noisy background does not affect co-variation. In summary, lateral inhibition onto SACs affects the glutamatergic and GABAergic synaptic fluctuation in the retinal direction-selective circuit.

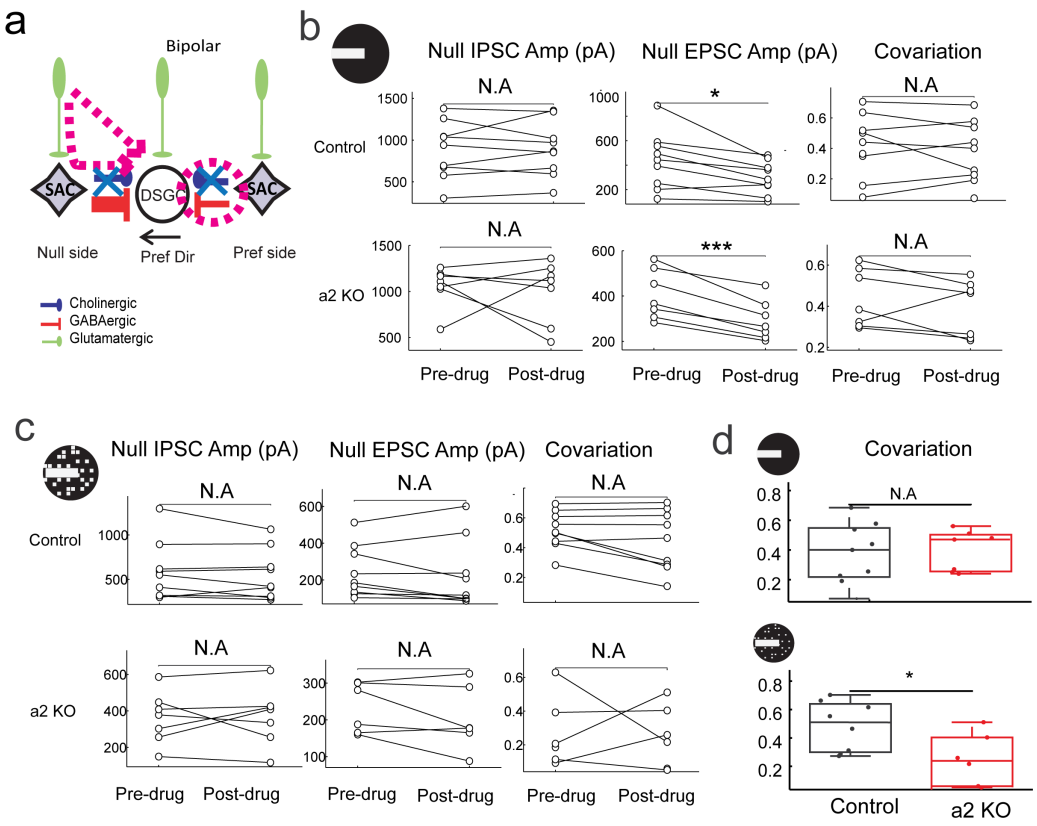

FIGURE 5.4: Covariation in noisy background arises from glutamatergic and GABAergic pathways.
a. Schematic shows the shared origins of excitatory and inhibitory inputs onto DSGCs.
b. Summary plots of Null motion evoked IPSC amplitude,EPSC amplitude, IPSC-ESPC covariation before and after application of cholinergic receptor antagonist, without presence of flickering noise.
c. Summary plots of Null motion evoked IPSC amplitude, EPSC amplitude, IPSC-ESPC covariation before and after application of cholinergic receptor antagonist, in the presence of flickering noise.
d. Summary plots of IPSC-EPSC covariation, in the presence of cholinergic receptors antagonist, in control and Gabra2 KO mices.
* $p<0.05$, ** $p<0.005$, *** $p<0.0005$, paired student t-test (b-c), two-sampled student t-test (d)
Control: 4 mice, 9 cells; KO 4 mice, 7 cells

Lateral inhibition could affect covariation in two major ways: first, through regulating synaptic gain, as previous modeling studies suggested; second, providing common inputs onto bipolar and SACs to correlate glutamatergic and GABAergic transmission. Indeed, our data demonstrated a linear relationship between the synaptic fluctuation covariation (Figure 5.5a) and geometric mean of IPSC/EPSC amplitudes. However, this linear relationship would not exclude the other possibilities. Given

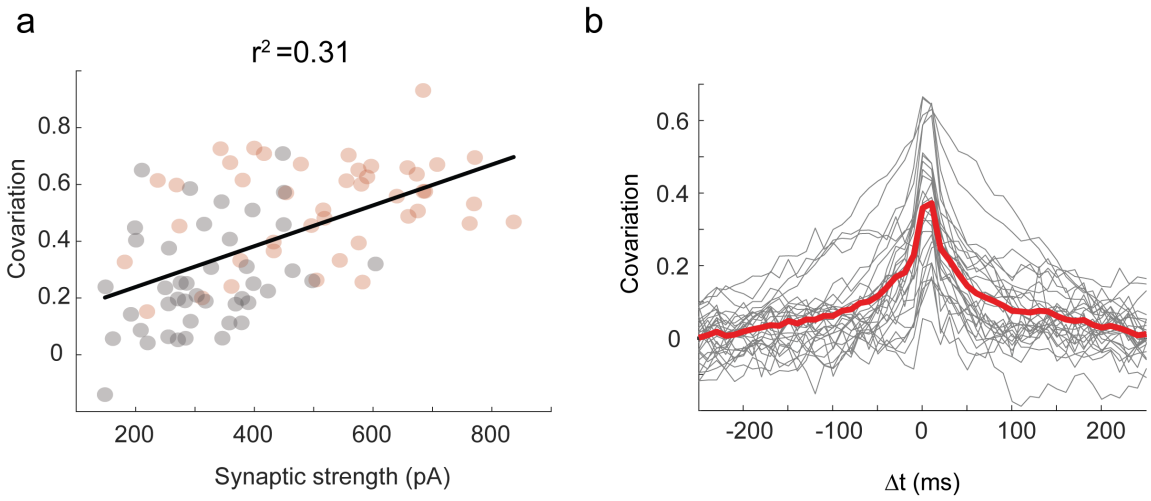

FIGURE 5.5: Properties of synaptic covariations ont DSGCs.
a.Scatter plots shows the linear relationship between covariation and synaptic strength. Synaptic strength is computed as $\sqrt{Amp_{IPSC} \cdot Amp_{EPSC}}$, in which Amp is the peak amplitude of synaptic currents evoked by moving bar stimuli. Red dots indicate data from null miton, gray dots indicate data from prefer motion.
b.Temporal profile of cross correlation between inhibition and excitatory synaptic noise evoked by null direction motion. δt is the temporal offset between inhibition and excitation, positive values means inhibition is leading.

that feedforward circuity is composed of direct excitation onto DSGC and indirect (two synapses) inhibition through SACs. If the glutamatergic and GABAergic arises from this substrate, we would expect the peak of covariation centered around the time scale for one synapse transmission (≈30ms). On the other side, if the covariation arises from common amacrine cells-to-bipolar or amacrine cell-to-SACs synapse, we would not expect delay of peak. To test this idea, we plotted and quantified the temporal profile of the cross-correlation, the temporal offset for maximal covariation is 5.2 ms between inhibition and excitation. Together, these data suggested a common input from amacrine cells onto bipolar terminal and SACs that synchronized the inhibition and excitation onto DSGCs in noisy background. However, the anatomical substrates remained to be determined.

5.4 Summary

In this chapter, we explored the implementation of correlated synaptic fluctuations in the retinal direction selectivity circuit. Multiple functional motifs exist in the direction selective circuit to synchronize the excitation and inhibition through parallel channels. Our data suggested that common amacrine cells inputs could play an important role particularly in noisy environment when the covariation from neurotransmitters corelease is absent. In previous chapter, we studied the mutual inhibitory motif and found that mutual inhibition prevents use-dependent synaptic depression. This mechanism maintains the fidelity of direction selectivity in a time window around hundreds of ms (Figure. 6a). Here, we dissected the function role of multiple circuitry mechanisms for fine-time scale (a few ms) synaptic covariation. Together, retinal direction selective circuit engages distinct sets of circuitry motifs that operating at different time scales to maintain the robustness of its computation.

5.5 Materials and Methods

5.5.1 Animals

The C57BL/6 wild-type (WT) or transgenic mice of either sex were used in this study. The $Gabra2^{flox/flox}$ mouse line was a generous gift from Dr. Uwe Rudolph at Harvard Medical School. Drd4GFP mice were initially developed by MMRRC (http://www.mmrrc.org/strains/231/0231.html) in the Swiss Webster background, and were subsequently backcrossed to C57BL/6 background. All strains in our laboratory were crossed to C57BL/6 background and crossed with each other to create the lines used in the study. Mice of both sexes aging from postnatal 21 to 60 days were used in the experiments. All procedures to maintain and use mice were in accor-

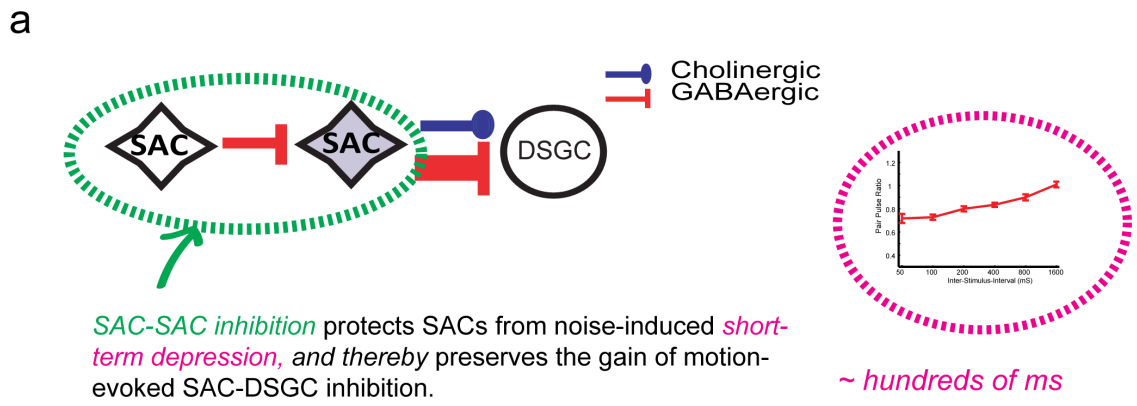

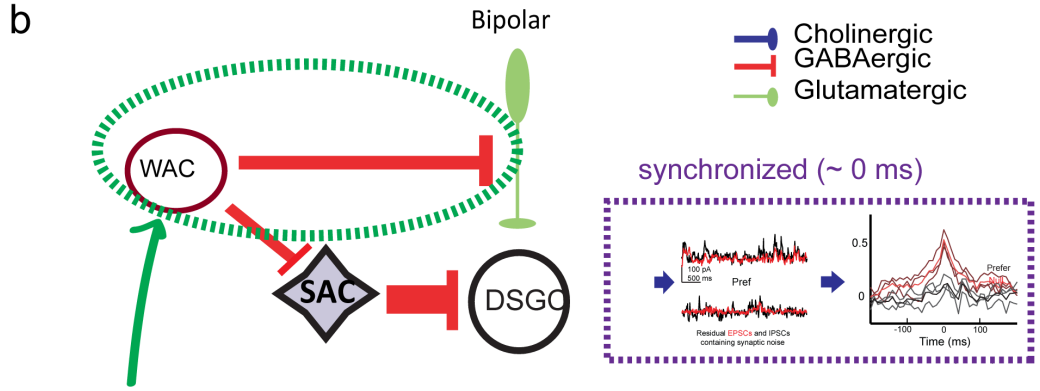

FIGURE 5.6: Based on the pharmacological and genetic manipulations, we propose that GABAergic inputs onto On SACs are differentially regulated at different time scales to mediate noise resilence of retinal DS.
a.mutal inhibition between SACs protects the SACs noise-induced short-term depression to render robust synaptic transmission from SACs onto DSGCs at a time window spanning ~hundreds of ms.
b.Shared origin of inputs from bipolar or WACs underlies the covariation between IPSCs and EPSCs that maintains robust DS in shorter time scale.

dance with the University of Chicago Institutional Animal Care and Use Committee (Protocol number ACUP 72247) and in conformance with the NIH Guide for the Care and Use of Laboratory Animals and the Public Health Service Policy.

5.5.2 Whole-mount retina preparation

The procedures of isolating the retina from pigment epithelium has been previously described (Wei, 2010). In short, mice were dark adapted for at least 45 minutes, anaesthetized with isoflurane, then decapitated. The retina was then isolated under infrared illumination at room temperature in oxygenated ($95\%O_2$ $5\%CO_2$) Ames medium (Sigma-Aldrich, St. Louis, MO). Isolated retinas were then cut into dorsal or ventral pieces and mounted on top of a 1mm2 hole in small piece of filter paper (Millipore, Billerica, MA) with ganglion-cell-layer up. The orientation of prefer direction (posterior) of Drd4-GFP positive cells was labelled for each piece. Retinas were kept in darkness at room temperature in oxygenated Ames medium until use (0-8 hrs).

5.5.3 Visual stimulation

A white organic light-emitting display (OLEDXL, eMagin, Bellevue, WA; 800 x 600 pixel resolution, 60 Hz refresh rate) was controlled by an Intel Core Duo computer with Windows 7 operating system and presented to the retina at 1.1 m/pixel resolution. Moving stimulus were generated by MATLAB and Psychophysics Toolbox (Brainard, 1997), and focused through the condenser lens of microscope to the photoreceptor layer. Positive contrast bar (220 μm wide, 440 μm long) moved along long axis and was presented in 8 or 12 pseudo-randomly chosen directions at a speed of 440 μm/sec over a 660 m-diameter field on the retina. Three to five trials were recorded for each moving direction. The intensity of the moving bar was $\sim 6.3 \cdot 10^4$ isomerizations (R*)/rod/s, in the photopic range. For homogeneous background, the intensity of background is 1800 R*/rod/s, lying at the lower end of photopic range. For noisy background, the noise was generated as randomly flickering checker. Individual checker was 55 μmx55 μm in size, with intensity at either background (0)

or $\sim 1 \cdot 10^4$ R*/rod/s drawn from a binomial distribution. The checker pattern was refreshed at 15 Hz.

5.5.4 Two-photon guided recording of fluorescence-positive neurons for light response

The retinas were perfused with oxygenated Ames at $34 - 36\,^{\circ}\mathrm{C}$ during recordings. Drd4-GFP positive pDSGCs or td-Tomato positive SACs were identified using a two-photon microscope (Bruker Nano Surface Division) and a Ti: sapphire laser (Coherent Chameleon Ultra II) tuned to 920 nm. Then cells were visualized with infrared light (>900 nm) and an IR-sensitive video camera (Watec). The inner limiting membrane was removed by an empty glass electrode to expose the targeted cell. For loose-attach recording of spikes, an electrode of 3-5 MΩ was filled with filtered Ames medium. For voltage-clamp whole cell recording, recording electrode was filled with a cesium-based internal solution containing 110 mM CsMeSO4, 2.8 mM NaCl, 4 mM EGTA, 5 mM TEA-Cl, 4 mM adenosine 5-triphosphate (magnesium salt), 0.3 mM guanosine 5-triphosphate (trisodium salt), 20 mM HEPES, 10 mM phosphocreatine (disodium salt), 5 mM N-Ethyllidocaine chloride (QX314), 0.025 mM Alexa 488 (for SACs) and 0.025 mM Alexa 594 (for pDSGCs), pH 7.25. Light evoked IPSCs and EPSCs onto pDSGCs were isolated by holding at 0 mv and -60 mv respectively.

5.5.5 Pulse-train recording for simultaneous EPSC and IPSC recording

The pulse-train protocol was previous reported and adopted in the lab to allow simultaneous EPSC and IPSC recording. Whole-cell voltage clamp was established with recording electrode filled with Cs-base internal. For each trial, the holding potential was alternated every 5 ms between the reversal potential of excitation and inhibi-

tion. The process was repeated 3-6 trials. Then EPSC and IPSC were extracted from the current recorded during the pulse-train protocol by interpolating near the last sample point before the next holding potential change. This process allows 100 Hz sampling rate of EPSC and IPSCs and capture the majority of excitatory and inhibitory conductance.

5.6 References

Barlow, H.B., and Hill, R.M. (1963). Selective Sensitivity to Direction of Movement in Ganglion Cells of the Rabbit Retina. Science (80-.). 139, 412412.

Barlow, H.B., and Levick, W.R. (1965). The mechanism of directionally selective units in rabbits retina. J. Physiol. 178, 477504.

Barlow, H.B., Hill, R.M., and Levick, W.R. (1964). Retinal ganglion cells responding selectively to direction and speed of image motion in the rabbit. J. Physiol. 173, 377407.

Brinkman, B.A.W., Weber, A.I., Rieke, F., and Shea-Brown, E. (2016). How Do Efficient Coding Strategies Depend on Origins of Noise in Neural Circuits? PLOS Comput. Biol. 12, 1005150.

Cafaro, J., and Rieke, F. (2010). Noise correlations improve response fidelity and stimulus encoding. Nature 468. Chen, Q., Pei, Z., Koren, D., and Wei, W. (2016). Stimulus-dependent recruitment of lateral inhibition underlies retinal direction selectivity. Elife 5.

Fried, S.I., Mnch, T.A., and Werblin, F.S. (2002). Mechanisms and circuitry underlying directional selectivity in the retina. Nature 420, 411414.

Hartline, H.K. (1938). The response of single optic nerve fibers of the verterbrate eye to the illumination of the retina. Am. J. Physiol. 121, 400415.

Lee, S., Kim, K., and Zhou, Z.J. (2010). Role of ACh-GABA Cotransmission in Detecting Image Motion and Motion Direction. Neuron 68, 11591172.

Mauss, A.S., Vlasits, A., Borst, A., and Feller, M. (2017). Visual Circuits for Direction Selectivity. Annu. Rev. Neurosci. 40, 211230.

Taylor, W.R., and Vaney, D.I. (2002). Diverse synaptic mechanisms generate direction selectivity in the rabbit retina. J. Neurosci. 22, 77127720.

Zylberberg, J., Cafaro, J., Turner, M.H., Shea-Brown, E., and Rieke, F. (2016). Direction-Selective Circuits Shape Noise to Ensure a Precise Population Code.

6

Conslusion and perspective

In retina direction-selective circuit, direction selectivity first arises in the dendrites of starburst amacrine cells (SACs), a class of interneuron that provides directionally tuned inhibition to the direction selective ganglion cells (DSGCs). The activities of both SACs and DSGCs are shaped by neighboring SACs and non-SAC amacrine cells. Regardless of the apparent complexity of the circuit, it can be further divided into multiple functional motifs that operate in parallel and ultimately converge onto DSGCs (Fig. 6.1). The main thesis of my graduate work is trying to understand how different functional motifs and cellular properties, like synaptic plasticity, work together to maintain a dynamic balance of excitation and inhibition for robust retinal computation. In particular, my work focuses on dissecting the functional relevance of inhibitory motifs for retinal direction selectivity. All previous studies on this topic have applied GABA receptor antagonists to the entire retina, and therefore cannot unambiguously identify the synaptic loci that are involved. Furthermore, all published studies have focused on synaptic interactions in the On sublamina of the retina due to greater accessibility of On SACs for functional analysis, the synaptic mechanisms underlying direction selectivity in the Off pathway have been largely ignored.

We, for the first time, dissected the inhibitory inputs onto both On and Off SACs using a combination of synapse-specific genetic manipulations, two-photon calcium imaging, electrophysiology and pharmacology. We found that:

- Different inhibitory motifs contribute differently to the direction selectivity of bright and dark moving objects, which are encoded by the On and Off pathway, respectively.
- Engagement of one particular form of lateral inhibition, mutual inhibition, is stimulus dependent. In the On pathway, mutual inhibition is recruited when stimuli moves against noisy background, resembling more natural conditions.
- Amacrine cell (AC)-SAC-DSGC serial inhibition does not serve the conventional disinhibition function role during noise processing. Instead, the visual noise in the background generates a network dynamics that engage these canonical circuit motifs in different time-scale for noise resilience of retinal direction selectivity.

6.1 On and off pathway asymmetry

The somas of On SACs are located in the ganglion cell layer so that On SACs were first named as displaced amacrine cells. Later another population of SACs, Off SACs, whose somas are located in the inner nucleus layer (INL), were found. Due to the accessibility for electrophysiological recording, most of the physiological properties we know about SACs are derived from On SACs. While On and Off SACs have been assumed to be mirror symmetric, anatomical difference between On and Off SACs has been documented, while largely overlooked (Famiglietti, 1985; Vaney, 1990). Meanwhile, On SACs synapses onto On DSRGCs in addition to On-Off DSRGCs.

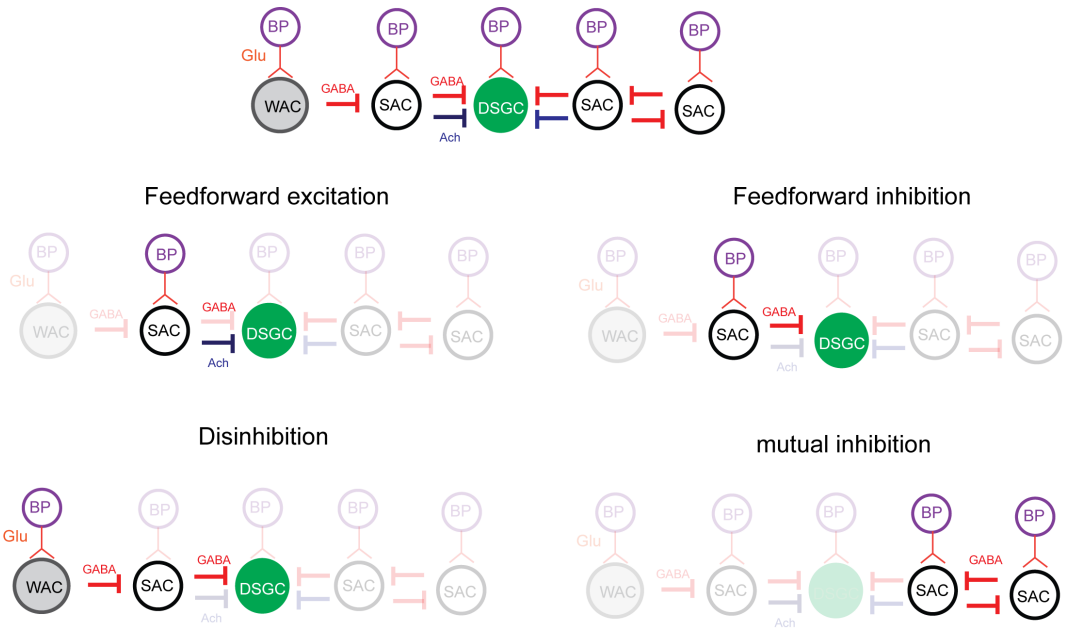

FIGURE 6.1: Functional circuitry motifs in retinal direction selective circuit.

It is tempting to hypothesize that On SACs might express additional properties to drive both On and On-Off DSRGCs. Another study investigated the difference in synaptic inputs onto DSGCs in On versus Off pathway (Taylor and Vaney, 2002). They found that the On pathway shows stronger asymmetry in inhibitory inputs from SACs, while the temporal delay is larger between inhibition and excitation in the Off pathway. Several recent recordings from Off SACs demonstrated distinct circuitry mechanisms underlying SACs direction selectivity. In Chapter 3 of this thesis, we investigated the role of individual inhibitory inputs onto SACs. We found that On SACs direction selectivity is intact without inhibitory inputs onto SACs in homogeneous background (Chen et al., 2016). However, the inhibition from wide field amacrine cells is apparently required from direction selectivity in Off SACs. Connectomic analysis revealed that both On and Off SACs receive spatially segregation bipolar inputs (Ding et al., 2016; Greene et al., 2016; Kim et al., 2014). However, Only On SACs receive proximal excitation from bipolar cell types with sustained temporal kinetics (Ding et al., 2016; Kim et al., 2014). In another study, direct elec-

trophysiological recording from On and Off SACs showed that only Off SACs reveal J-shaped I-V curves, a signature of NMDA receptors mediated currents (Fransen and Borghuis, 2017). Additional nonlinearity introduced by wide field amacrine cells and NMDA receptors might contribute to the enhanced contrast sensitivity as required under natural condition in the Off pathway (Turner and Rieke, 2016). Furthermore, On SACs receive tonic glutamate release from bipolar cells which could regulate dendritic isolation of SAC dendrites through activation of mGluR2. It turns out Off SACs, however, did not receive tonic glutamate release from bipolar cells (Borghuis et al., 2013). Thus, Off SACs might utilize a different mechanism regulating dendritic compartmentalization.

The division of On-Off pathway raises the question about the functional purpose of such asymmetry. While previous studies indicate that such asymmetry might arise from adaption towards natural image statistics. For example, natural images exhibits more regions of intensity decrements, so some retina pathways have smaller receptive field sizes to map the dark regions with higher resolutions. How does the introduction of additional wide field amacrine cells inputs and expression of NMDA receptors in Off SACs contribute to the efficient encoding of nature images would require more complete analysis of interactions of natural scenes and circuitry motifs.

6.2 Stimulus-dependency of motif recruitment

Direction-selective retinal circuit expresses a variety of mechanisms to compute direction selectivity at multiple levels as reviewed in Chapter 1. Such level of circuitry intricacy might reflex the complexity of performing the task of motion detection in natural environment. In fact, natural environment differs dramatically from the simple artificial stimuli in the laboratories. Natural scenes exhibit significant level of fluctuations in luminance and contrast, as well as spatial and temporal background

noise. Simple artificial stimuli could reveal some but not all aspects of properties of retinal circuitry. For example, it has been shown that natural stimuli could reveal characteristics of visual neurons otherwise unseen with simple stimuli (David et al., 2004; Felsen and Yang, 2005; Talebi and Baker, 2012).

In consistence of this notion, while the ultimate retinal output remains relatively invariant, the recruitment of circuitry mechanisms showed significant stimulus dependency.

- Firstly, the recruitment of direction selective mechanisms is luminance dependent. One recent study showed that spiking wide field amacrine cells synapse onto presynaptic bipolar terminals (Hoggarth et al., 2015). The activation of those TTX-sensitive amacrine cells could sharpen the tuning of DSRGCs. Recruitment of the spiking wide field amacrine cells is ambient light level dependent since certain brightness is needed to reach the spiking threshold of those amacrine cells. Another potential way ambient light level could affect the DSRGCs circuitry is through mediating tonic glutamate release onto SACs. As described previously, bipolar cells tonically release glutamate onto On SACs (Borghuis et al., 2013). The level of tonic excitation could affect the mGluR2 activation, thus regulate the dendritic compartmentalization of SACs dendrites.

- Secondly, the recruitment of direction selective mechanisms is contrast dependent. Low contrast preferentially activate cholinergic pathways versus glutamergic pathways onto DSRGCs (Sethuramanujam et al., 2016). In this case, DSRGCs receives both excitation and inhibition predominantly directly from SACs.

- Thirdly, the recruitment of direction selective mechanisms depends on background noise. In Chapter 3, we described that engagement of lateral inhibition onto SACs prevents the degradation of direction selectivity. In fact, additional

dendritic mechanism is expressed by DSGCs for noise resilience. The NMDA receptor signaling of DSGC would amplify correlated excitation and inhibition inputs to improve the signal (correlated) to noise (uncorrelated) ratio of the DSGCs output (Poleg-Polsky et al., 2016).

6.3 Mutual inhibition and noise reduction

In Chapter 3, we reported that in noisy visual environment, retinal direction selectivity is degraded without lateral inhibition onto SACs. In Chapter 4, we further characterized the underlying synaptic mechanisms. We found that without lateral inhibition onto SACs, DSGCs receive reduced amount of inhibition from SACs. This finding contrasts the conventional notion about the AC-SAC-DSGC serial inhibition, in which dis-inhibition of SAC would increase the inhibitory inputs from SACs onto DSGCs. This paradigm, however, assumes the synaptic transmission in the circuit is rather static. However, it has been reported previously SAC-DSGC synapse undergoes short-term depression in rodent retina during development. To resolve this discrepancy, we investigated the role of short-term plasticity during visual stimulation. We found that, without lateral inhibition onto SACs, noise stimuli would evoke short-term depression in SACs that suppress the response to following signal. In particular, mutual inhibition among SACs suffice to protect the neighboring SAC from undergoing short-term depression.

Mutual inhibition motif has been indicated to be the building block of point attractor network and participates in important brain functions such as decision making, pattern completion, and noise reduction ((Hopfield, 1982; Machens et al., 2005). Our work, for the first time, showed how noise and signal response interacts at cellular level for noise reduction in retinal direction selective circuit. While adaptation of inhibition in amacrine cells has been attributed to sensitization in the retina (Kast-

ner and Baccus, 2013), our finding indicates that for certain retinal pathway, such sensitization could be problematic when neural response to null-stimuli is also sensitized. While mutual inhibition among neurons and short-term plasticity are common features across multiple brain areas, the interaction between mutual inhibition and short-term plasticity we revealed in the study, would have further implications beyond retina direction selective circuit.

6.4 Summary

The availability of genetic tools and functional recording methods now allows us to study neural circuits in unprecedented details. Our findings provide important mechanistic insights into the direction selective circuit, highlight the importance of using both simple and complex stimuli when studying multiple levels of neural mechanisms underlying visual processing.

6.5 References

Borghuis, B.G., Marvin, J.S., Looger, L.L., and Demb, J.B. (2013). Two-photon imaging of nonlinear glutamate release dynamics at bipolar cell synapses in the mouse retina. Journal of Neuroscience 33, 10972-10985.

Chen, Q., Pei, Z., Koren, D., and Wei, W. (2016). Stimulus-dependent recruitment of lateral inhibition underlies retinal direction selectivity. Elife 5, e21053.

David, S.V., Vinje, W.E., and Gallant, J.L. (2004). Natural stimulus statistics alter the receptive field structure of v1 neurons. Journal of Neuroscience 24, 6991-7006.

Species-specific wiring for direction selectivity in the mammalian retina. Nature 535, 105-+.

dendrites of starburst amacrine cells. Nature 418, 845. Famiglietti, E.V. (1985).

Starburst amacrine cells: morphological constancy and systematic variation in the anisotropic field of rabbit retinal neurons. Journal of Neuroscience 5, 562-577.

Felsen, G., and Yang, D. (2005). A natural approach to studying vision. Nature neuroscience 8, 1643.

Fransen, J.W., and Borghuis, B.G. (2017). Temporally Diverse Excitation Generates Direction-Selective Responses in ON-and OFF-Type Retinal Starburst Amacrine Cells. Cell Reports 18, 1356-1365.

Greene, M.J., Kim, J.S., and Seung, H.S. (2016). Analogous convergence of sustained and transient inputs in parallel on and off pathways for retinal motion computation. Cell reports 14, 1892-1900.

Hopfield, J.J. (1982). Neural networks and physical systems with emergent collective computational abilities. Proc. Natl. Acad. Sci. U. S. A. 79, 25542558.

Hoggarth, A., McLaughlin, A.J., Ronellenfitch, K., Trenholm, S., Vasandani, R., Sethuramanujam, S., Schwab, D., Briggman, K.L., and Awatramani, G.B. (2015). Specific Wiring of Distinct Amacrine Cells in the Directionally Selective Retinal Circuit Permits Independent Coding of Direction and Size. Neuron 86, 276-291.

Kastner, D.B., and Baccus, S.A. (2013). Spatial segregation of adaptation and predictive sensitization in retinal ganglion cells. Neuron 79, 541554.

Kim, J.S., Greene, M.J., Zlateski, A., Lee, K., Richardson, M., Turaga, S.C., Purcaro, M., Balkam, M., Robinson, A., and Behabadi, B.F. (2014). Space-time wiring specificity supports direction selectivity in the retina. Nature 509, 331.

Famiglietti, E. V (1985). Starburst amacrine cells: morphological constancy and systematic variation in the anisotropic field of rabbit retinal neurons. J. Neurosci. 5, 562577.

Machens, C.K., Romo, R., and Brody, C.D. (2005). Flexible control of mutual inhibition: A neural model of two-interval discrimination. Science (80-.). 307, 11211124.

Poleg-Polsky, A., and Diamond, J.S. (2016). NMDA Receptors Multiplicatively Scale

Visual Signals and Enhance Directional Motion Discrimination in Retinal Ganglion Cells. Neuron 89, 1277-1290.

Sethuramanujam, S., McLaughlin, A.J., Hoggarth, A., Schwab, D.J., and Awatramani, G.B. (2016). A central role for mixed acetylcholine/GABA transmission in direction coding in the retina. Neuron 90, 1243-1256.

Talebi, V., and Baker, C.L. (2012). Natural versus synthetic stimuli for estimating receptive field models: a comparison of predictive robustness. Journal of Neuroscience 32, 1560-1576.

Taylor, W.R., and Vaney, D.I. (2002). Diverse synaptic mechanisms generate direction selectivity in the rabbit retina. Journal of Neuroscience 22, 7712-7720.

Turner, M.H., and Rieke, F. (2016). Synaptic rectification controls nonlinear spatial integration of natural visual inputs. Neuron 90, 1257-1271.

Vaney, D.I. (1990). The mosaic of amacrine cells in the mammalian retina. Progress in retinal research 9, 49-100.